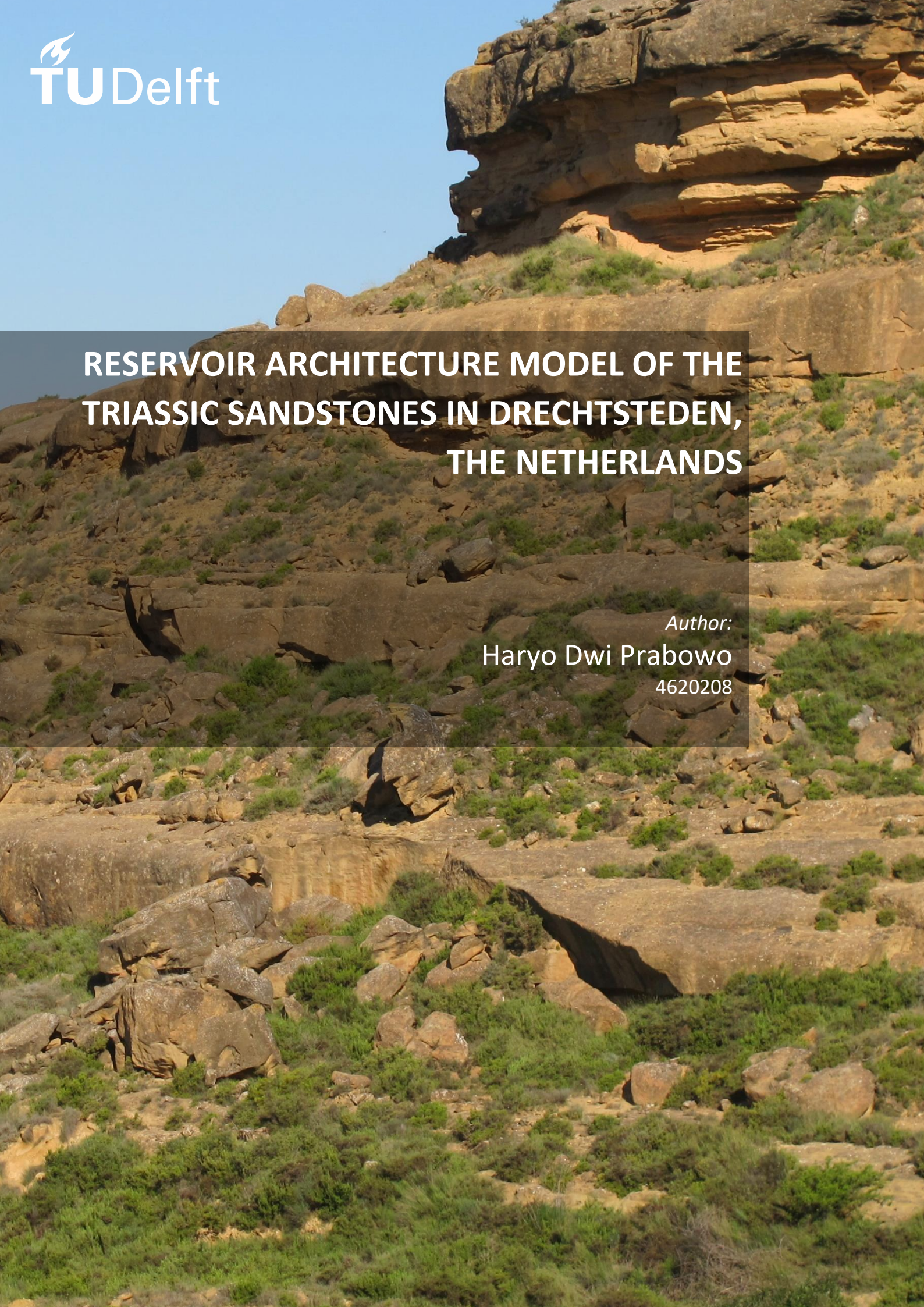

RESERVOIR ARCHITECTURE MODEL OF THE TRIASSIC SANDSTONES IN DRECHTSTEDEN, THE NETHERLANDS

Author:
Haryo Dwi Prabowo
4620208

Reservoir Architecture Model of the Triassic Sandstones in Drechtsteden, The Netherlands

By

Haryo Dwi Prabowo

in partial fulfillment of the requirements for the degree of

Master of Science
in Petroleum and Geosciences
Specialization of Reservoir Geology

at the Delft University of Technology,
to be defended publicly on August 31, 2018, at 2:00 PM.

Student number	: 4620208
Project duration	: November 17, 2017 – August 31, 2018
Supervisor	: Dr. M. E. Donseelar TU Delft, Chairman
Thesis Committee	: Charlotte de Wijkerslooth HVC
	Gerhard Diephuis TU Delft
	Axel Sanden Veegeo Energy

Acknowledgements

This research is the final project which conclude my two years study in the Petroleum and Geosciences faculty at TU Delft. In this opportunity I would like to express my gratitude to Indonesia Endowment Fund for Education for sponsoring my Master's Degree at the TU Delft.

I would like to thank my university supervisor, Dr. M. E. Donseelar for introducing me to this interesting topic. My external supervisors, Charlotte de Wijkerslooth (HVC), Gerhard Diephuis and Axel Sanden (Vegeeo Energy) for the guidance, constructive remarks and insightful guidance in the achievement of this project.

Lastly, I would like to thank my family and friends as well, for their never-ending support since the beginning of my study.

Haryo Dwi Prabowo
Delft, August 2018

Abstract

In the Netherlands, the geothermal application is implemented to produce heat from a sedimentary aquifer in the subsurface for greenhouses and district heating. The most commonly used configuration is a doublet of wells, in which one injection- and one production well is drilled to produce warm water and re-inject cool water in the same target reservoir. One of the most important issues in operating this project is to maintain pressure communication of the doublet, with injector-producer well distance limitation and geological heterogeneity provide the main challenge to be solved. Moreover, as this application depends on flow behavior from injector to producer well, thus the determination of doublet wells location and spacing must be correctly evaluated to reduce the risk of an unsuccessful project.

In this research, the Triassic successions within the Drechtsteden area in the West Netherlands Basin (WNB) are evaluated for its potential for geothermal energy production. A reservoir characterization approach is implemented to answer the above challenges by utilizing subsurface data such as 3D seismic and well data. The process consists of seismic interpretation, reservoir sedimentology, and petrophysical evaluation analysis to determine the reservoir architecture and properties within the study area.

The regional study shows that most of the sandstone intervals within the Triassic successions occur in the Röt-, Hardegsen-, Detfurth- and Volpriehausen Formation. Based on reservoir sedimentology analysis, the sandstone intervals are composed of the stacked low sinuous river and sheet flood deposits with some interbedded lake margin deposits. The regional correlation suggests that the sand bodies within each formation can be correlated over distances of kilometers and were deposited along an SE-NW direction. The petrophysical evaluation result displays some variation in the reservoir properties (N/G, average porosity, and permeability) at a different location within the study area. A notable decrease is observed in reservoir porosity and permeability at greater depths which might indicate a compaction effect due to several tectonic episodes during and after the deposition of the Triassic Successions.

At the end of this research, two doublet locations are determined based on the analysis results which fulfill the required conditions for geothermal application. Both of the proposed doublets are designed to follow the SE-NW overall trend of the deposition and main faults orientation to maintain the pressure communication and avoid the presence of faults in between the wells. The injector is designed to be located at the shallower level than the producer to allow for gravity-driven flow propagation. A rough estimation of temperature distribution in doublet location displays that the proposed locations have sufficient estimated temperature for greenhouses and district heating. The expected reservoir properties at the proposed doublet locations are estimated from the depth range of penetrated doublet, the generated isopach maps, and petrophysical averages on the evaluated wells within the study area by a statistical approach.

Table of Contents

List of Tables

List of Figures

1 Background

1.1. Introduction

Geothermal exploitation has gained renewed attention in the Netherlands in the past couple years as a result of increased energy demand and worldwide targets for the reduction of CO_2 emission. Geothermal energy is touted as a future source of energy since it has a low emission level compare to the conventional sources such as oil and gas. In the Netherlands, one of the geothermal applications is to produce heat from a sedimentary aquifer in the subsurface for greenhouses and district heating. The most commonly used configuration is a doublet of wells, in which one injection- and one production well is drilled to produce warm water and re-inject cool water in the same target reservoir. This operation is an interesting option to be considered to divert from gas for heating purposes since it takes more than half of Netherlands total energy consumption (Sanner, Ria, Land, & Mutka, 2011).

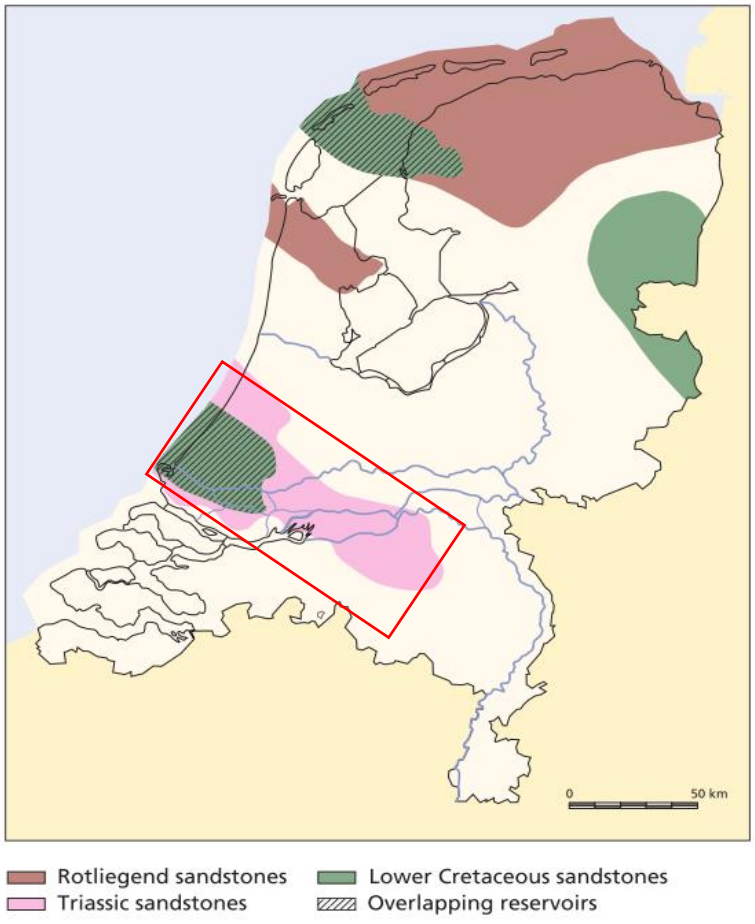

Figure 1. The distribution of deeper aquifers which are potentially most suitable (T > 60◦C and sufficient transmissivity) for the extraction of geothermal energy in the Netherlands (Lokhorst & Wong, 2007). *Red rectangle shows the West Netherlands Basin location.*

The average thermal gradient in the Netherlands is 31°C/km, at conventional depths, this is regarded as a low enthalpy geothermal source. Heat generation for greenhouses and district heating generally require 70ºC of inlet temperature which only found in aquifers deeper than 2000 m (Lokhorst & Wong, 2007). Extensive studies have been carried out since 1980's found that potential sedimentary aquifers for geothermal purposes in the Netherlands occur in the Permian, Lower Triassic and Lower Cretaceous sandstones and in two Tertiary sand units (Lokhorst & Wong, 2007) with estimated total HIP of all prospective aquifers is more than 820,000 PJ (Kramers, van Wees, Pluymaekers, Kronimus, & Boxem, 2012).

In this research, the investigation of the deep aquifer in Triassic sandstone will be conducted in the southernmost part of the West Netherlands Basin (WNB) (Figure 1), in a group of municipalities called Drechtsteden (Figure 2). The produced heat from the targeted reservoir will be used as a district heating source in that area. The main target of interest for this study is the Triassic Fluvio-Lacustrine Sandstone which is a proven oil and gas reservoir. Many of the exploration and development wells have been drilled. Moreover, the past experiences and knowledge regarding geological setting in oil and gas production will surely provide valuable information for characterizing the reservoir for geothermal purpose and give a good platform for the geothermal project.

However, apart from its high prospectivity and successful experiences in oil and gas production, there are complexities and challenges that have to be investigated in more detail before developing this operation. One of the most important issues is to maintain pressure communication of doublets, with injector-producer well distance limitation and geological heterogeneity provide the main challenge to be solved, since this application depends on flow behavior from injector to producer well. Thus, doublet wells location and spacing must be correctly evaluated to reduce the risk of an unsuccessful project.

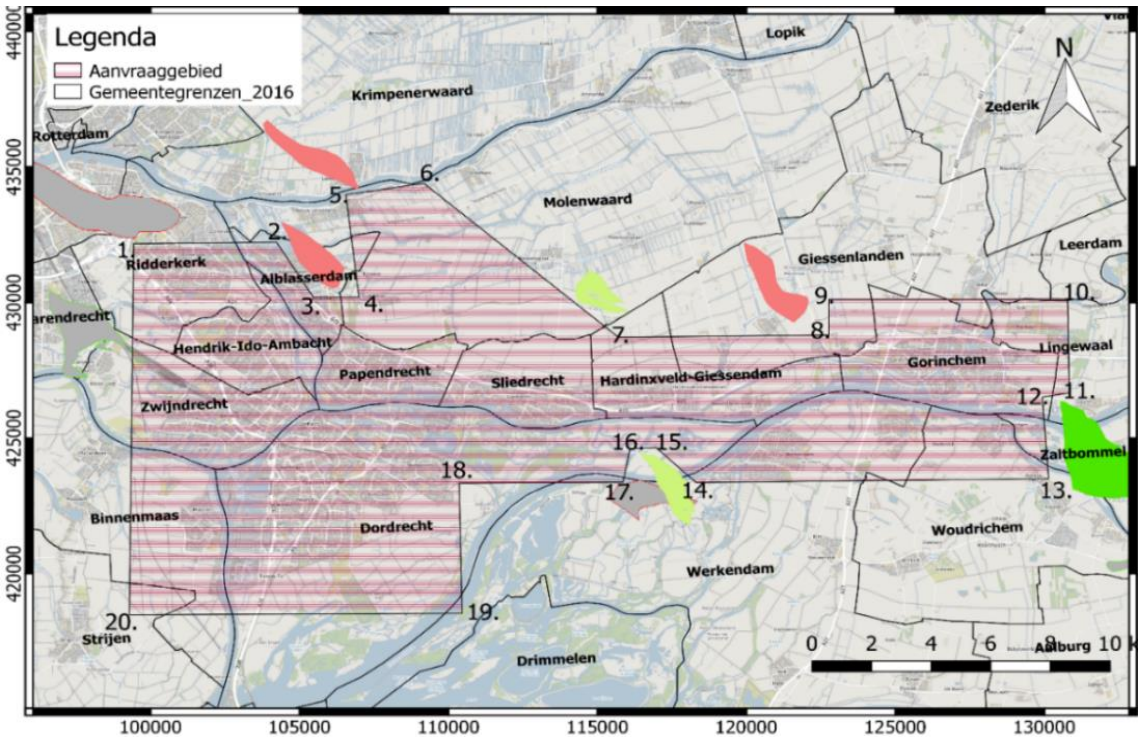

Figure 2. The research area of Drechtsteden geothermal project. (HVC Groep, 2017)

1.2. Research Objective

In order to answer the challenges raised in the previous chapter, a comprehensive reservoir characterization approach is proposed to reduce the uncertainty in implementing this operation. Subsurface data such as 3D seismic and well data are utilized to evaluate the structural and sedimentological aspects within the study area.

In this research project, there are several parameters which need to be investigated as stated below:

- The size, shape, spatial distribution and connectivity (reservoir architecture) of the Triassic Sandstones, and;
- Reservoir properties (porosity and permeability) distribution of the Triassic Sandstones.

The mentioned parameters above will be the main research questions in this thesis. In the end, it will also be used to develop a reservoir architecture model to investigate the most suitable area for geothermal application, which is the main objective of this research.

1.3. Structure of the Report

This research report covers five chapters, consisting of the background of the project in the first chapter which includes the introduction, research objective, and structure of the report. The second chapter will discuss the geological framework of the study area in regional coverage with the general review of Triassic stratigraphy within the research area. In the third chapter, the implemented research method and all available data which been used during this research will be presented.

Next, the results from seismic interpretation and reservoir sedimentology section will be reviewed in the fourth chapter which utilized the available data mentioned in the previous chapter. In the last chapter, an in-depth analysis and discussion regarding the suitable area for geothermal exploitation will be outlined and the final conclusion will be summarized.

2 Geological Framework

2.1. Regional Geology

The research area is located in the southernmost part of the West Netherlands Basin (WNB), in the basin fringe area next to the Roer Valley Graben (RVG). The WNB is bounded by the Zandvoort Ridge in the north and London-Brabant Massif in the south (Figure 3). In general, the WNB was formed as a response to world-wide reorganizations of lithospheric plates (Ames & Farfan, 1996). The basin originally developed on a former fringe area of the Southern Permian Basin area, Merged as a broad platform which attached to the London-Brabant Massif as a northern rim part of Variscan Orogenic belt which developed during Pangaea assembly in the Paleozoic time (Geluk, Plomp, & van Doorn, 1996).

According to Geluk (2007), the breaking up of Pangaea during the Late Permian denoted the pre-rift stage of this basin development, in which the main target of this project (Triassic Successions) was deposited. Major rifting in the syn-rift stage started during the Middle Jurassic to Early Cretaceous, followed by differentiated subsidence which resulted in tilted blocks, a half-graben structure with NW-SE striking trend. A compressional tectonic episode during the Late Cretaceous transformed the basin into an inverted type basin which also reactivated the pre-existing faults.

The WNB structural style is mainly influenced by these rifting and inversion stages which are characterized by tilted blocks, folded and asymmetrical anticlinal structures (Figure 4) and becoming the structural traps for most of the oil and gas province in the southern part of the Netherlands. In terms of depositional sequences, there are four subdivisions which can be determined according to Racero-Baena and Drake (1996) I) a pre-rift clastic sequence from the Permian to Early-Mid Jurassic, II) a syn-rift sequence of the Late Jurassic to Early Cretaceous age, III) a post-rift sequence of the Early to Late Cretaceous and IV) a syn- to post inversion sequence of the Late Cretaceous-Tertiary to Quaternary age. However, in this project in-depth investigation will be conducted in the pre-rift sequence of Triassic deposits. More detail of the Triassic deposits overview will be discussed in the next part.

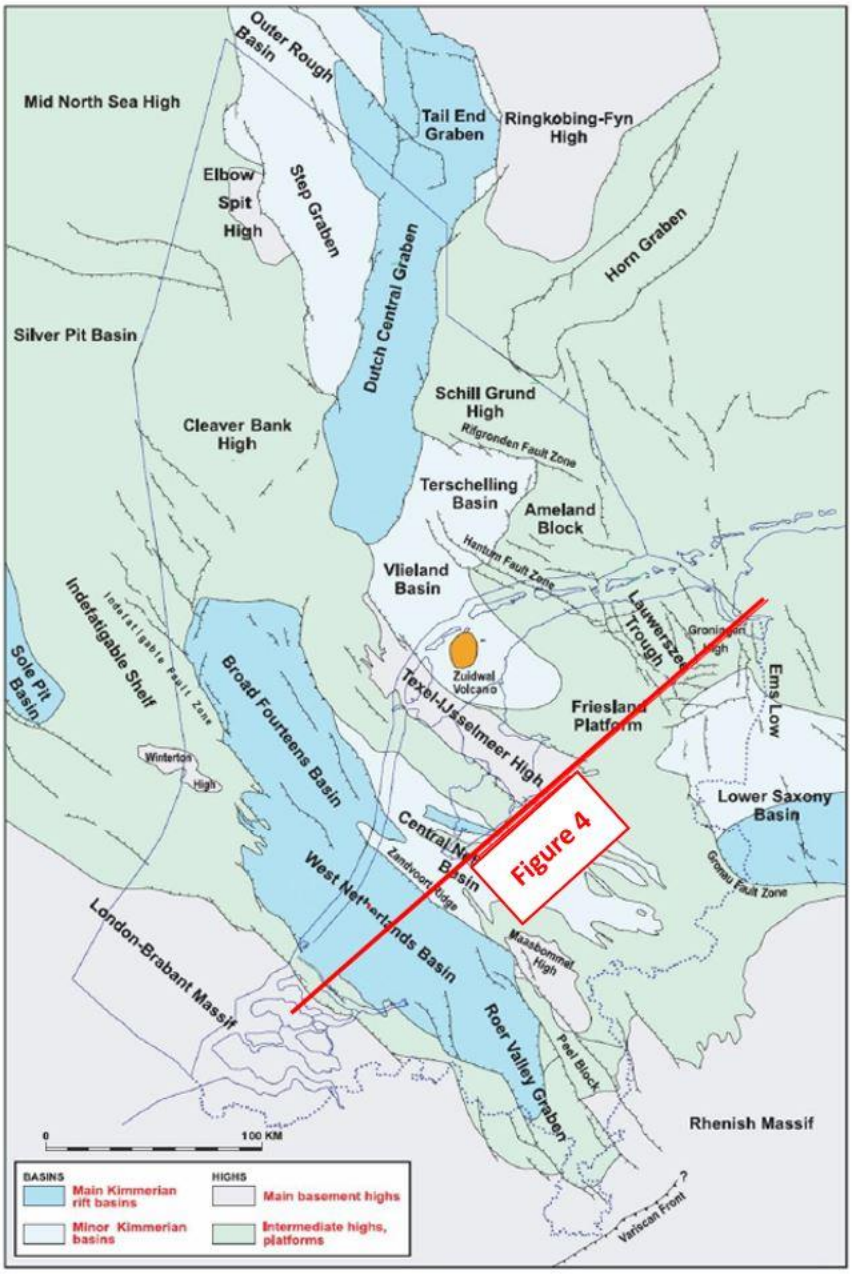

Figure 3. The map showing the WNB area (Geluk, 2007). *The SW-NE cross-section of WNB location is shown below.*

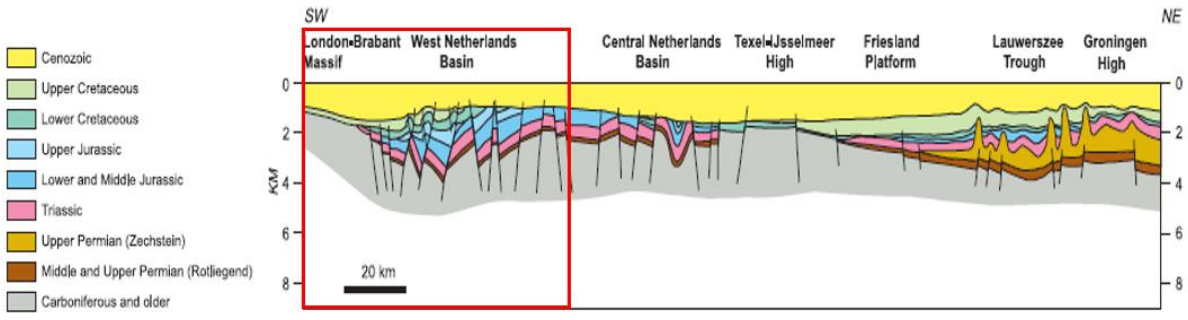

Figure 4. The SW-NE cross section of WNB area as highlighted by red rectangle (Geluk, 2007).

2.2. Overview of the Triassic stratigraphy

During the Triassic, sedimentation continued in the area of the former Southern Permian Basin as a part of the post-Variscan megacycle. In this age, the deposition occurred in an arid to a semi-arid condition which is characterized by braided stream complexes with aeolian, interdune, flood-plain and crevasse-splay environments and terminated in playa lakes (Ames & Farfan, 1996). The sediments were mainly transported from the southeastern part of the Netherlands, in which the RVG acted as a major seaway connection (Geluk et al., 1996).

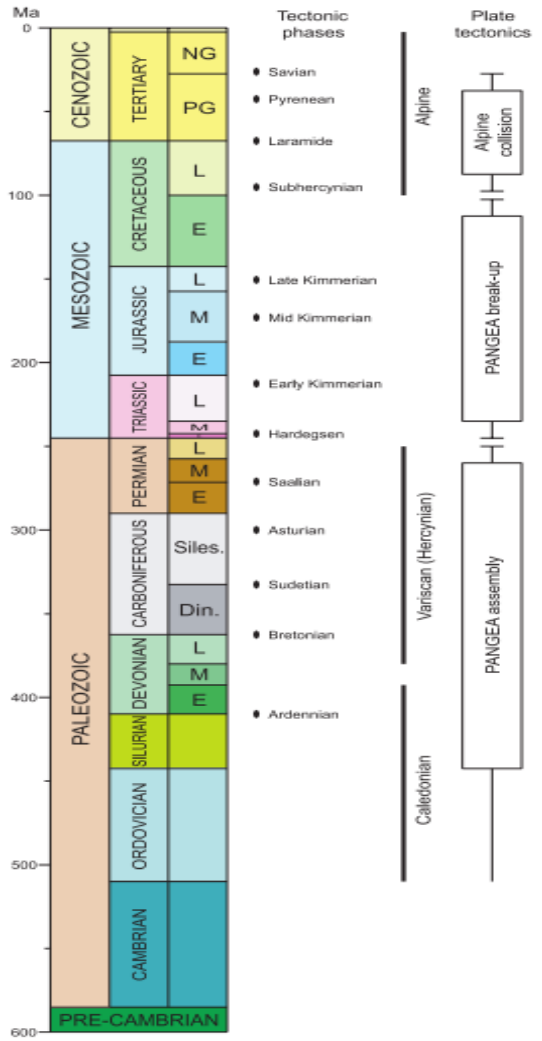

Figure 5. Summary of tectonic events and its relation plate movement in Netherlands. (De Jager, 2007)

The Triassic deposition was also influenced by an extensional tectonic episode which occurred until the Cretaceous, as a response of Pangaea break-up in the Late Permian. As a result, differentiated subsidence and uplift movement are pronounced in most areas in the Netherlands and therefore affected the sedimentation process (Geluk, 2007). Some thickness variations and unconformities within this succession are also found and mainly caused by two extensional tectonic phases (Figure 5).

- The Hardegsen Phase; Controlling the thickness variation and distribution of Main Buntsandstein deposit, and;
- The Early Kimmerian Phase; Affecting the distribution of Upper Germanic Triassic deposit.

In general, the Triassic stratigraphy can be classified into two groups; the Upper and Lower Germanic Triassic which is separated by the Solling unconformity. Based on the classification of Van Adrichem Boogaert & Kouwe (1997), The lower Germanic Triassic consists of the Lower Buntsandstein, Volpriehausen, Detfurth and Hardegsen Formations where the last three formations formed the Main Buntsandstein sub-group. The Upper Germanic Triassic is divided into the Solling, Röt, Muschelkalk and Keuper Formations. The stratigraphy column of Triassic deposits is presented in Figure 6. A more detailed description of each formation in surrounding research areas will be discussed below:

- **Lower Buntsandstein Formation**

  This formation is composed of fine-grained lacustrine sandstone with clay-siltstone alternation. In the study area, it consists of the Rogenstein and Main Claystone member. It directly overlies the Permian Zechstein Claystone Member in most part of the area which also indicates the start of continental deposition condition during the Early Triassic (Geluk, 2007).

- **Volpriehausen Formation**
  The Volpriehausen Formation forms the lower-most part of the Main Buntsandstein Sub-group. In the study area, two members of this formation are present which are the Lower- and Upper Volpriehausen Member. This formation is deposited widely in The Netherlands and reached the greatest thickness up to 150 m in the RVG (Geluk, 2007). Composed of basal-fine grained sandstone with coarsening upward trend in the sequence. In the basin fringe area, it gradually changes into fine-grained cemented sandstone successions.

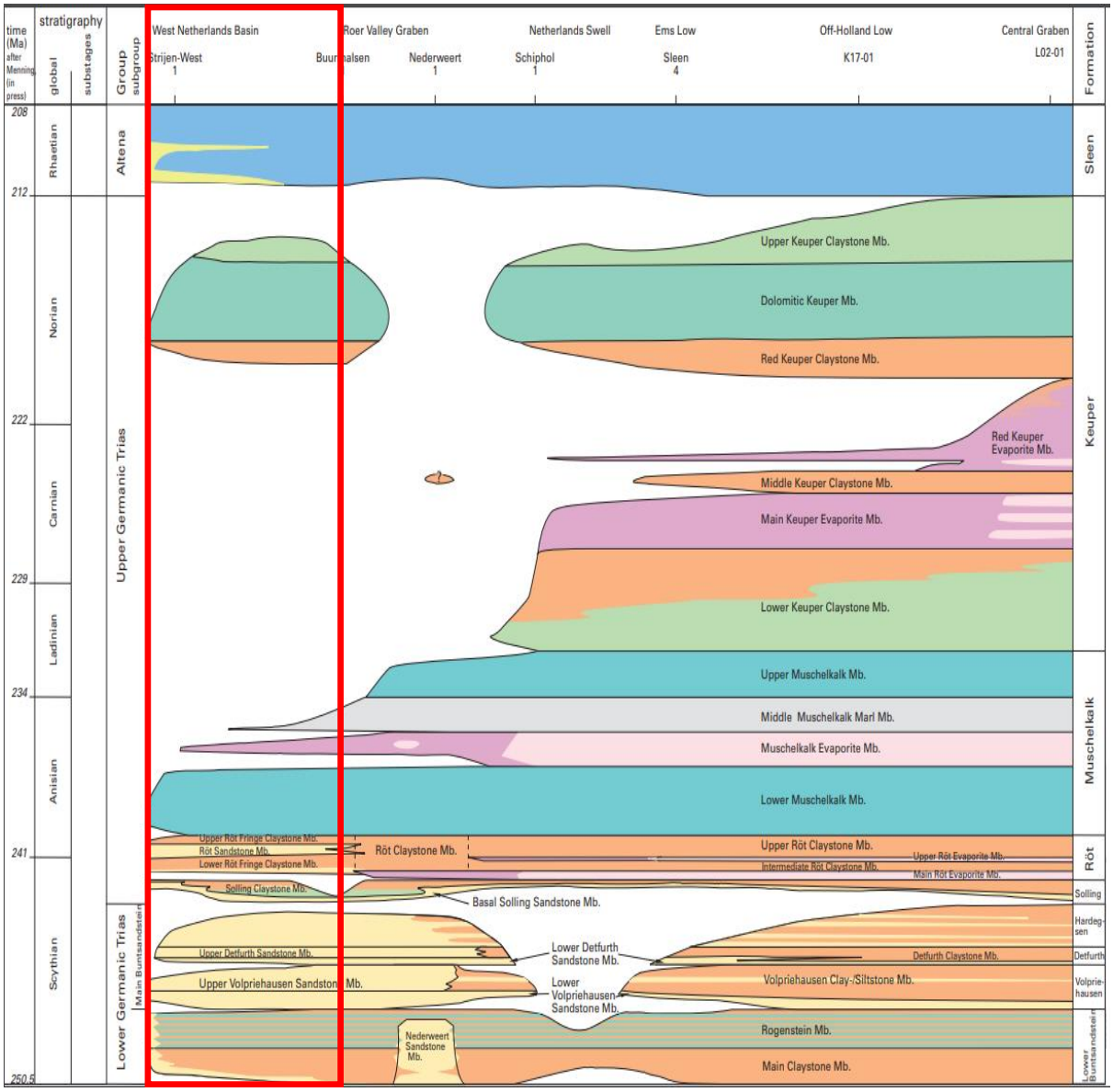

Figure 6. Stratigraphic column of Triassic deposit (Van Adrichem Boogaert & Kouwe, 1997). *Red rectangle shows the WNB area.*

- **Detfurth Formation**
  The Detfurth Formation consists of the Lower- and Upper Detfurth Sandstone Member in the basin fringe area. It consists of arkosic sandstone with relatively high Quartz percentage (up to 50%) and high average porosity range from 15-20% (Geluk et al., 1996). The upper part of this formation mainly displays an intercalation of sandstone-claystone with less reservoir quality compared to the lower part.

- **Hardegsen Formation**
  The Hardegsen Formation is the uppermost of Main Buntsandstein sequence. It is comprised of massive sandstone deposits with maximum porosity up to 20% in the WNB (Geluk et al., 1996). The distribution of this formation is limited to lows and majorly influenced by the Hardegsen extensional phase which explains the absence of this succession in some part of the research area.

- **Solling Formation**
  The Solling Formation denotes the beginning of the Upper Germanic Triassic Group. The start of deposition is marked by pronounced uplift and erosion which is indicated by an unconformity, separating the Lower and Upper Germanic Triassic Group (Geluk, 2007). It is composed of basal sandstone with reddish claystone overlain the succession. In most parts of the basin fringe area, this formation is found to sit directly at the top of the Hardegsen or Detfurth Formation.

- **Röt Formation**
  This formation is comprised of an evaporitic lower part and a clastic upper part. In the basin fringe area, such as the WNB, the evaporitic part is not present (Geluk et al., 1996). The clastic part consists of mainly claystone with sandstone intercalations. Hence, only two members of this formation; the Röt Claystone and Sandstone Member which can be found in the study area.

- **Muschelkalk Formation**
  The Muschelkalk Formation is comprised of limestone and dolomite in the lower part, an evaporitic in the middle and claystone with dolomite in the upper section. During its deposition, the strongest subsidence occurred in the RVG area. Therefore, it influenced the distribution of this formation with only up to 50 m in thickness in the study area (Geluk et al., 1996).

- **Keuper Formation**
  The Keuper Formation sits at the uppermost part of the Triassic deposit. It consists of a claystone and carbonate-dolomite succession. In the study area, the sedimentation was affected by the Early Kimmerian phase where some of the uplift movement occurred and resulted in the erosion of most of the Keuper Formation (Geluk, 2007).

3

Research Methodology and Available Data

3.1. Research Methodology

Figure 7. The general workflow of the project

A reservoir characterization approach is implemented in this research to address the objectives set in the first chapter. The general workflow is presented in Figure 7. The overall process utilizes subsurface data such as 3D seismic, well logs and core data within and around the research area. The detailed description and objectives for each step of the workflow are explained below:

- **Literature Study**
  This part will cover several geological aspects such as regional, structural and sedimentology characteristic of the research area correspond to research objectives.

- **Seismic Interpretation**
  In this step, the geometry and framework of the targeted reservoir will be interpreted by utilizing seismic and well data. The process consists of a seismic-well tie, horizon-fault interpretation, and time-depth conversion.

- **Reservoir Sedimentology**
  The Triassic sandstone unit will be evaluated using well data such as well logs and core data. First, the description of the selected core interval will be performed manually by hand. In the end, the well correlation, core and facies description, paleo-flow direction and connectivity will be analyzed to create a sedimentological model.

- **Petrophysical Evaluation**
  The objective of the petrophysical evaluation is to carry out a detailed analysis of the available well data. Petrophysical parameters that need to be obtained are reservoir thickness, net to gross ratio, porosity, and permeability.

- **Doublet Placement Determination**
  The developed sedimentological model of Triassic Sandstones and their expected reservoir properties are presented in this step. The doublet location will be assessed based on this evaluation.

3.2. Available Data

3.2.1. Coordinate System

In this project, the Rijksdriehoekstelsel New (RD New) coordinate system is used for location determination. Most of the data are originally available in this format such as 3D Seismic and well data. However in the process, some additional data such as regional geological map both in depth and time domain are used for interpretation guide. Hence, a conversion is done as they are only available in UTM (ED50) format. All the conversions are performed in Petrel software.

3.2.2. Seismic Data

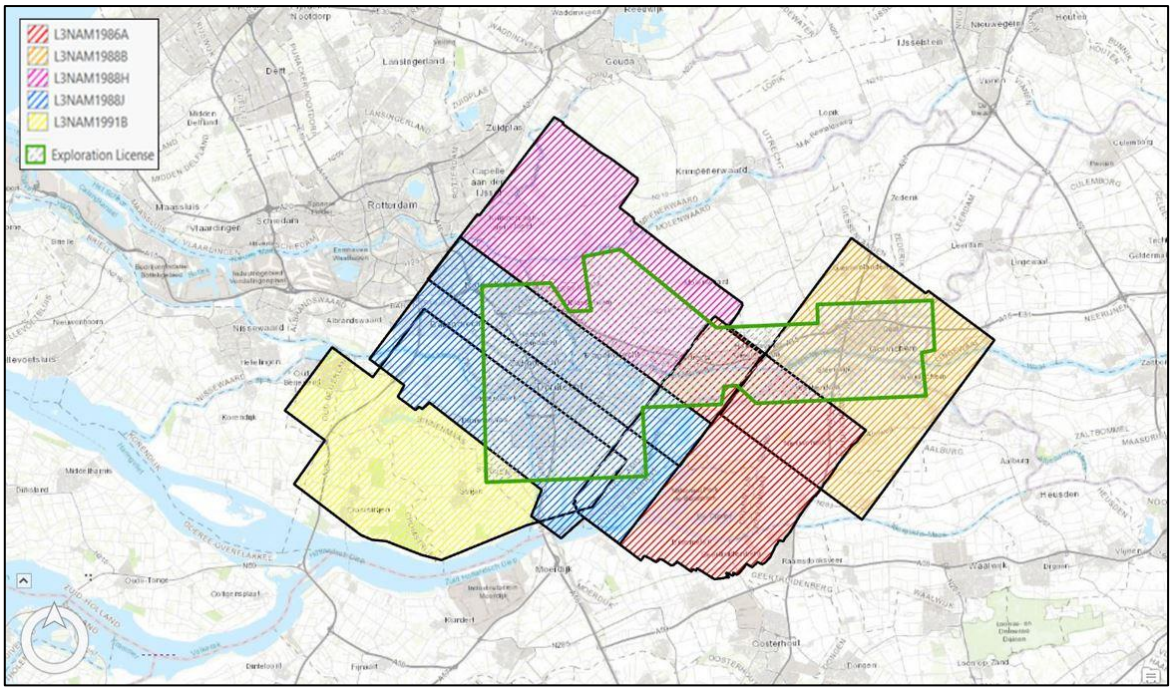

Figure 8. The available 3D seismic Post-Stack Time Migration data and exploration license for the Drechtsteden project. Note that for Seismic Interpretation part only L3NAM1988B IS utilized, as new 3D PSDM data are received.

The Drechtsteden area is fully covered by 3D seismic data. Initially, four onshore 3D seismic Post-Stack Time Migration data are utilized for seismic interpretation part (Figure 8). Below is the list of available 3D seismic Post-Stack Time Migration data on the research area coverage:

- L3NAM1986A
- L3NAM1988B
- L3NAM1988H
- L3NAM1988J
- L3NAM1991B

However in the process, a new 3D seismic Pre-Stack Depth Migration (PSDM) data is received and used for the most of seismic interpretation part. The new data covers almost all the research area, except the most northeastern part of the area in L3NAM1988B coverage (Figure 9). Therefore, seismic interpretation in the area which is covered by PSDM data will be done in depth domain, while the north-eastern part in the time domain.

Both of the seismic data are in SEG convention. In this project, 3D seismic interpretation is displayed in non-SEG convention and hence the color scale is reversed as the hard-kick is represented by a through (red-color), and vice versa.

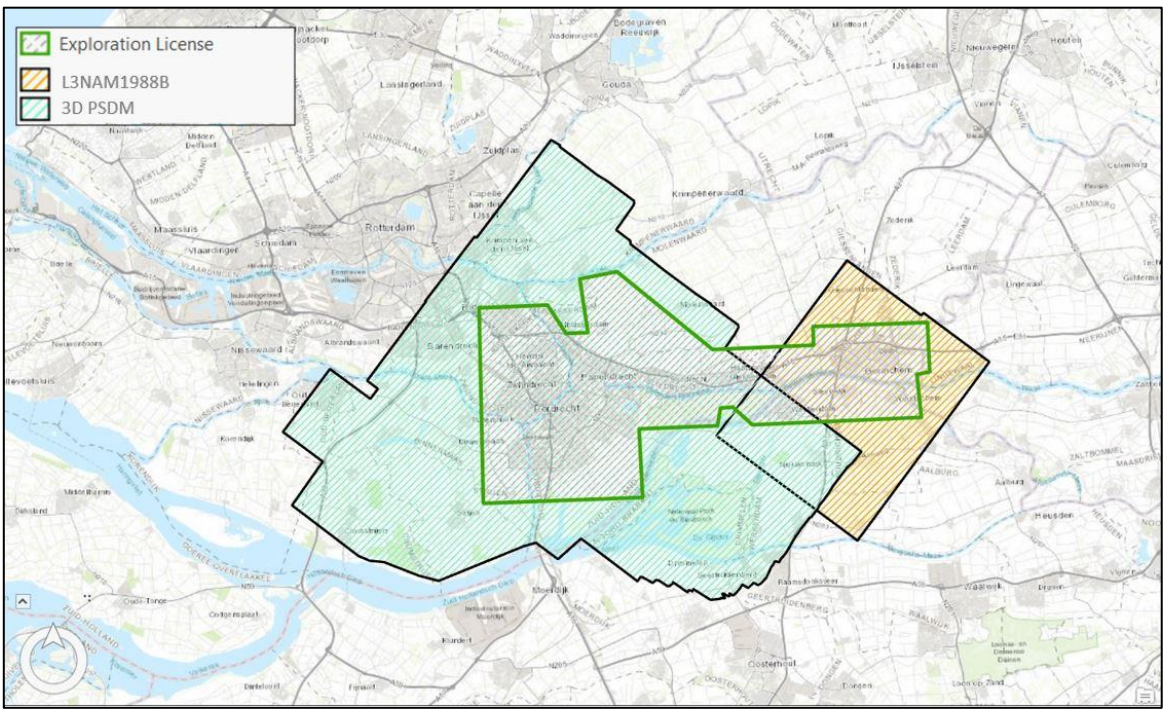

Figure 9. Base map shows the coverage of 3D PSDM and 3D Post-Stack Time Migration data.

The 3D PSDM data consists of 3754 inline and 1724 Xline with the interval of 20 m. The 3D Post-Stack Time Migration data covers the smaller area in North-eastern part of the area which is composed of 530 inline and 779 xline with 20 m interval. The detail of the configuration of each dataset can be found in Appendix A.1 and A.2.

3.2.3. Well Data

A large number of well data within the research area are listed for seismic interpretation, petrophysical and sedimentology analysis steps. Well data such as borehole location, deviation path, well marker, well logs, core data, and reports are retrieved from the nlog.nl site.

A selection is made by listing the available well data inside the 3D seismic coverage mentioned above. There are in total 172 wells in the area, but only 22 wells were drilled through the Triassic level. Of the Triassic wells, only 10 wells have the core data. The available well data inside the study area are presented in Figure 10-13. All the required data for analysis are collected and put in a well database which can be found in the Appendix B.1.

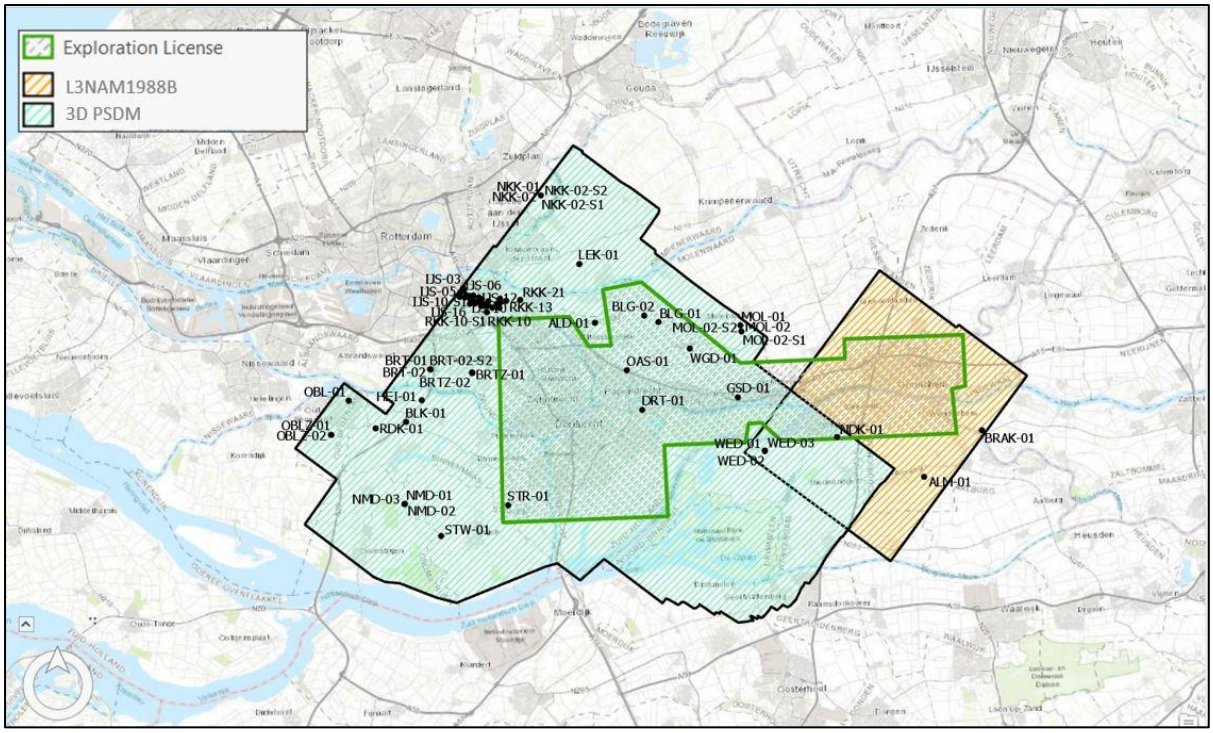

Figure 10. The available 172 well data inside the research area coverage.

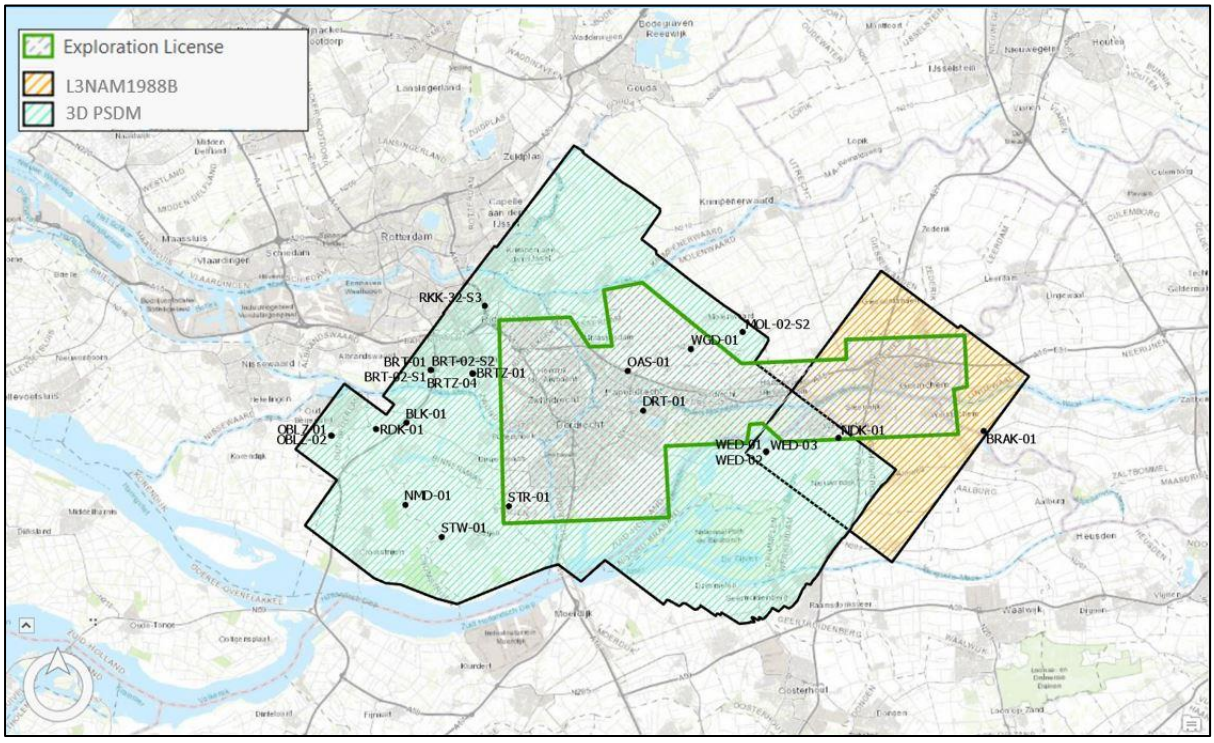

Figure 11. Numbers of wells that penetrated Triassic level.

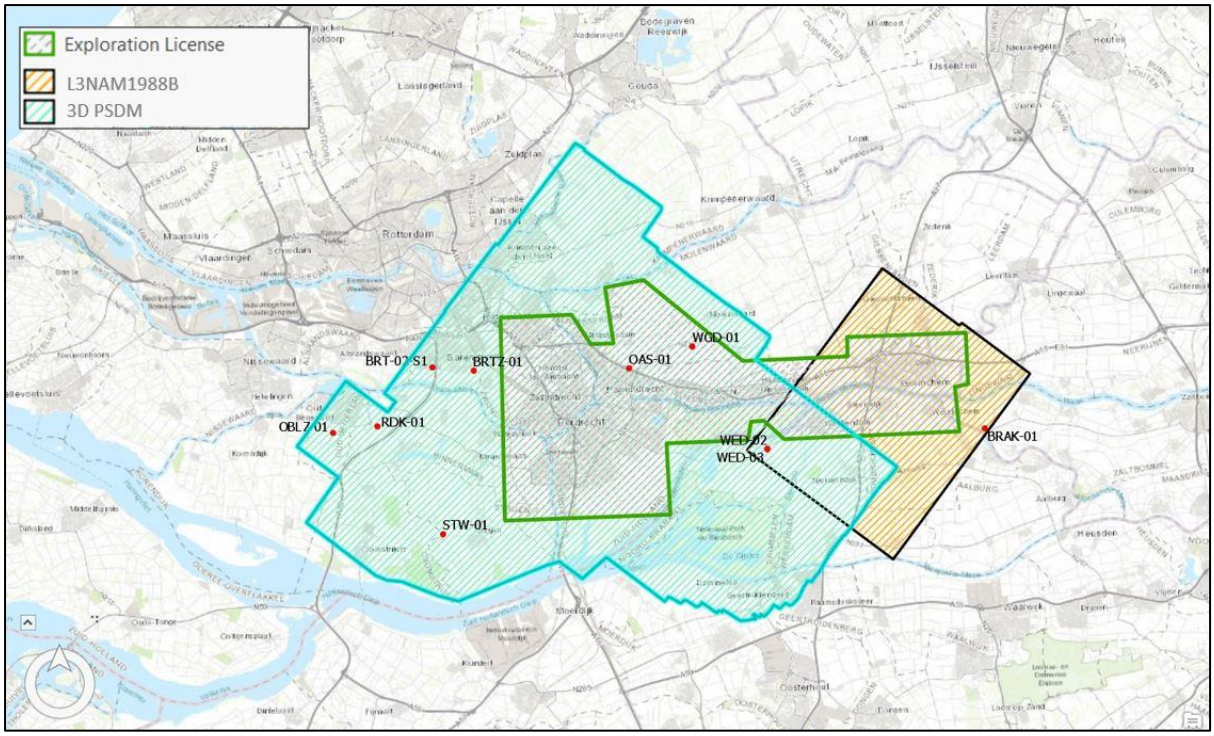

Figure 12. Numbers of wells with core available.

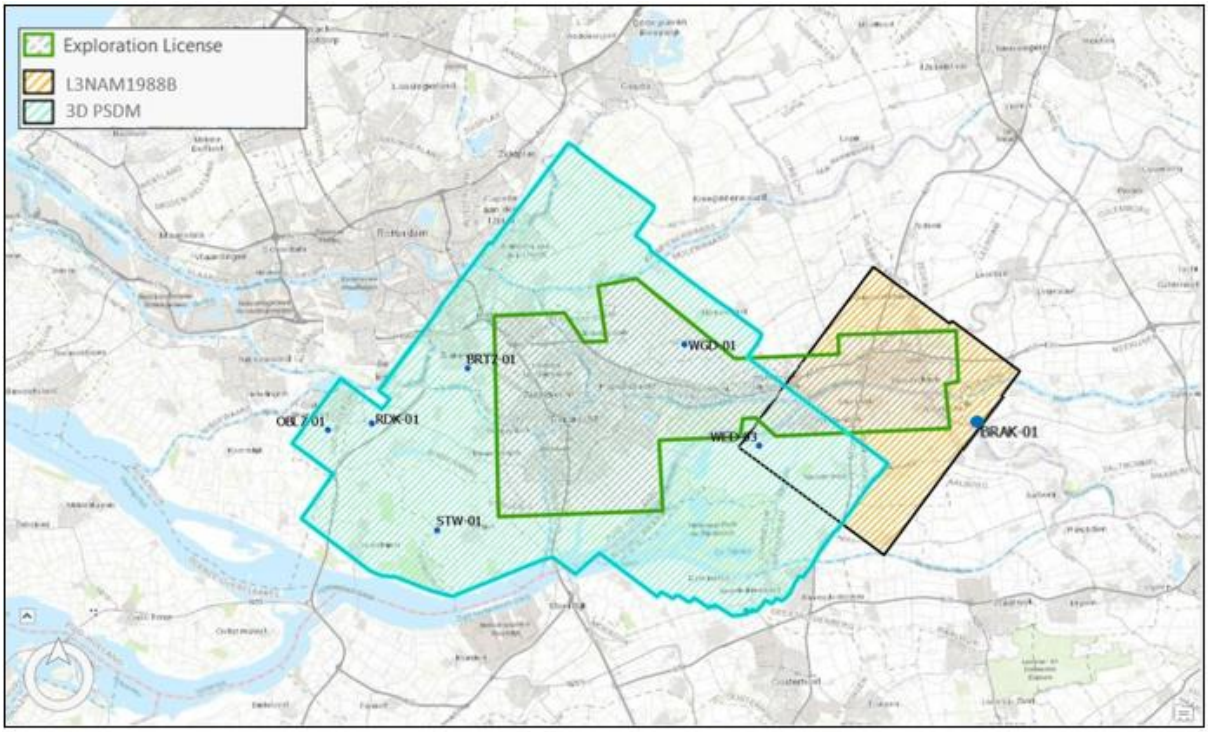

Figure 13. Numbers of wells for petrophysical evaluation part.

3.2.4. Additional Data

During seismic interpretation step, several horizons and fault maps of the Digital Geological Model (DGM) from the nlog.nl site are used as a reference. All the interpreted horizon maps are available in RD format, while the fault map has to be converted first from UTM (ED50) coordinate system to RD format.

Two interpreted horizons of the DGM-deep onshore 4.0 maps of Base Posidonia and Base Altena level in depth and time domain are imported for horizon interpretation comparison. The maps are presented in Figure 14-15. In general, the interpreted horizons are in line with the reference maps.

During fault interpretation phase, fault distribution from DGM 2.0 fault map is utilized as shown in Figure 16. Based on the imported map, the major NW-SE and E-W fault trends in the WNB area can be observed. In the process, this fault map distribution is combined with the variance attribute map to be a reference for fault indication in the Triassic level.

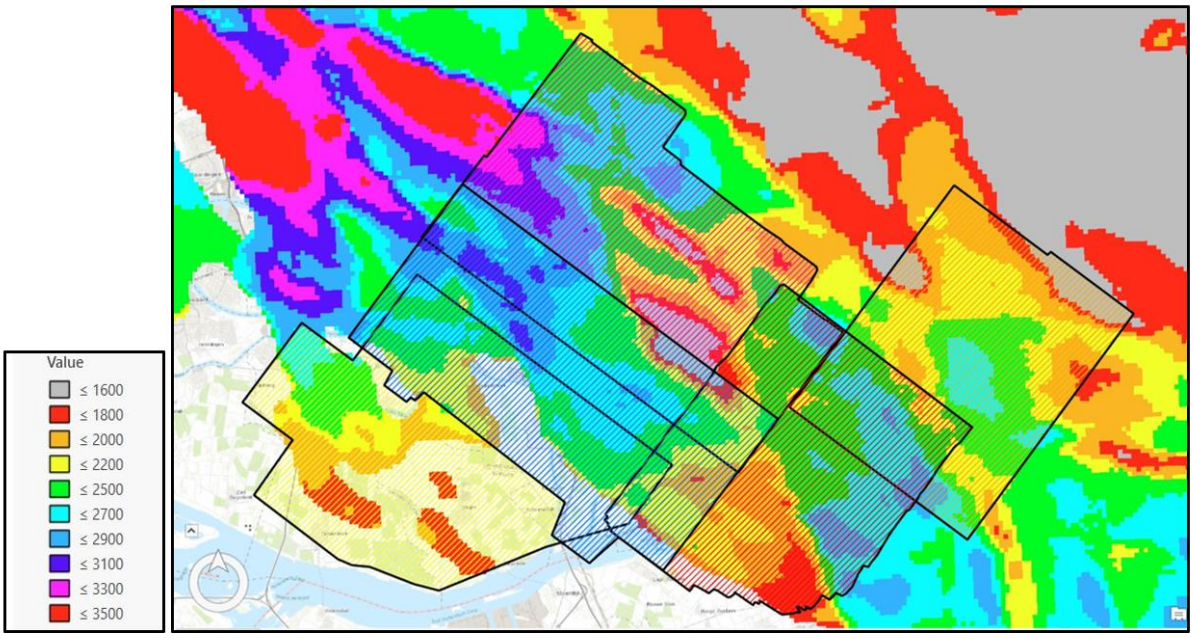

Figure 14. The interpreted horizon map of DGM-4.0 for Base Posidonia level. The comparison with the final interpretation result is shown in Figure 15.

.

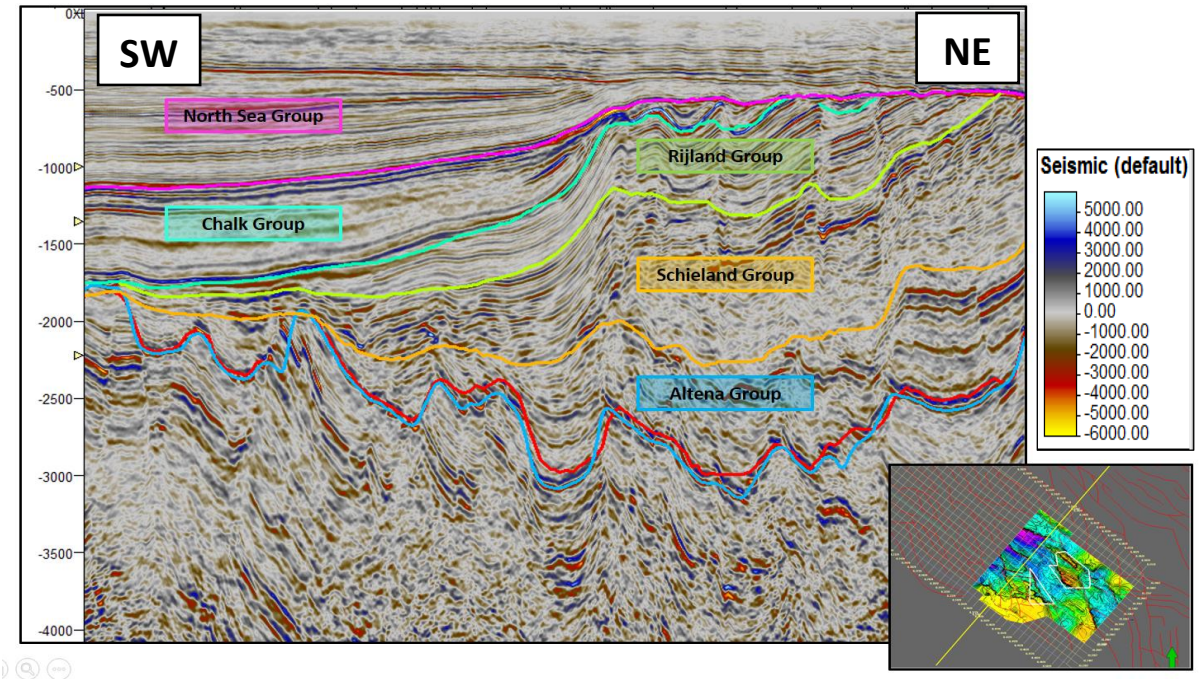

Figure 15. The comparison between the interpreted horizon from DGM 4.0 map (Red) and the final result of interpretation (Blue) of Base Posidonia level.

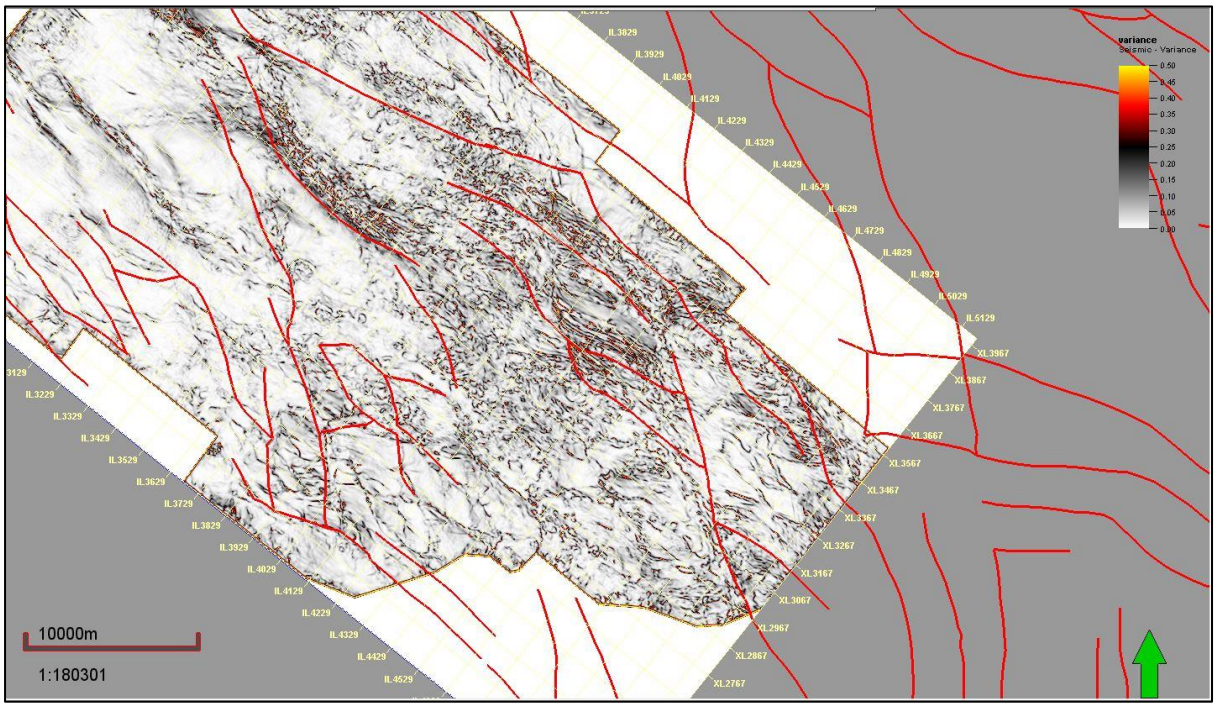

Figure 16. Combination of fault distribution of DGM 2.0 map and variance attribute for Base Altena level.

4 Results

4.1. Seismic Interpretation

As mentioned in the previous chapter, two different domains of 3D seismic data (PSDM and Post-Stack Time Migration) are utilized in this phase. Therefore, a different workflow is applied to each dataset. For time domain data the interpretation is done firstly in the time domain and will be converted into depth domain later. A more direct interpretation is performed for depth domain data, as no time-depth conversion is required and could directly yield the mapped horizons for each reservoir level in depth domain. Most of the interpretation is performed in 3D PSDM data and only the northeastern part of the area is done in 3D Post-Stack Time Migration data.

All of the processes are performed in Petrel 2014 software. A more detailed information about the interpretation for each 3D seismic dataset will be explained in below sub-chapters. In general, the interpretation steps for each dataset are illustrated in the figure below.

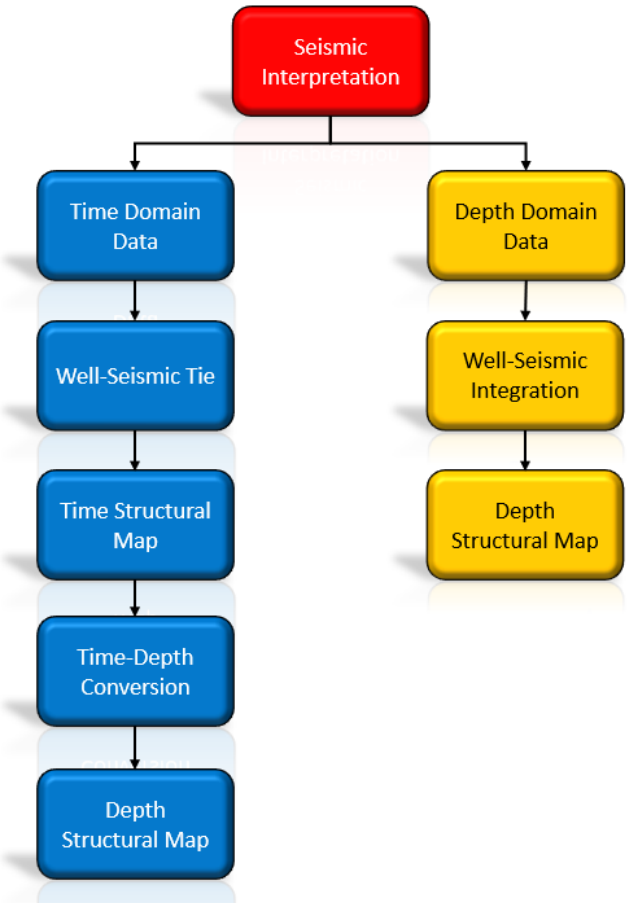

Figure 17. The general workflow of seismic interpretation phase for two different domain seismic data.

4.1.1. Well and Seismic Data Integration

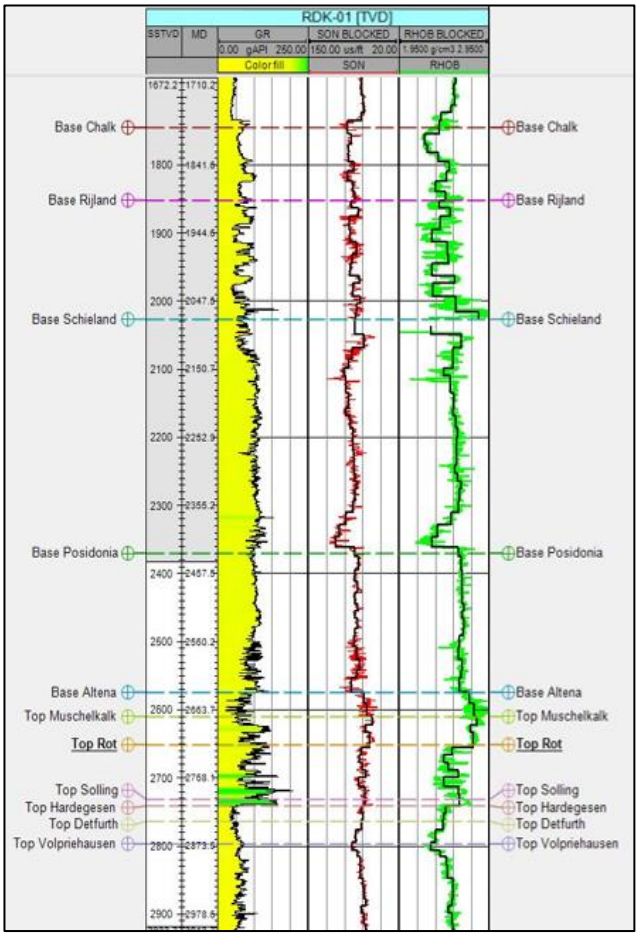

Figure 18. Well logs example from RDK-01 well. The reflectivity response is estimated from sonic and density logs. Note that Base Altena (Top Triassic) is characterized by hard kick response as sonic and density logs increase from the above formation.

The first step in the seismic interpretation phase is integrating the well and seismic data.

In seismic with time domain dataset, a domain conversion for the well data is required. The well data contains important information such as well tops and well logs which are the primary information for seismic interpretation. Since the seismic data is in the time domain, thus the well data should be converted from depth to time domain by applying checkshots data.

The next step is creating a synthetic seismogram for each well. This is done by convolving a wavelet and reflectivity series in each well. The reflectivity series is firstly should be investigated before the well-seismic tie process. It represents a difference in acoustic nature for each formation which can be estimated from sonic and density logs in each well (Figure 18).

The summary of the reflectivity response for each formation is presented in Table.1. The subdivision of each target is created in regard to its base formation. For the top of the Triassic successions, it is represented by the Base Altena (Table.1) as it directly overlain by the Altena group in the study area. Based on the logs response, the Base Altena is characterized by a hard kick reflectivity. This is logical as this illustrated by an increase of density and sonic logs due to a gradual change from sandy lithology of the Sleen Formation to Anhydritic claystone of the Keuper Formation (Figure 18).

Table 1. The Summary of reflectivity response.

Target	Reflectivity Response	Quality
Base NSG	Hard Kick	Excellent
Base Chalk	Soft Kick	Excellent
Base Rijland	Soft Kick	Moderate
Base Schieland	Hard Kick-Soft Kick (where Brabant fm absence)	Excellent
Base Posidonia	Hard Kick	Excellent
Base Altena	Hard Kick	Excellent

Butterworth wavelet is chosen during this well-seismic tie process as it gives the most representable synthetic seismogram. As the non-SEG display is applied for this phase, therefore the inverted type of that wavelet is chosen. The example of the well and seismic matching process is presented in Figure 19. The result from the other well can be seen in Appendix B.2.

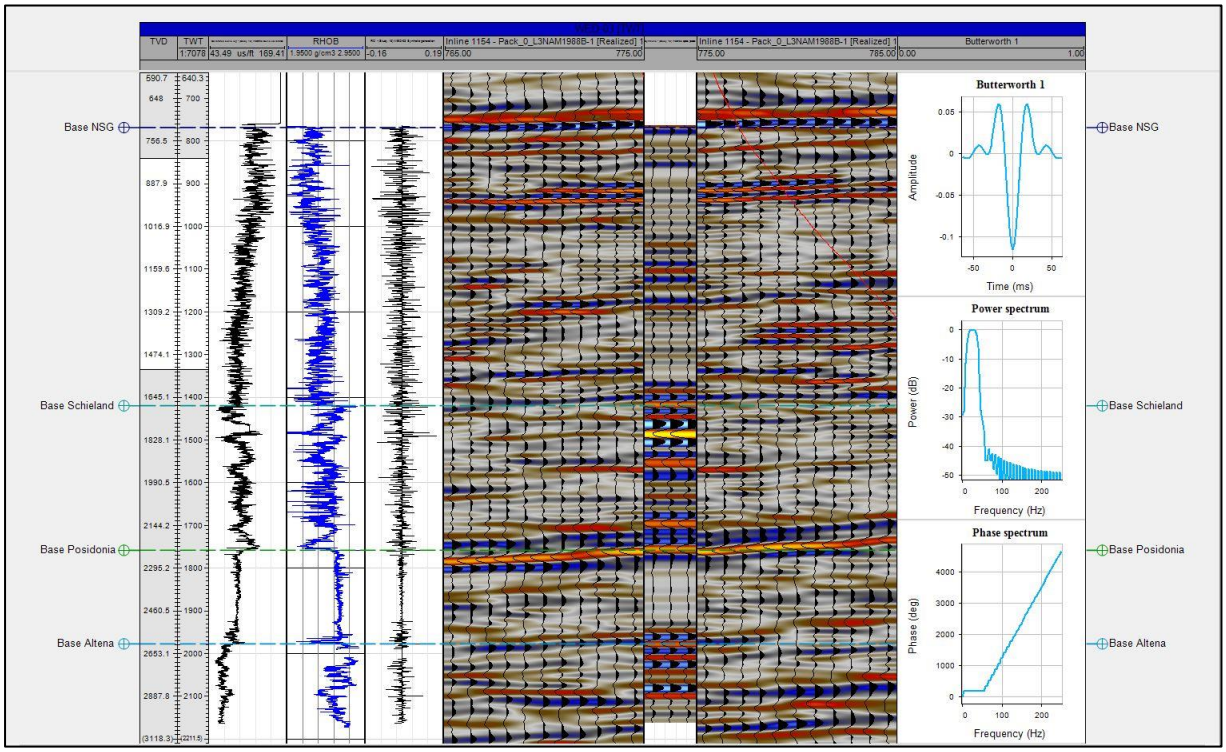

Figure 19. The well seismic tie for WED-03 well.

Unlike the process in the time domain, the well and seismic integration in depth domain data is done without creating a synthetic seismogram as both of the data are already in the depth domain. Overall, the well tops from each well are already located on the desired reflector. A good alignment between seismic and well tops is observed through the entire area as can be seen in Figure 20.

However, manual quality control still has to be performed to inspect whether the well top is matched with its reflectivity response for a certain level, as summarized in Table.1. Thus, a correction can be made before the interpretation to avoid a misinterpreted horizon.

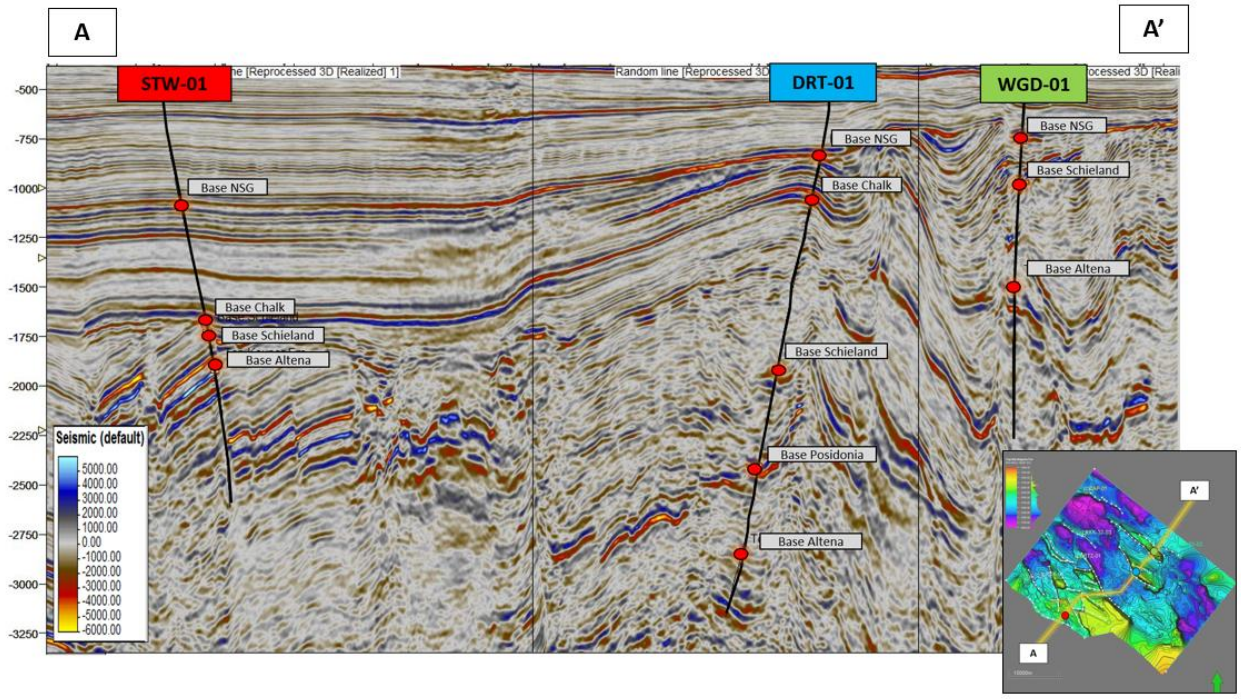

Figure 20. Seismic cross-section from 3D PSDM data shows good alignment between well tops and target reflector.

4.1.2. Horizon and Fault Interpretation

In this phase, six formation targets in Table.1 and fault distribution within the research area are interpreted. Some additional data such as horizon and fault maps from of Digital Geological Model (DGM) from the nlog.nl site are also used for comparison.

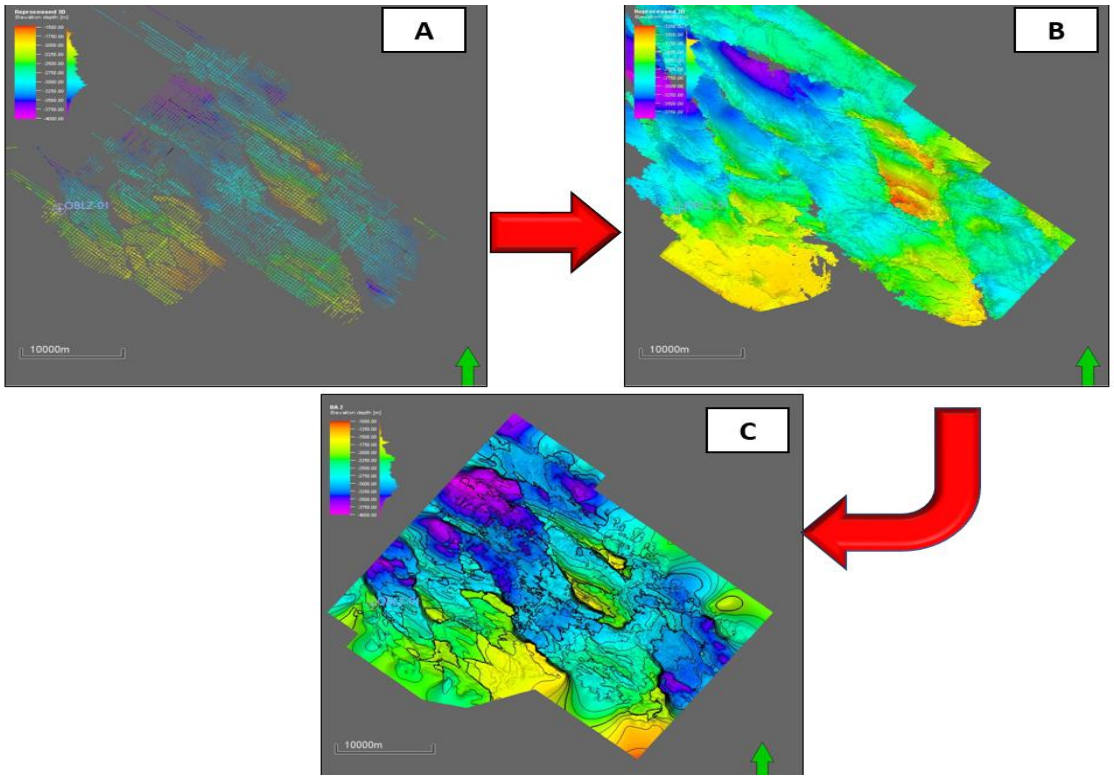

Figure 21. Horizon interpretation steps. Start from (A) 2D interpretation with Xline and Inline trends, (B) 3D guided autotracking and (C) Surface attribute using the result from B.

In the horizon interpretation part, although the target of this study is aiming for the Triassic level, the other five horizons in Table.1 are still interpreted to observe the structural features in the area and act as a reference point for interpretation. During the process, horizon interpretation is mainly performed in every 16th increment for both types of data. Tighter increments can also be applied in some parts of the area in which some irregularities of reflector might be found.

Firstly, several composite lines which intersect the available wells are created and interpreted to give an initial anchor point for each target formation (Figure 21). Next, the interpretation continues by following Xline and Inline trends with the mentioned increment. The interpretation is completed by applying the guided autotracking to fill in space in between interpretation (Figure 21).

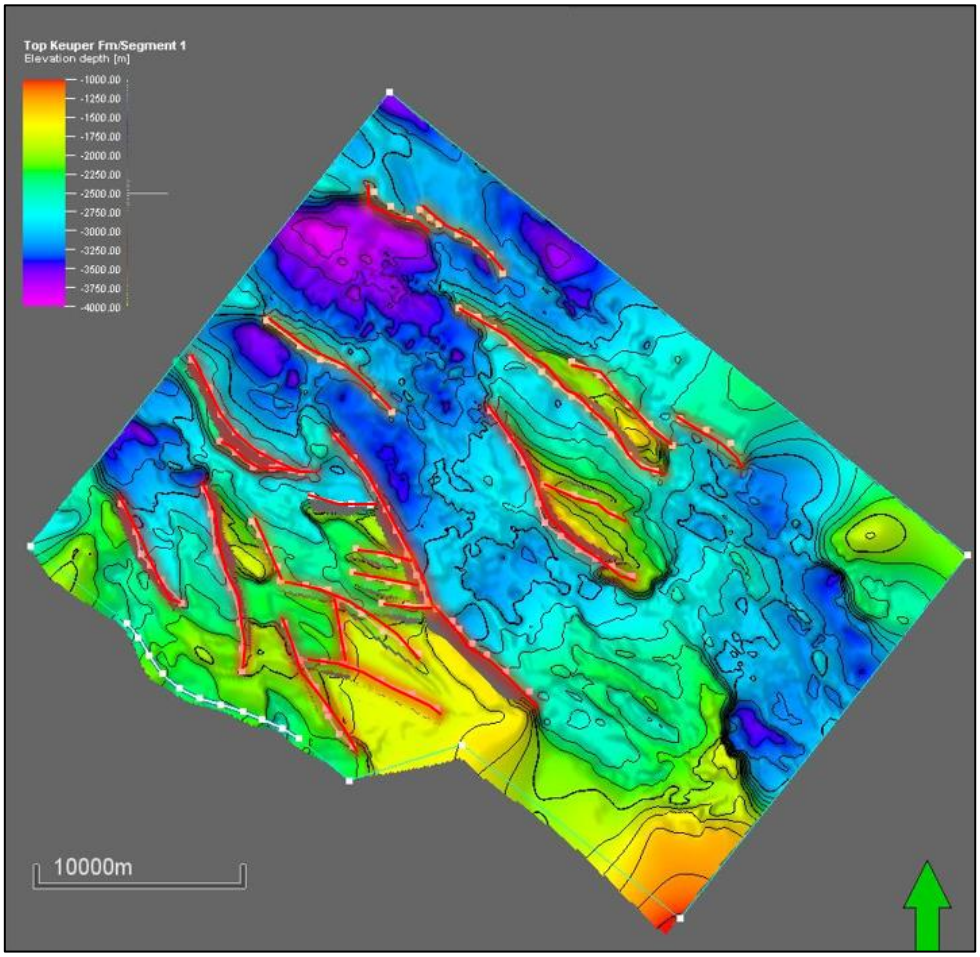

Figure 22. Fault distribution within the research area.

In general, the seismic expression at the shallower depth (Base NSG to Base Schieland) gives more clear amplitude response than the deeper part of seismic. As a result, the interpretation on that level can be traced in more certainty. The top of the Triassic successions (Base Altena) is still can be traced in some parts of the area despite its position in deeper level of the subsurface.

However, the individual formation within the Triassic successions is not clearly visible in most part of the area. This response might be influenced by the evaporitic succession in the upper part. Thus, the interpretation on that levels will be completed by using the isopach maps which are generated from the well tops with Base Altena horizon as a reference.

During the fault interpretation part, the regional fault map of the Triassic level is utilized in combination with the variance attribute. The faults are characterized by a clear discontinuity in one or multiple horizons. The study area is characterized by NW-SE major faults trending in which dissected the WNB into the half-graben structure as a response to the rifting process during the Cretaceous. Figure 22 shows the fault distribution within the Drechtsteden area. As can be seen, the faults divide the area into three compartments in which the Triassic level sits deeper in the middle section.

Pronounced syn-rift and inversion features such as half-graben structures and reactivation of the existing fault can be seen in some parts of the area. An NW-SE seismic cross-section (Figure 23) shows some tectonic overprints which occurred in the area. Bounding faults are observed with some existing fault being reactivated during the inversion phase. The reactivation of the existing fault can be recognized by a different pattern at the top and bottom part of the individual existing fault, which shows both a normal offset and reverse offset respectively. Series of flower structures are observed in the Cretaceous level. This might be formed as a response of maximum compressive stress during the inversion phase was generally not at the right angle which resulted in transpressional movement (De Jager, 2003).

In the Triassic level, mostly the NW-SE trend of existing faults are observed (Figure 23). These faults are probably already established during the Silurian to Early Devonian Age (De Jager, 2003). Some of the faults were reactivated during the syn-rift regime in which affected thickness distribution of the Triassic successions throughout the research area.

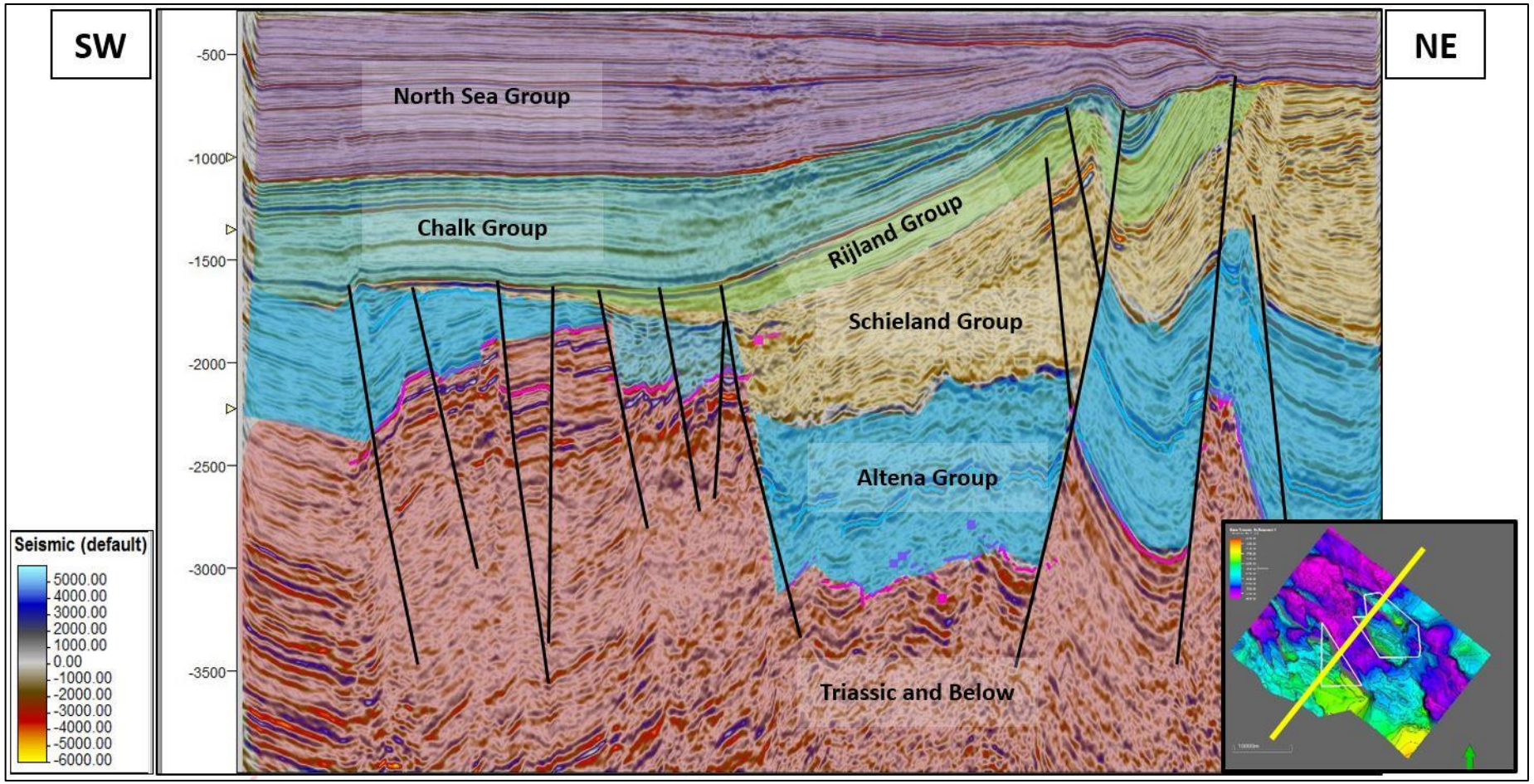

Figure 23. SW-NE (IL 4166) seismic cross-section of the study area with the interpreted horizons and faults.

4.1.3. Depth and Thickness Maps of Targeted Reservoir

In this part, the interpreted horizons and faults of the previous sub-chapter will be used to create depth maps of the target formation. First, the interpreted horizon is transformed from horizon attribute to surface attribute before it is merged with the interpreted fault. For the depth domain dataset, the interpreted horizons and faults can be transformed directly into the surface depth attribute. As the interpretation is also performed in the time domain dataset, hence a time depth conversion for this dataset is required.

The time depth conversion is performed by firstly estimating the interval velocity for each target zone. In this study, a layer cake model is used, and the intervals are set from the mean sea level to Base Posidonia and Base Posidonia to Base Altena. The interval velocity can be calculated by using the below equation:

$$V_{int} = 2 * \frac{Z_{top} - Z_{base}}{TWT_{top} - TWT_{bottom}} \quad (1)$$

The result of the interval velocity calculation is presented in Table.2. Mostly, the estimated difference in TVD depth for each top formation is below 30 m. This difference might be due to variation in depth and time of corresponding top formation as the area is characterized by several faults with big displacement.

Next, the estimated interval velocity for each zone is used to create a velocity model to convert the horizon and fault interpretation from time to depth domain. In order to correct the result in well locations, well tops adjustment is also used during the process. The result of the time to depth conversion is shown in Table.3. The time and depth structural maps for the Triassic level are presented in Figure 24 and 25.

Table 2. Interval velocity calculation for each target formation.

Interval 1	Mean Sea Level to Base Posidonia										
Wellname	TWT top interval	TWT base interval	TVD top interval	TVD base interval	Delta TWT	Delta TVDepth	Calculated Vint	Calculated Thickness	Difference in thickness	Calculated TVDepth	Difference in TVDepth
	[s]	[s]	[m]	[m]	[s]	[m]	[m/s]	[m]	[m]	[m]	[m]
BRAK-00	0.0000	1.4360	0.000	-1790.080	1.436	1790.0800	2493.1	1803.616	13.5	1803.6	13.5
WED-03	0.0000	1.7578	0.000	-2226.85	1.758	2226.8500	2533.6	2207.834	-19.0	2207.8	-19.0

Final choice Vint: 2512.0

Interval 2	Base Posidonia to Base Altena										
Wellname	TWT top interval	TWT base interval	TVD top interval	TVD base interval	Delta TWT	Delta TVDepth	Calculated Vint	Calculated Thickness	Difference in thickness	Calculated TVDepth	Difference in TVDepth
	[s]	[s]	[m]	[m]	[s]	[m]	[m/s]	[m]	[m]	[m]	[m]
BRAK-01	1.4360	1.6423	-1790.08	-2117.13	0.206	327.1	3170.6	339.6	12.5	2143.2	26.1
WED-03	1.7578	1.9770	-2226.85	-2601.07	0.219	374.2	3414.7	360.8	-13.4	2568.6	-32.5

Final choice Vint: 3292.0

Table 3 The result of time-depth conversion with well tops adjustment.

BP TIME	Well	X-value	Y-value	Z-value	Horizon after	Diff after	Corrected?	Information
	WED-03	117408.8	423041.8	-2226.85	-2226.85	-0.00	Yes	
	BRAK-01	131758.0	423216.0	-1790.98	-1790.98	0.00	Yes	
BA TIME	Well	X-value	Y-value	Z-value	Horizon after	Diff after	Corrected?	Information
	WED-03	117460.5	423109.3	-2601.07	-2601.07	-0.00	Yes	
	NDK-01	122048.6	423367.0	-2275.48	-2275.48	0.00	Yes	
	BRAK-01	131698.9	423054.9	-2117.13	-2117.13	-0.00	Yes	

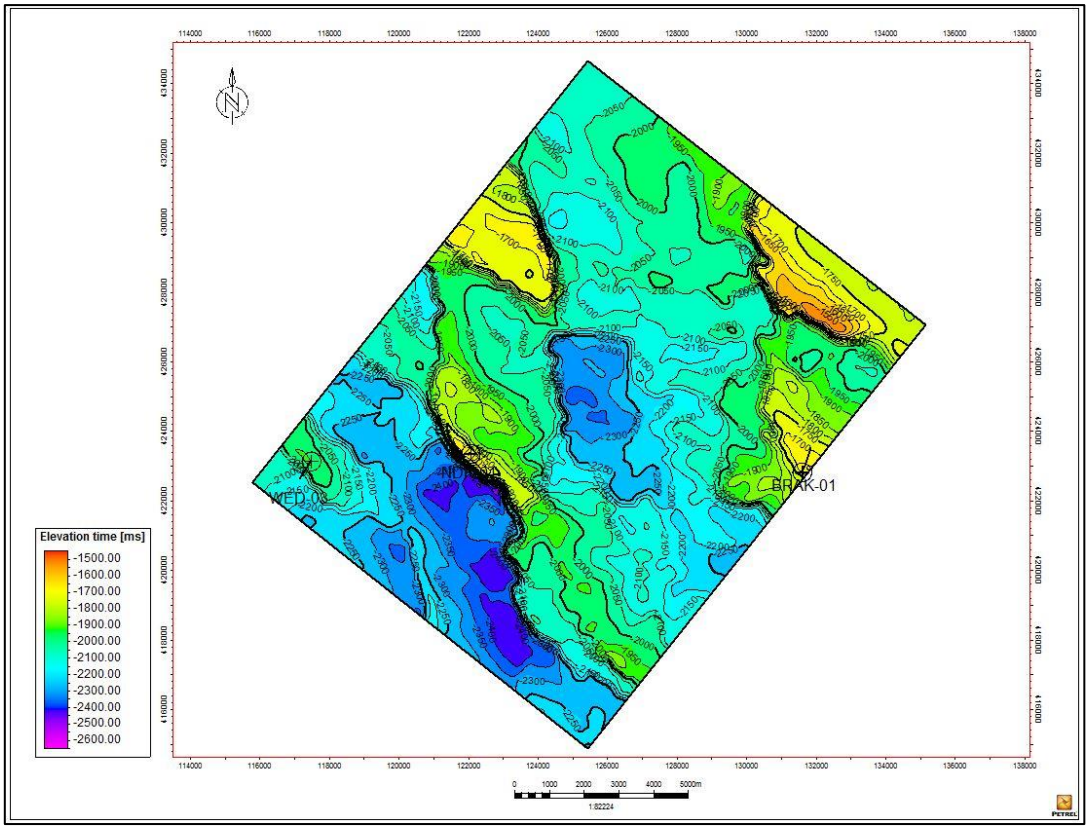

Figure 24. Time structural map of Base Altena (Top Triassic).

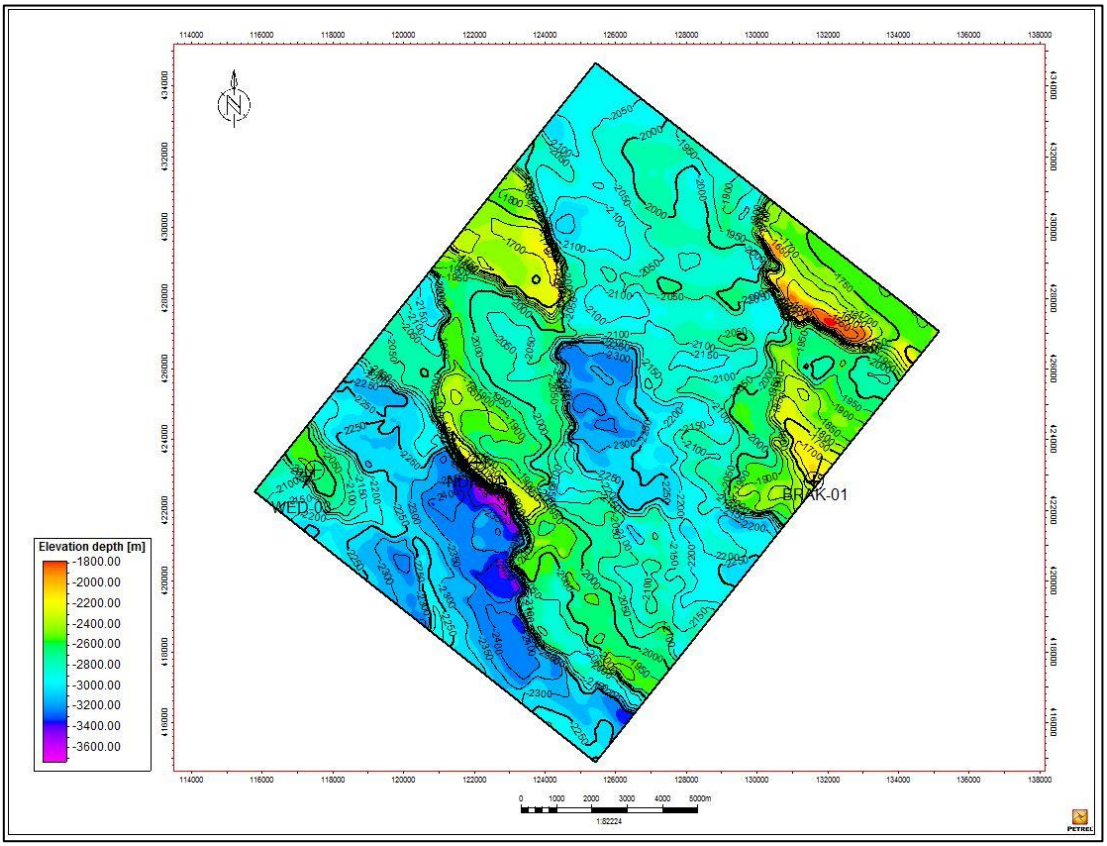

Figure 25. Depth structural map of Base Altena (Top Triassic).

As mentioned in the previous sub-chapter, the individual formations within the Triassic succession will be generated by utilizing isopach maps from the well tops. Based on these maps, a rough estimation of the thickness distribution of each formation within the Triassic successions can be investigated and might also suggest the source of sediment direction. The isopach maps for the Keuper, Röt, Hardegsen, Detfurth and Volpriehausen Formation are shown in Figure 26-30. Note that the well symbols which used here refer to their bottom hole location. The generated isopach maps show a different trend of thickness distribution for each Formation.

The Keuper Formation was formed as the upper boundary of the Triassic successions. It has varied thickness distribution based on its isopach map (Figure 26), ranging from 0 to 80 m. As stated in Chapter 2, this might indicate the impact of the Early Kimmerian rifting which occurred during its deposition. The rifting episode was identified to cause a pronounced uplift in the area of the WNB where erosion cut deeply into the Muschelkalk or even Röt Formation (Geluk et al., 1996). As a consequence, this formation is absent in some parts of the WNB and one of them can be seen within the study area.

A gradual change in thickness is observed in the Röt Formation isopach map (Figure 27). Based on the map, a NW to SE thickening trend is observed which might indicate the source of sediment from the RVG in the SE part of the study area (Geluk et al., 1996). The thickness is ranging from 60 to 130 m. The Röt Formation is composed of a clastic and evaporitic part in majority area of the Netherlands. However, in the WNB area, only the clastic part is identified while the evaporitic part is absent (Geluk, 2007). Thus, it suggests a promising sandstone interval to be evaluated for geothermal reservoir target.

The Hardegsen Formation has the most significant difference in thickness based on its isopach map (Figure 28). Its thickness is relatively thin with the average around 20 m. In some areas, this Formation is absent which might suggest the result of erosion during the deposition of the Solling Formation. Apart from its variation in thickness, this formation is observed as a sandstone prone interval and therefore it is an option to be evaluated.

The isopach map of the Detfurth Formation shows a significant decrease in thickness at the centre of the study area (Figure 29). This might represent the uplift period which occurred before the deposition of the Hardegsen Formation. Overall, the thickest zone is located at the northeastern part of the study area. The thickness ranges from 15-40 m in the centre of the study area and up to 65 m in the northeastern part. The Volpriehausen Formation shows the thickest interval among the others (Figure 30). The thickness ranges from 70 to 140 m in the study area. Based on the generated isopach map, it can be seen that the thickest zone is located in the southwestern part of the area.

At the end of the seismic interpretation step, the generated isopach maps and Base Altena surface are used as input for creating a depth map of each formation within the Triassic successions. The depth maps for the Keuper, Röt, Hardegsen, Detfurth and Volpriehausen Formation are presented in Figure 31-35. The result for the other formations can be found in the Appendix C.2. Note that the well symbols which used here refer to their bottom hole location.

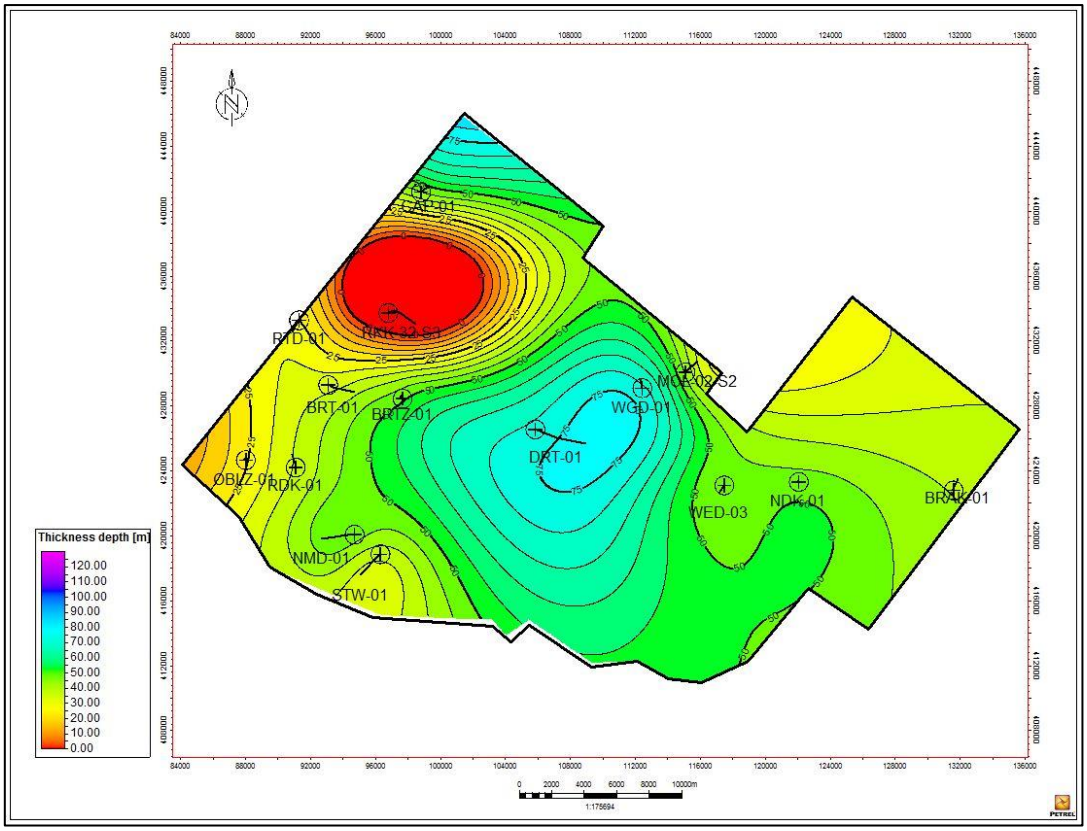

Figure 26. Isopach map of the Keuper Formation.

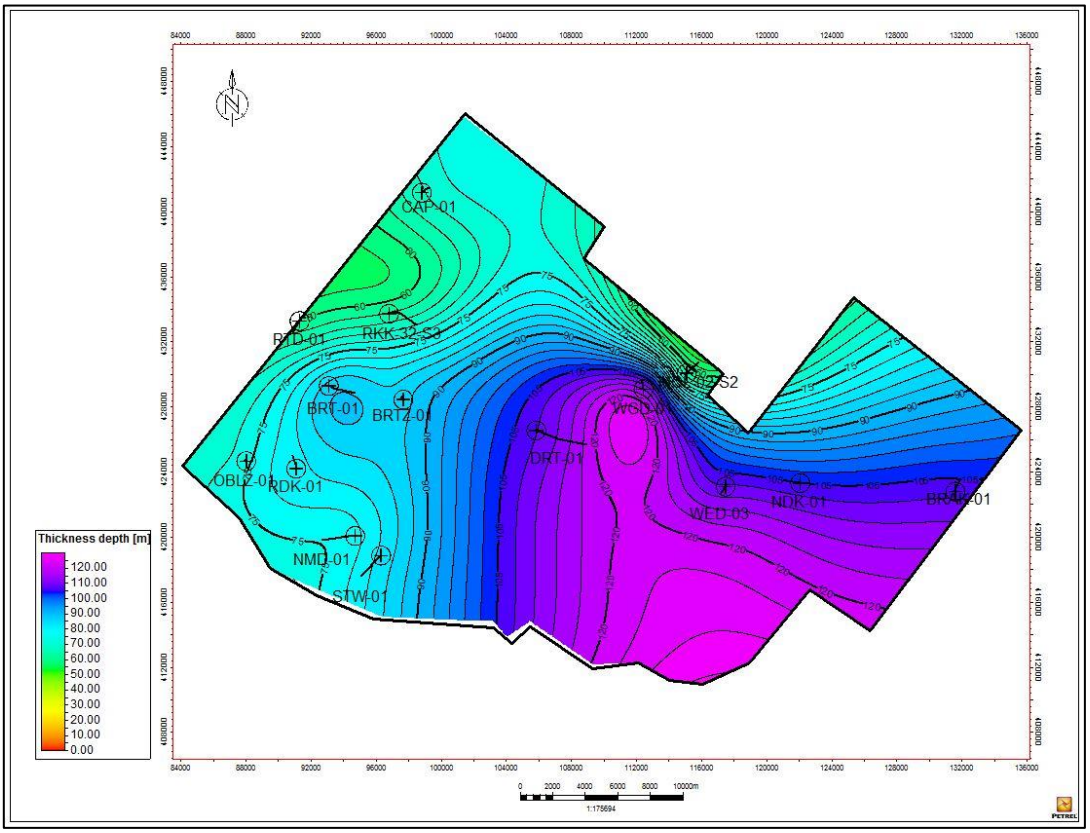

Figure 27. Isopach map of the Röt Formation.

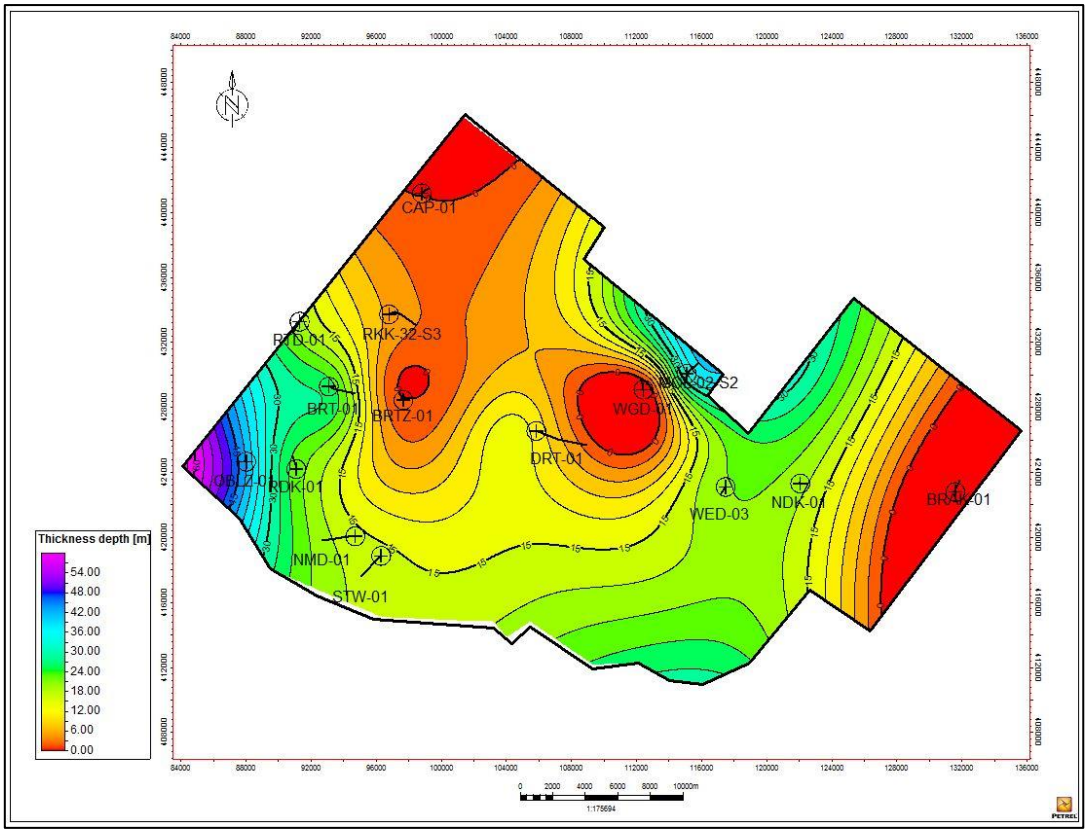

Figure 28. Isopach map of the Hardegsen Formation.

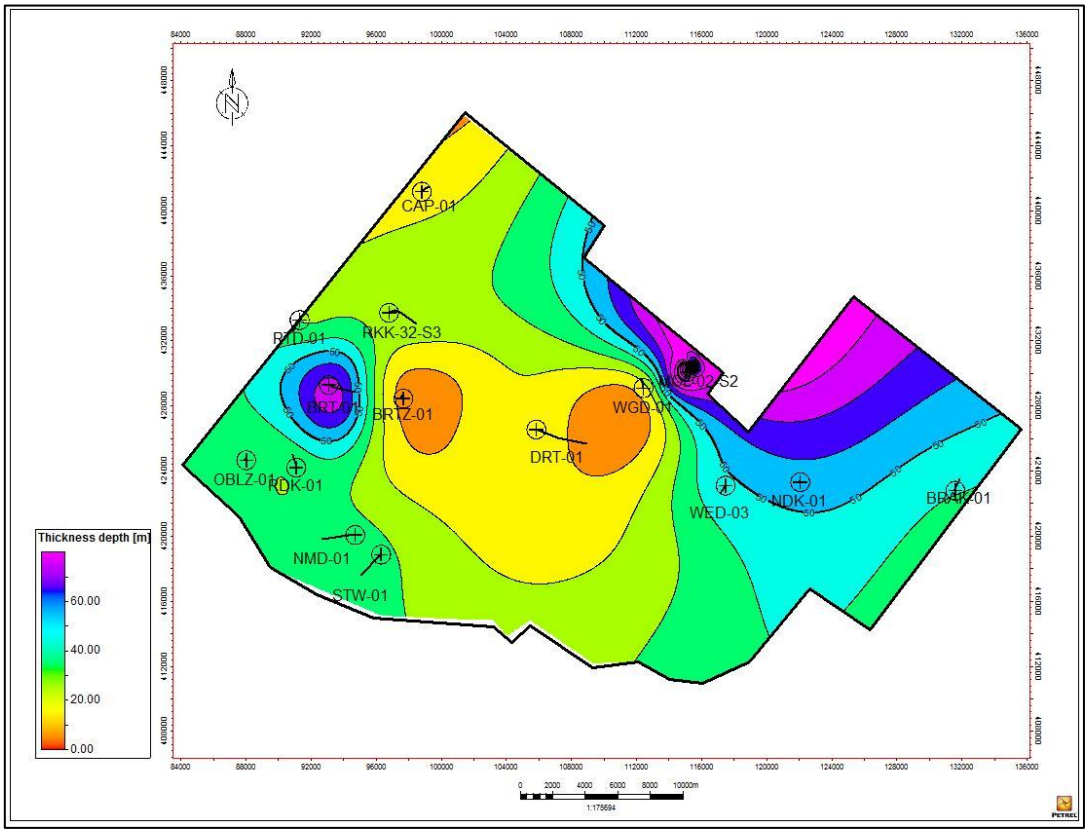

Figure 29. Isopach map of the Detfurth Formation.

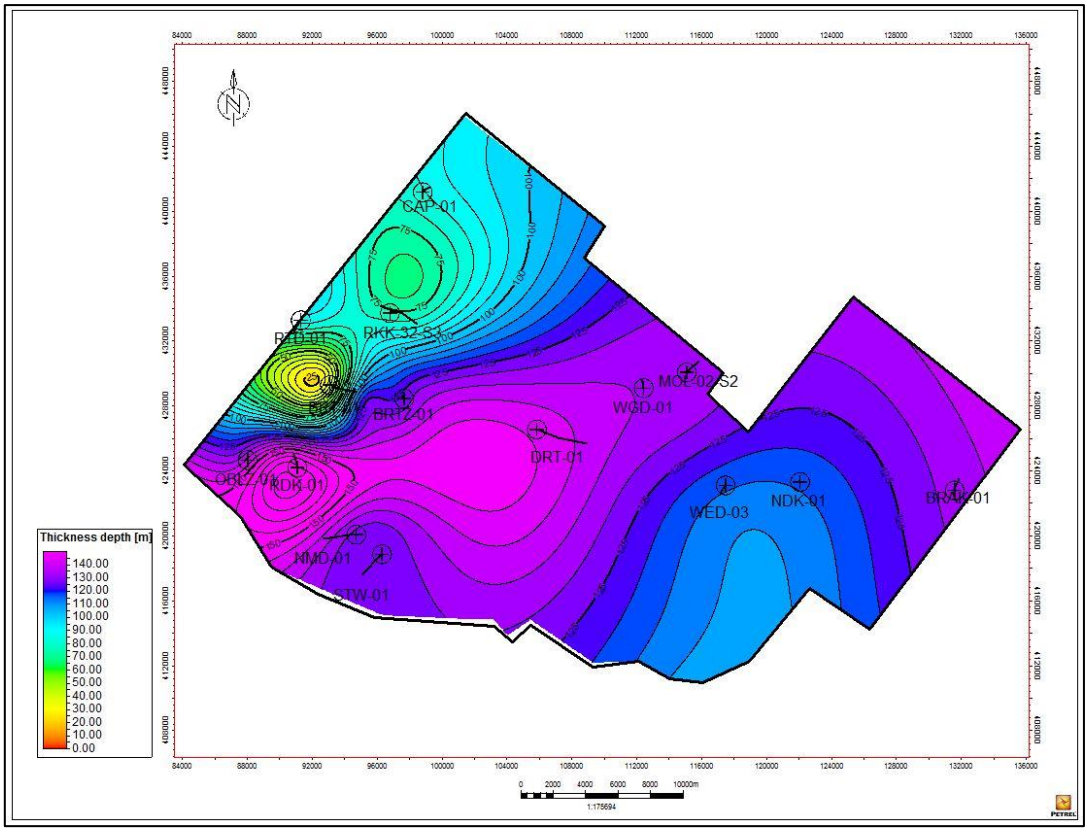

Figure 30. Isopach map of the Volpriehausen Formation.

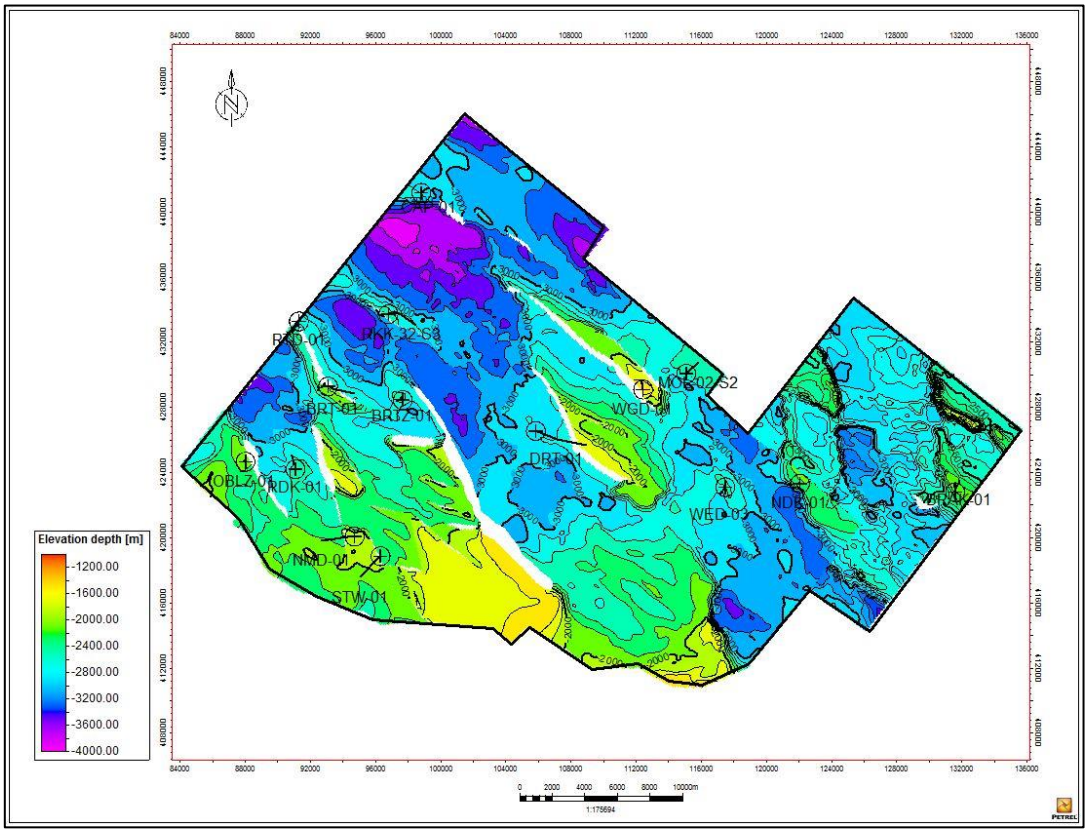

Figure 31. Isopach map of the Hardegsen Formation.

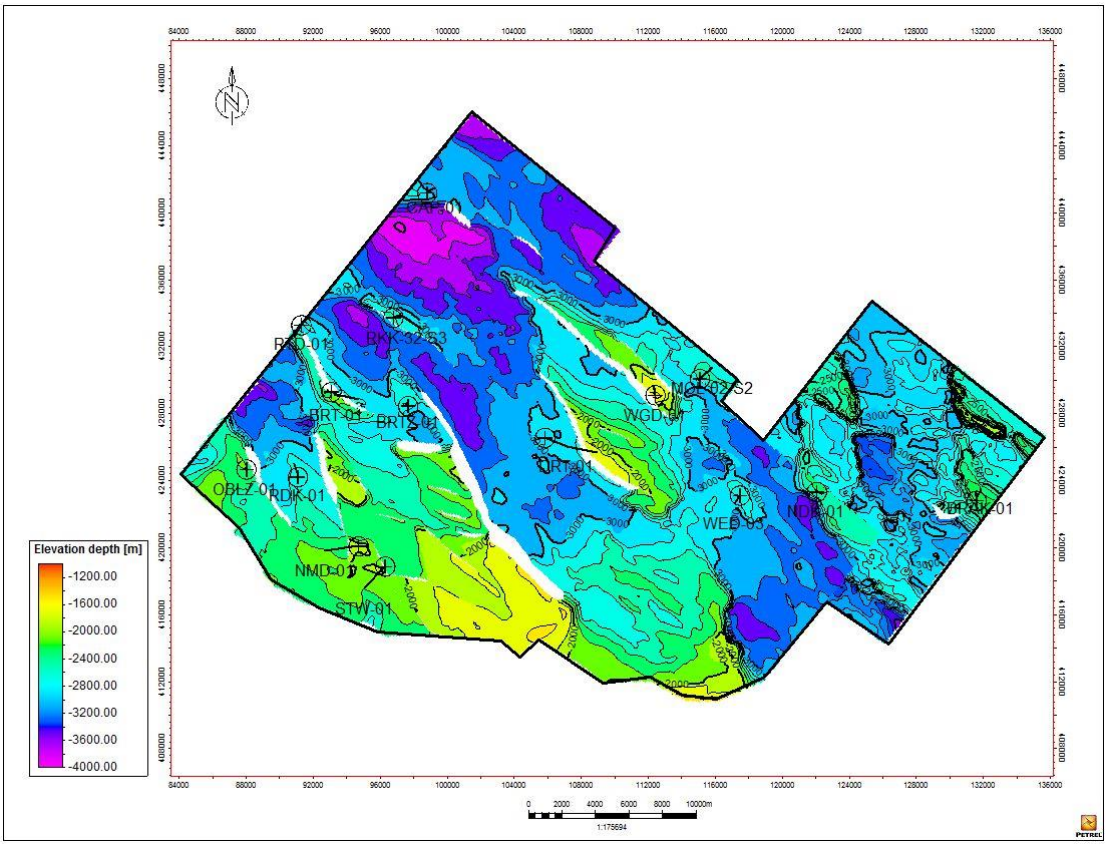

Figure 32. The depth map of the Röt Formation.

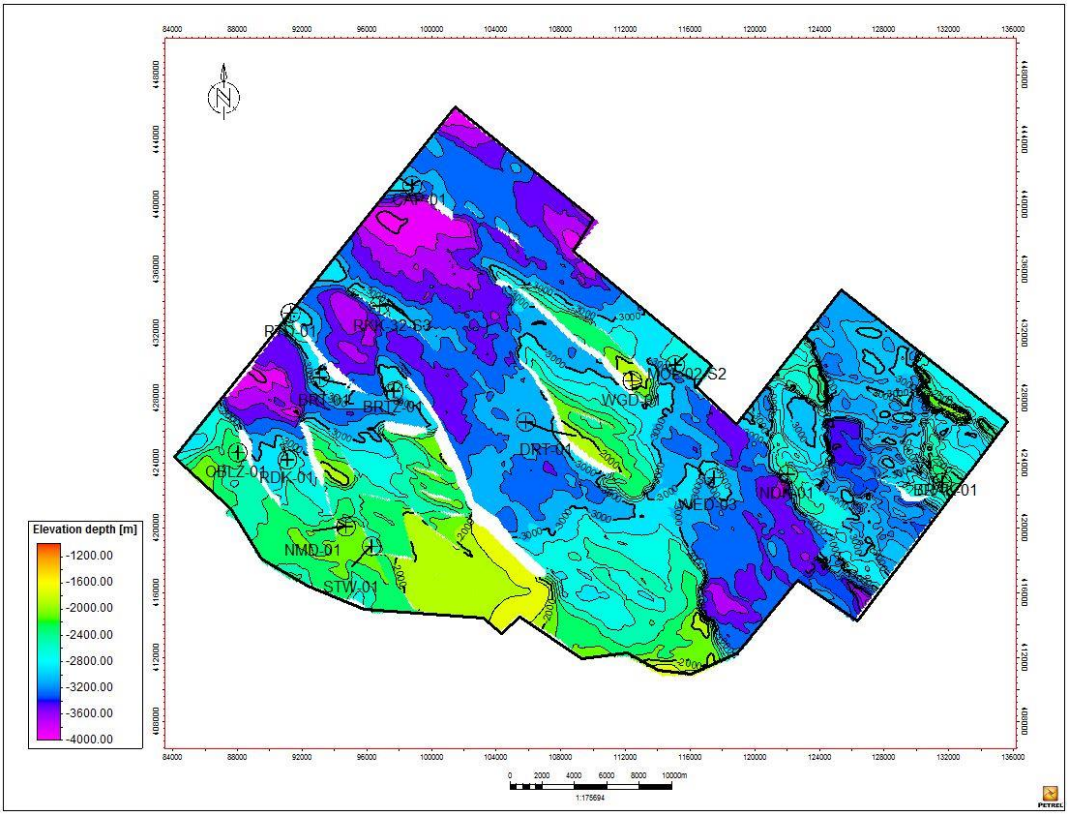

Figure 33. The depth map of the Hardegsen Formation

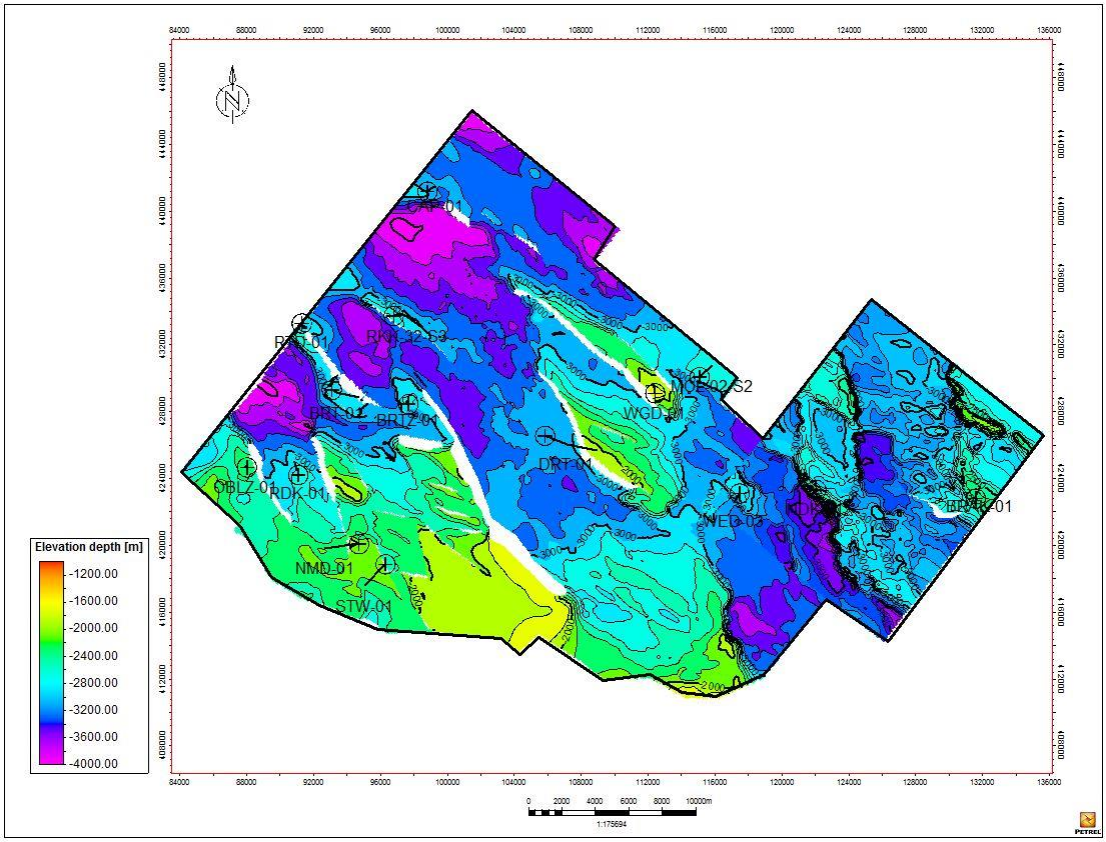

Figure 34. The depth map of the Detfurth Formation.

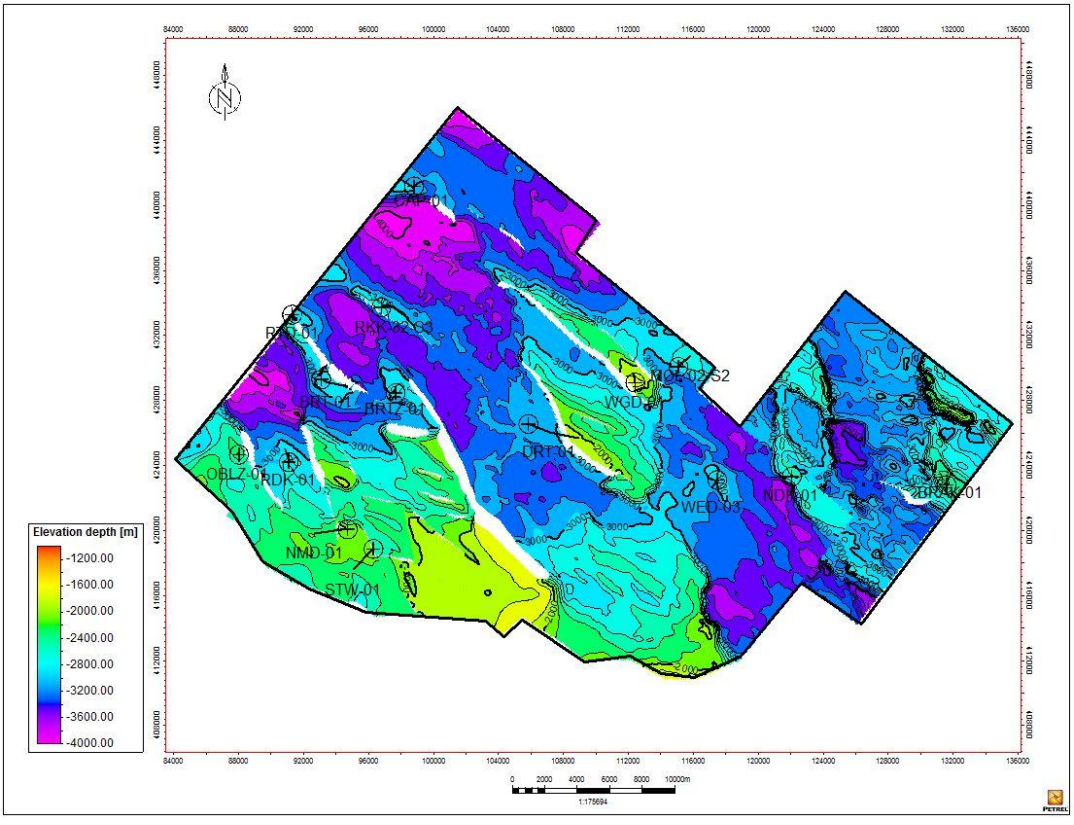

Figure 35. The depth map of the Volpriehausen Formation.

4.2. Reservoir Sedimentology

In this part, a sedimentological analysis is conducted on the selected core data in the research area. As stated in Chapter three, there are 10 wells in which the core data is available. However, due to time limitations, a selection of core data must be made based on the criteria as listed below:

- Covering the reservoir target;
- Good reservoir properties (Porosity and Permeability); and
- Good recovery.

Core data from the Röt and Hardegsen intervals of wells OBLZ-01 and WGD-01 are selected to be evaluated in this part. All of the core data are stored at NAM Core Laboratory in Assen. The core database within the study area is presented in Appendix D.1. The sedimentological analysis consists of several steps. First, a core description is performed manually by hand in the scale of 1:50. Next, the result will be used to generate a lithofacies classification and interpreted depositional environment. In the end, several correlation panels are constructed to evaluate the sandstone connectivity, size, and distribution within the described interval. More detailed explanation of the analysis will be discussed in several sub-chapters below.

4.2.1. Lithofacies Classification

The core description for both the Röt and Hardegsen intervals from the OBLZ-01 and WGD-01 are used as the main input to determine lithofacies grouping in this part. The grouping is made based on the observed lithologies, sedimentary structures, and grain size variation. In total, there are five lithofacies can be generated from the selected core interval. The terminology and method in this part are adopted from the NAM sedimentological report. The result of lithofacies determination are listed and explained below:

- **Mudstone (M)**

This lithofacies consists of the claystone dominated interval in which more than 50% of clay content is encountered. Some mm-scale of very-fine grained sandstones are interbedded in the interval. In the most of cored interval, this lithofacies is observed to be homogeneous with some horizontal to wavy bedding structures.

- **Wavy Stratification Sandstone (Sw)**

In this group, a very-fine to medium grain size of sandstone with a well-developed wavy structure is observed. In some parts, this lithofacies is bounded and admixed with the silt layer. This lithofacies can be found in all of the selected core intervals in both of OBLZ-01 and WGD-01 well.

- **Well Stratified Fine-Grained Sandstone (Ssf)**

This lithofacies predominantly consists of fine-grained sandstone with well-developed stratification. The observed stratifications are horizontal and sub-horizontal lamination. In some parts, a planar cross bedding with low angle stratification also presents in the succession.

- **Well Stratified Medium-Grained Sandstone (Ssm)**

This lithofacies differs from the previous group in respect of grain size. Mainly consist of medium grain size sandstone with some horizontal to sub-horizontal stratification structures such as parallel lamination, planar and through cross-bedding are observed. This lithofacies can be found quite abundant in both core data of OBLZ-01 and WGD-01 well.

- **Non-Stratified Sandstone (Ssn)**

It is composed of very fine to medium grain size of sandstone in which no visible structure is observed. Characterized by a homogeneous and massive interval of sandstone with some clay pebbles are admixed in the succession.

After lithofacies grouping is created, a more general classification of lithofacies is made. Lithofacies association term is used for this grouping which consists of several lithofacies. This is done with the objective to interpret the depositional environment based on its association with specific lithofacies. In general, there are two subdivisions can be made based on the dominated lithological unit. The list of lithofacies association are explained below:

Mudstone Dominated Sequence

- Mudstone (M)

This lithofacies association is composed of Mudstone lithofacies (M) as the main member. It has some supported lithofacies of Well Stratified Fine-Grained Sandstone (Ssf) and Wavy Stratification Sandstone (Sw) with very-fine to fine grain size.

This lithofacies association might indicate a lake to lake margin environment with some sheet flood deposits are admixed, as it consists of claystone with very-fine to fine-grained sandstones. In the case where a thick claystone interval is encountered, a lake environment is more pronounced. Whilst, the presence of thin sandstone interval might suggest a sheet flood deposit.

Sandstone Dominated Sequence

- Sandstone-1 (S1)

The Well Stratified Fine-Grained Sandstone (Ssf) lithofacies is the main member of this association. It is supported by Well Stratified Medium-Grained Sandstone (Ssm) and Wavy Stratification Sandstone (Sw) with very-fine to fine grain size. Horizontal stratification structure is common to be found in this class with some low angle stratification types are also observed.

As arid to the semi-arid environment prevailed during the deposition, thus the observed structures might suggest a different type of flow. A horizontal bedding structure could indicate a more unconfined flow such as sheet flood deposit. Whilst, a low to high angle bedding might reflect a deposition by a stream channel.

- Sandstone-2 (S2)

This lithofacies composed of Well Stratified Medium-Grained Sandstone (Ssm) lithofacies as the main member and supported by Well Stratified Fine-Grained Sandstone (Ssf) and Wavy Stratification Sandstone (Sw) with very-fine to fine grain size lithofacies. Horizontal to sub-horizontal bedding and ripple structures are common in this lithofacies association. In general, this lithofacies is bigger in grain size than S-1.

The different grain size could suggest a different position of deposition from the source of sediment. The S-2 with bigger grain size might indicate a relatively more proximal environment while the S-1 is the other way around. The presence of clay pebbles in some parts of the interval also give an information of the stronger type of flow.

4.2.2. Core Analysis of the Röt Formation

Two cored interval from OBLZ-01 and WGD-01 well are subjected to core analysis in this part. Both of the core data cover the Röt Formation but within a different member. The first core from OBLZ-01 well covers the Upper Fringe Claystone Röt Member while the core from WGD-01 well was taken from the Röt Sandstone Member.

Core No.1 (2202-2220.44 mAH) of OBLZ-01 Well

This cored interval was taken from the upper part of The Röt Formation which is the Upper Fringe Claystone Röt Member. The core mainly consists of grey to buff sandstone layers with very fine to medium grain size. The thickness varies from cm to m in vertical scale. In some parts, the sandy layer is interbedded with mm to cm claystone layer and marked by a sharp boundary (Figure 36.B). Clay pebbles are quite abundant to be found at the bottom part of the sandy interval and usually have a wavy boundary. The N/G ratio is 0.85. Sedimentary structures such as parallel lamination, planar to through crossbedding (Figure 36.A) and current ripple are common in the cored interval. The detailed description of this core interval is presented in Appendix D.2.

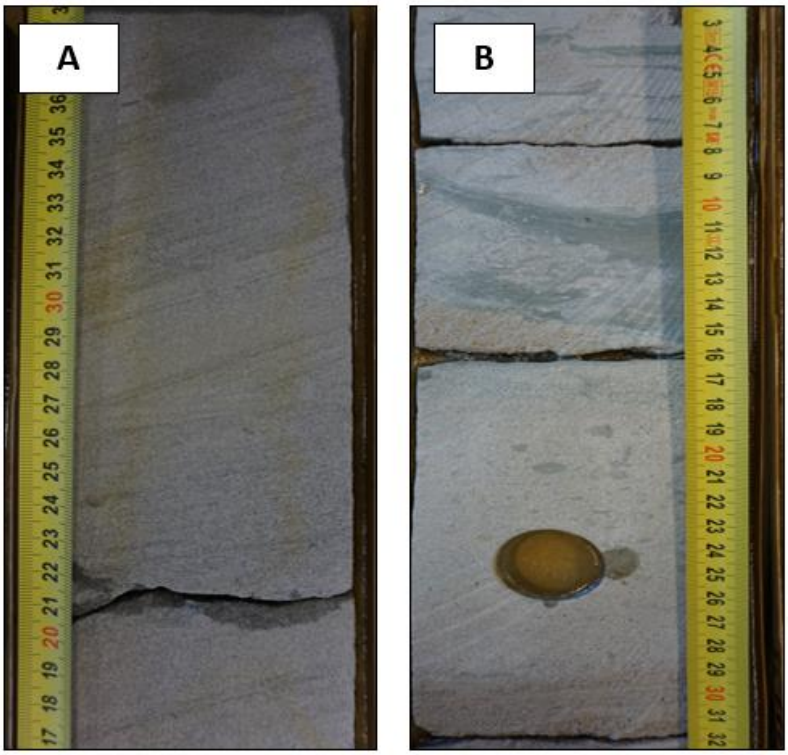

Figure 36. Some of the observed sedimentary structures in Core No.1 of OBLZ-01 well. (A) A planar crossbedding shows some inclination in lamination at 2213-2212.50 m. (B) The sharp boundary between silty and sandy layer at 2215-2214 m.

Core No.1 (1746.65-1775.15 mAH) of WGD-01

This 28.05 m long core sample was taken from the Röt Sandstone Member. The interval predominantly consists of buff to brownish very fine to medium upper grained sandstone with some intercalations of mm to cm silty layer. The N/G ratio is 0.92, which is higher than the previous core. Clay pebbles are observed in the most of sandy layers and bounded by an irregular boundary (Figure 37.A). Various sedimentary structures such as planar-through crossbedding (Figure 37.B), climbing ripple and parallel lamination are present. The complete description of this cored interval is presented in Appendix D.4.

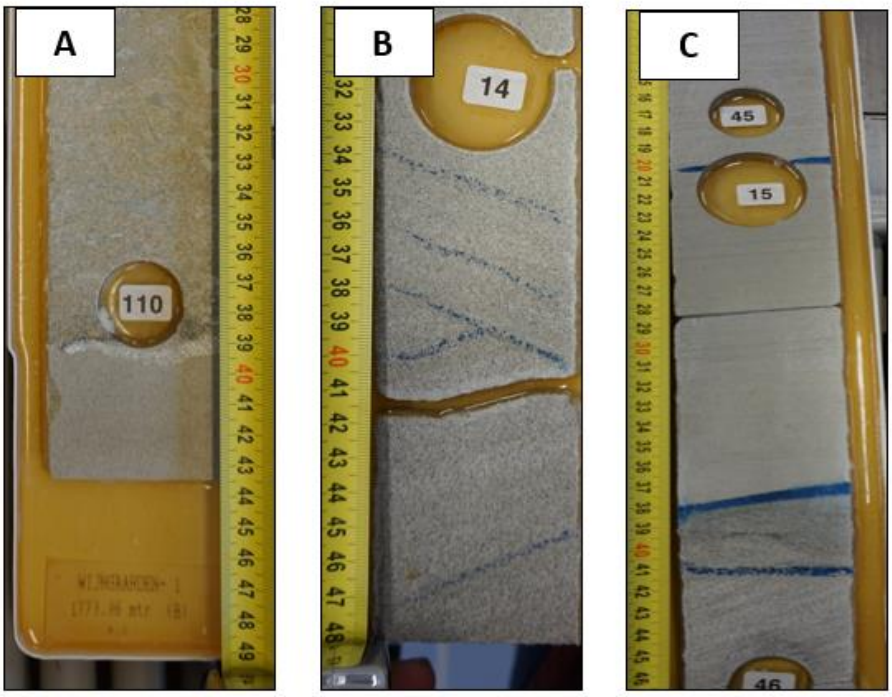

Figure 37. (A) A wavy boundary with clay pebbles at 1773-1773.30 m. (B) A through crossbedding set at 1751.80-1752 m, and (C) alternation of finer and coarser sandy layer with a sharp boundary at 1752.80-1753 m.

Lithofacies Association Interpretation

Lithofacies association interpretation is performed on the basis of the grain size and sedimentary structure variation. Overall, both of the core data show several alternation series of S1 and S2 lithofacies with some M lithofacies in between (Figure 38.C and 39.C). This lithofacies interpretation is also linked with the gamma-ray response to be correlated with the non-cored wells later. The A/S (accommodation space versus sediment supply) ratio is used in this analysis as it represents the change in relative base level and sediment supply. The A/S ratio is denoted in the triangle in which the high ratio is shown by a pointing up triangle and increase of gamma ray. A low A/S ratio is marked by a triangle pointing downward.

Lithofacies association S1 can be recognized in the most part of the cored interval from both wells and characterized by an intercalation of fine-medium grained sandstone layer and very fine-fine sandstone or silty layer within a 15-20 cm package. A sedimentary structure such as parallel lamination is commonly observed within this interval. This depositional couplets can be interpreted as a characteristic of sheetflood deposit, in which a coarser sandy layer is overlain by a finer sandstone or silty layer due to the variation of water level (Nichols, 2009). It is supported by the presence of parallel bedding structure which suggests an unconfined flow type that usually occurs in a sheetflood deposit. Based on the gamma-ray analysis, the S1 lithofacies is indicated by a relatively high A/S ratio and gamma-ray value with fining upward sequence. This might illustrate the condition of rising accommodation space which is possibly encountered during a high intensity of rainy period. Therefore, the catchment area is inundated by water and creates a perfect setting for sheetflood deposit to occur (Nichols, 2009).

The S2 lithofacies association shows a thicker package of coarser sandy layers than S1 lithofacies. The thickness varies from 0.5-1.5 m. Several high to low angle crossbeddings are observed within the sandy interval. In the most part of the core, clay pebbles are found at the bottom of the sandy interval with a clear boundary to its below succession. The S2 lithofacies

mostly occurs during low A/S condition which can be interpreted as a period where sediment supply exceeds the accommodation space rate. As a result, this lithofacies shows a stacking pattern of the sandy layers with an overall coarsening upward trend. Therefore, this might represent an amalgamation of a river system. The presence of clay pebbles in S2 lithofacies might represent a stronger type of flow than S1 which is associated with a more confined flow scheme in stream channel system (Nichols, 2009). It is supported by a low to high angle cross-bedding within the package. The absence of clay interlayer at the top of sandy layer indicates this lithofacies to be a low sinuous river deposit than a sinuous river.

The presence of M Lithofacies Association is indicated by a silty grain size interval. The thickness ranges from 0.5-1 m. Some wavy and horizontal structures are observed in this interval but mostly a more homogeneous layer is found. It is characterized by an increase in gamma-ray value and fining upward trend as a response from the higher magnitude of accommodation space. The finer grain size of sandstone or claystone can be expected in this condition and can be interpreted as relatively a distal environment deposit. In arid-semi arid condition, this might suggest a lake to lake margin environment in distal part of alluvial plain settings. The interpreted depositional environment for each core data is presented in Figure 38.D and 39.D.

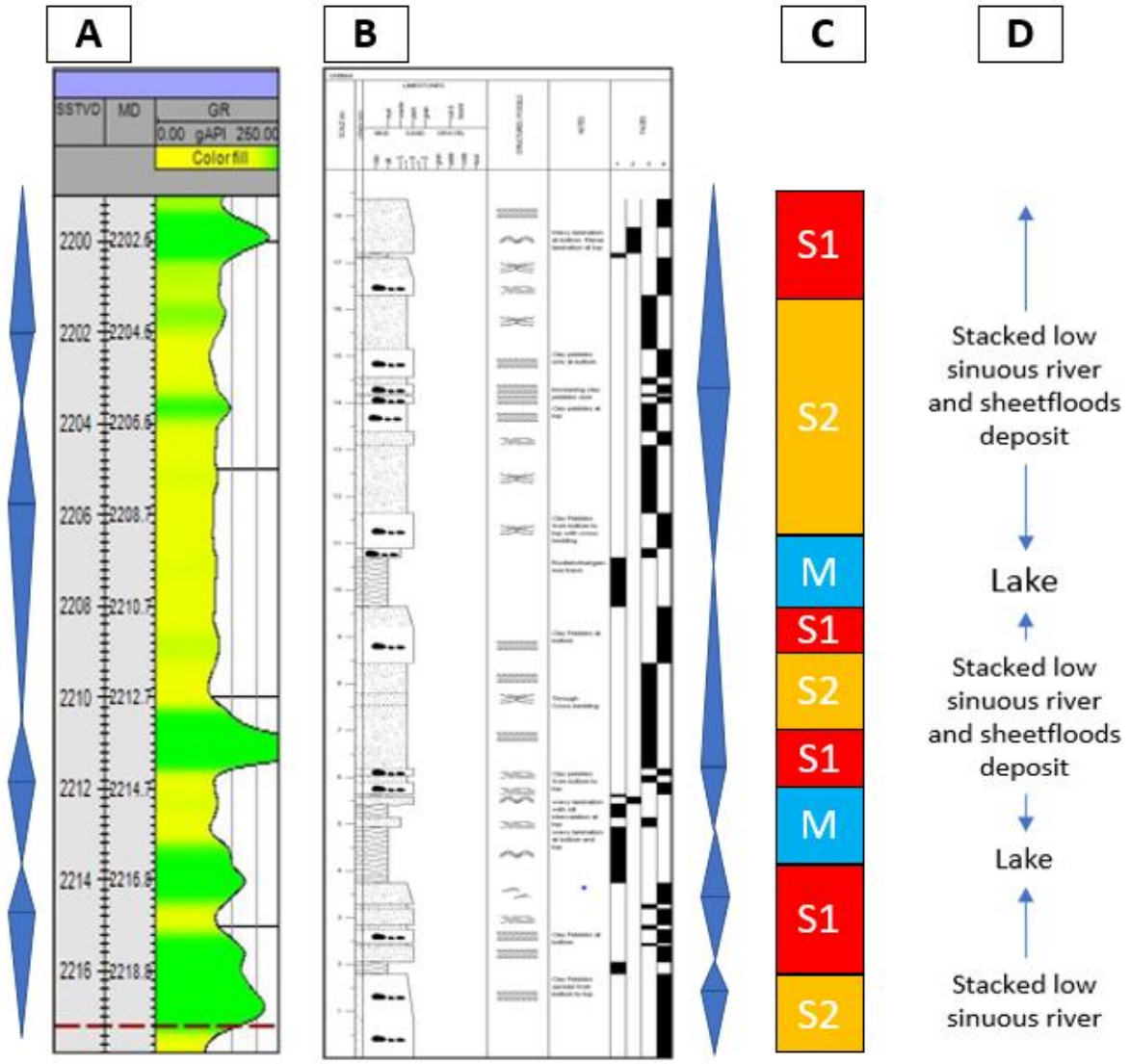

Figure 38. Core analysis of Core No.1 of OBLZ-01 well. (A) The gamma-ray logs response, (B) the core description, (C) the interpreted lithofacies association and (D) the interpreted depositional environment. Note that the triangle represents the A/S ratio in which high A/S ratio is shown by a pointing down triangle and vice versa.

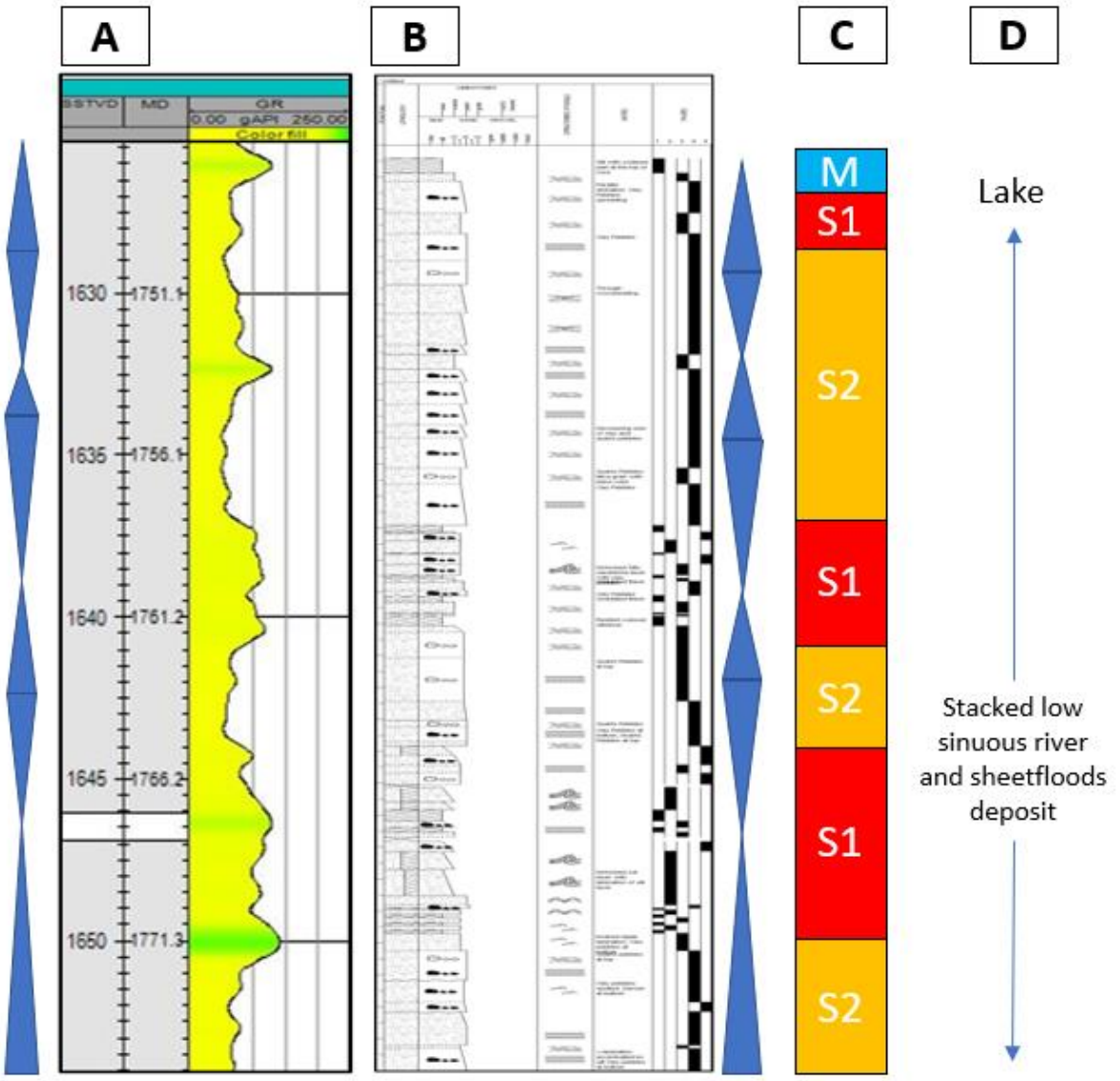

Figure 39. Core analysis of Core No.1 of WGD-01 well. (A) The gamma-ray logs response, (B) the core description, (C) the interpreted lithofacies association and (D) the interpreted depositional environment. Note that the triangle represents the A/S ratio in which high A/S ratio is shown by a pointing down triangle and vice versa.

Well Correlation for Predicting Sandstone Distribution

The link between the interpreted lithofacies and the gamma-ray response has allowed the correlation to the non-cored wells to be performed. The sequence stratigraphy approach is implemented during this correlation to connect the sandstone bodies chronostratigraphically. Time strata relationships are defined in the form of sequence boundaries and flooding surfaces. However, since the study area is located in a continental setting thus to define such boundaries is quite challenging. Due to its location, a marine incursion is probably limited or may be absent. Moreover, the lack of marker beds such as paleosols and coal layers in the core data leaves the correlation to rely on the observation of wireline logs data only. The sequence boundary is defined as there is a sudden drop in gamma-ray response. It gives an indication of an increase in sandy content which is possessed by a low A/S ratio. While the flooding surface is characterized by a rapid increase of gamma-ray value and mud content as shown by a high A/S ratio.

Two correlation panels in SW-NE and SE-NW orientations for the Röt Formation are presented in Figure 40 and 41. The prediction of the sand body is performed by following the interpreted time strata boundaries. Three units of reservoir target can be generated within the Röt Formation. The subdivision is made based on the interpreted lithofacies, gamma-ray response, and N/G ratio.

The first unit is the Lower Röt Fringe Claystone Member. In general, it is composed of the lake to lake margin deposits with some stacked of the low sinuous river and sheet flood deposits in the middle. A relatively low net sand content is observed within the interval. According to the regional facies interpretation by Geluk (2005), a marine incursion was introduced as the connection with the Tethys ocean in the basin centre was formed during the deposition of this unit. It resulted in the rising of relative base level which affected the basin margin area to be covered by a lacustrine deposit as it is shown by a fining upward trend. The SE-NW correlation shows that this unit is relatively continuous and can be correlated over several km distances.

The unit-2 covers the Röt Sandstone Member. This unit is marked by the falling of relative base level which is indicated by a sudden drop in the gamma-ray. Therefore, a much higher amount of sediment supply is expected during the deposition of this unit. As a result, a higher net sand content is observed. It mainly consists of stacked deposits of low sinuous river and sheet flood deposits as it characterized by several coarsening upward sequences. Both of the correlation panels show that the sand body in this unit is continuous laterally. According to Nichols (2009), the alluvial fan radius can reach a distance up to 10 km. Based on that, the connected sand bodies are possibly resulted from an amalgamation of several alluvial fans which surrounded the area. Several layers of lake deposit are observed in the northwestern part of the study area which probably occurred during a high base level period. This might indicate an overall trend of deposition with SE-NW trend.

Unit-3 is the Upper Röt Fringe Claystone Member. Based on its gamma-ray response, this unit is interpreted as a low net sand interval. Overall, this unit has a similar trend as the unit-1. It is characterized by several fining upward sequences. It is mainly composed of the lake to lake margin deposits with some sheet flood and low sinuous river deposits. The unit was probably deposited following the transgression period after the deposition of unit-2.

The result from the correlation shows that the unit-2 is the most promising target as high sand content is observed. Moreover, the spatial prediction of this unit shows a continuous distribution of the sand body over several km in the study area. Next, a detailed evaluation regarding its reservoir properties will be conducted in the next sub-chapter in petrophysical evaluation part.

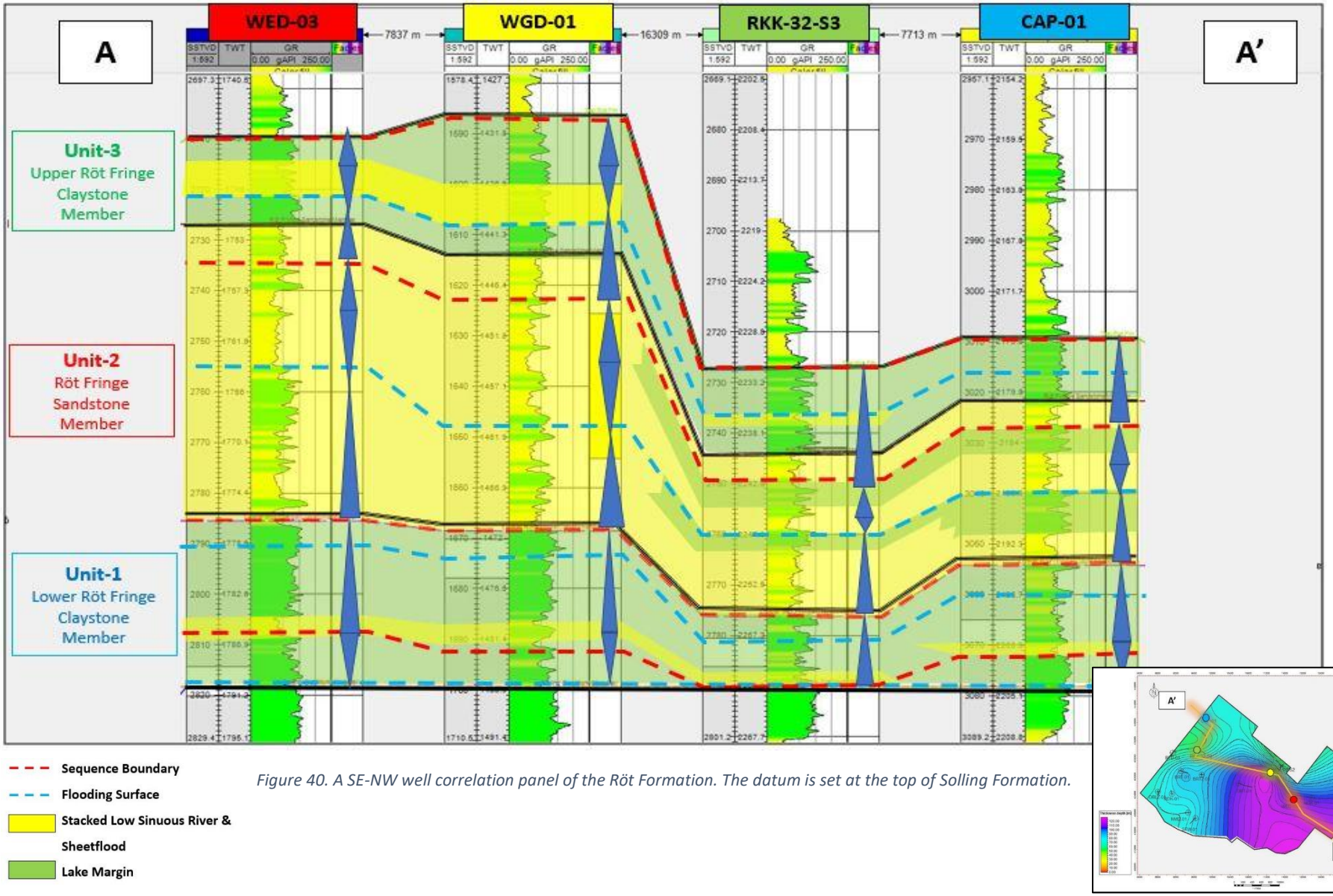

Figure 40. A SE-NW well correlation panel of the Röt Formation. The datum is set at the top of Solling Formation.

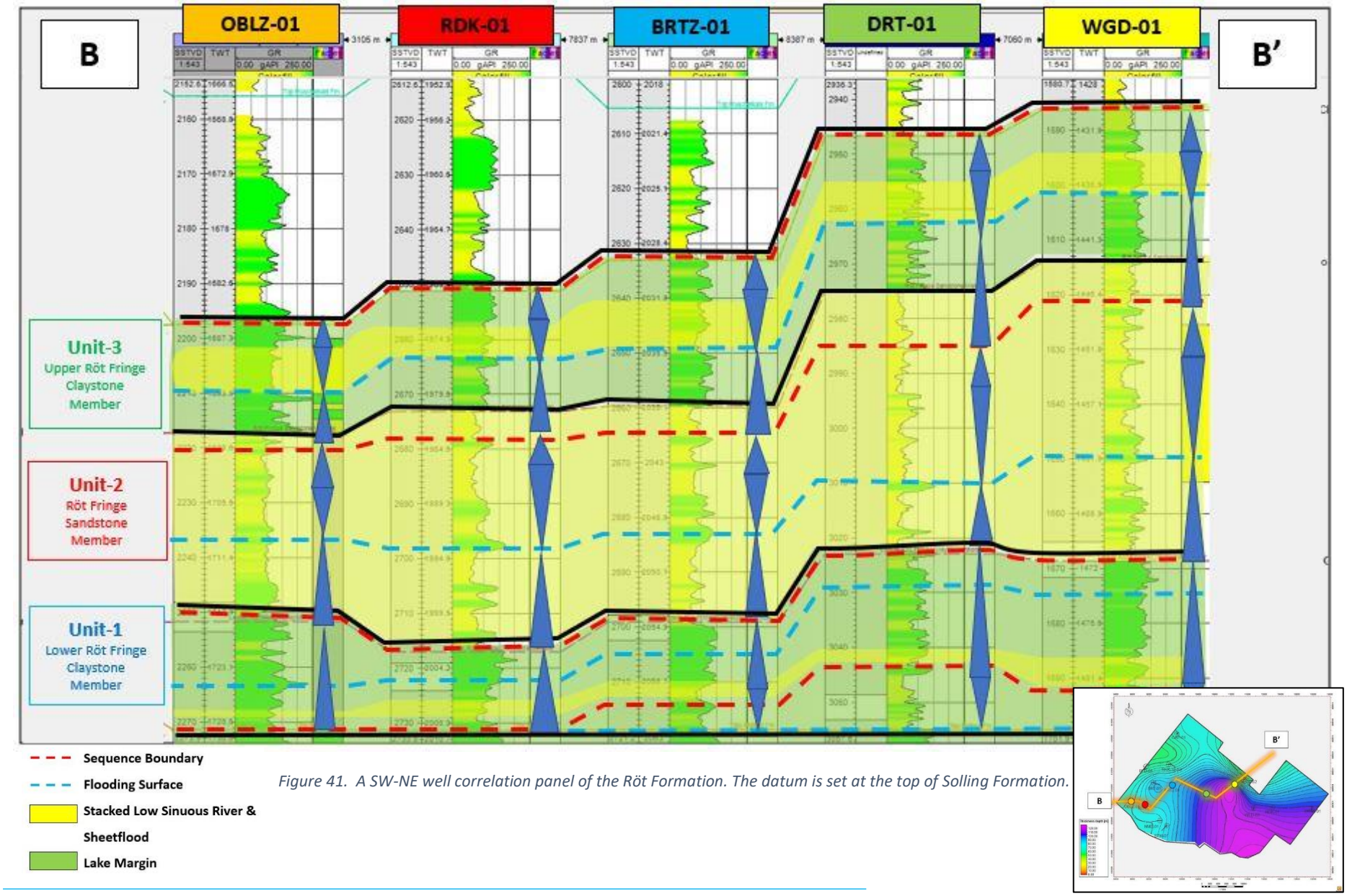

Figure 41. A SW-NE well correlation panel of the Röt Formation. The datum is set at the top of Solling Formation.

4.2.3. Core Analysis of the Hardegsen Formation

Core No.2 (2275-2296.58 mAH) of OBLZ-01

The second interval of core data from the OBLZ-01 well covers the Solling and Hardegsen Formation on the interval of 2275-2296.58 mAH. The cored interval is generally composed of grey to brownish sandstone layers with fine to medium grain size and some silty layers in the middle and top of the interval. The thickness ranges from 20 cm to 2 m in a sand layer package and 30 cm to 2 m for a silty layer. Clay pebbles are present in the sandy interval. The N/G ratio is 0.8. Sedimentary structures such as parallel lamination, planar to through crossbedding and current ripple are common in the cored interval. A good porosity indication is shown at depth (2295.55 to 2295.30 m) as the epoxy went through the rock as can be seen in Figure 42.A. The detailed description of this core interval is presented in Appendix D.3.

Figure 42. (A) An indication of a porous layer as the epoxy adsorption is visible at 2295.55-2295.30 m. (B) Parallel lamination and alternation of finer and coarser sandy layer at 2285.75-2286.30 m.

Lithofacies Association Interpretation

Based on the core description, the Lithofacies Association interpretation is conducted through the whole interval. As shown in Figure 43.C, the S1 and S2 lithofacies dominate the most part of the interval while the M lithofacies is interpreted only at the upper part. Using the same approach as the previous description, the alternation of S1 and S2 lithofacies is interpreted as the stacked of the low sinuous river and sheet flood deposit. Whilst, the M lithofacies might indicate a lake to lake margin environment.

This alternation of S1, S2 and M lithofacies can be interpreted as a response to a gradual shift of the fan which might be influenced by a change in climate condition and tectonic activity.

This affected the sediment supply and accommodation space. As a result, an alternation of sheet flood and stream channel deposit is occurred and bounded by a lake deposit. At the base of the Basal Solling part, a wavy boundary with clay pebbles is observed. This might represent the erosion during the start of deposition of the Solling Formation in which denoted by an unconformity. The presence of the M lithofacies association at the top of the interval is taken from the Solling Formation. The thickness reaches 4 m in this interval and probably reflects a lake to lake margin deposit.

The variation of A/S ratio is interpreted and compared to the gamma-ray log response. Based on the interpretation, the gamma-ray log captures less variation than the core description. An increase of the gamma-ray value is only observed at the beginning of the Solling Formation and can be correlated to the M lithofacies. This might illustrate a gradual increase of accommodation space when a major transgressive period was occurring during the Solling Formation deposition according to Geluk (2007). However, the distinction of S1 and S2 lithofacies cannot be clearly recognized from the gamma-ray pattern. Therefore, the two lithofacies will be interpreted as one sandstone body in the next well correlation part. The result of the analysis shows that the Hardegsen Formation is an interesting target to be investigated. As it consists of great thickness of stacked deposit of low sinuous river and sheet flood as shown by the relatively blocky low gamma-ray response.

Well Correlation for Predicting Sandstone Distribution

Two correlation panels in SW-NE and SE-NW orientations are constructed to investigate the connectivity of the sand bodies within the Hardegsen Formation. The correlation panels are presented in Figure 44 and 45.

Based on the correlation result, mainly the stacking of low sinuous river and sheet flood deposits dominate the Hardegsen interval. The gamma-ray pattern shows a uniform blocky appearance throughout the wells. Hence, a high net sand content is expected in this interval. However, significant differences in thickness are observed within the study area as can be seen in both correlation panels. The thickness is observed to be drastically decreased towards the northwest direction whereas the sand-rich zone is observed in the southeast part of the area. The variation in thickness might indicate the impact from the Hardegsen extensional phase, in which the Hardegsen Formation was subjected to the erosional period at the beginning of the Solling Formation deposition.

Based on the core analysis and correlation result, the Hardegsen Formation shows a promising indication of net sand interval and therefore can be one of the targets for geothermal operation. Nevertheless, the significant variation in gross thickness might limit its exploitable zone. More detailed evaluation of its reservoir properties will be conducted in next sub-chapter.

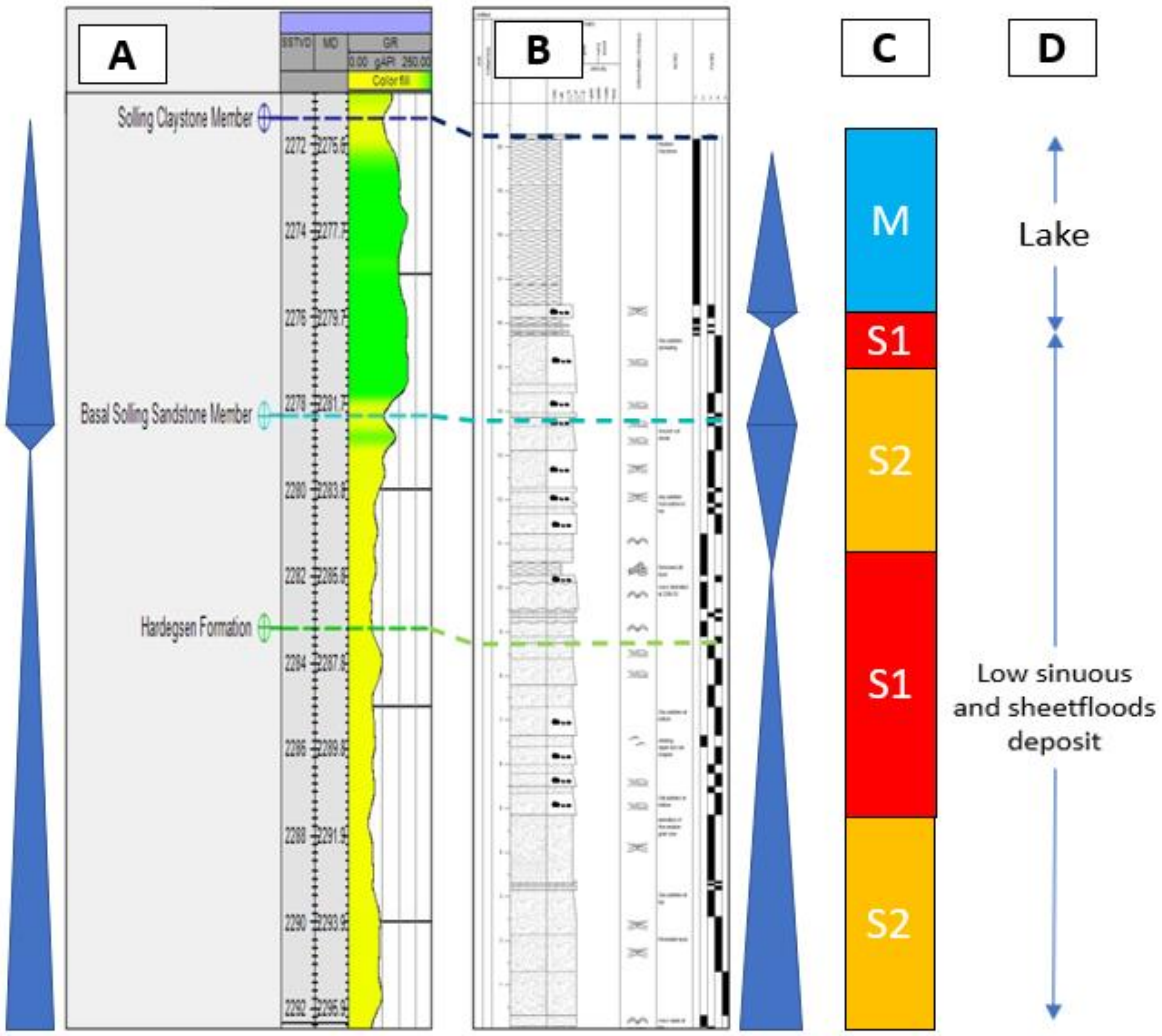

Figure 43. Core analysis of Core No.2 of OBLZ-01 well. (A) The gamma-ray logs response, (B) the core description, (C) the interpreted lithofacies association and (D) the interpreted depositional environment. Note that the triangle represents the A/S ratio in which high A/S ratio is shown by a pointing down triangle and vice versa.

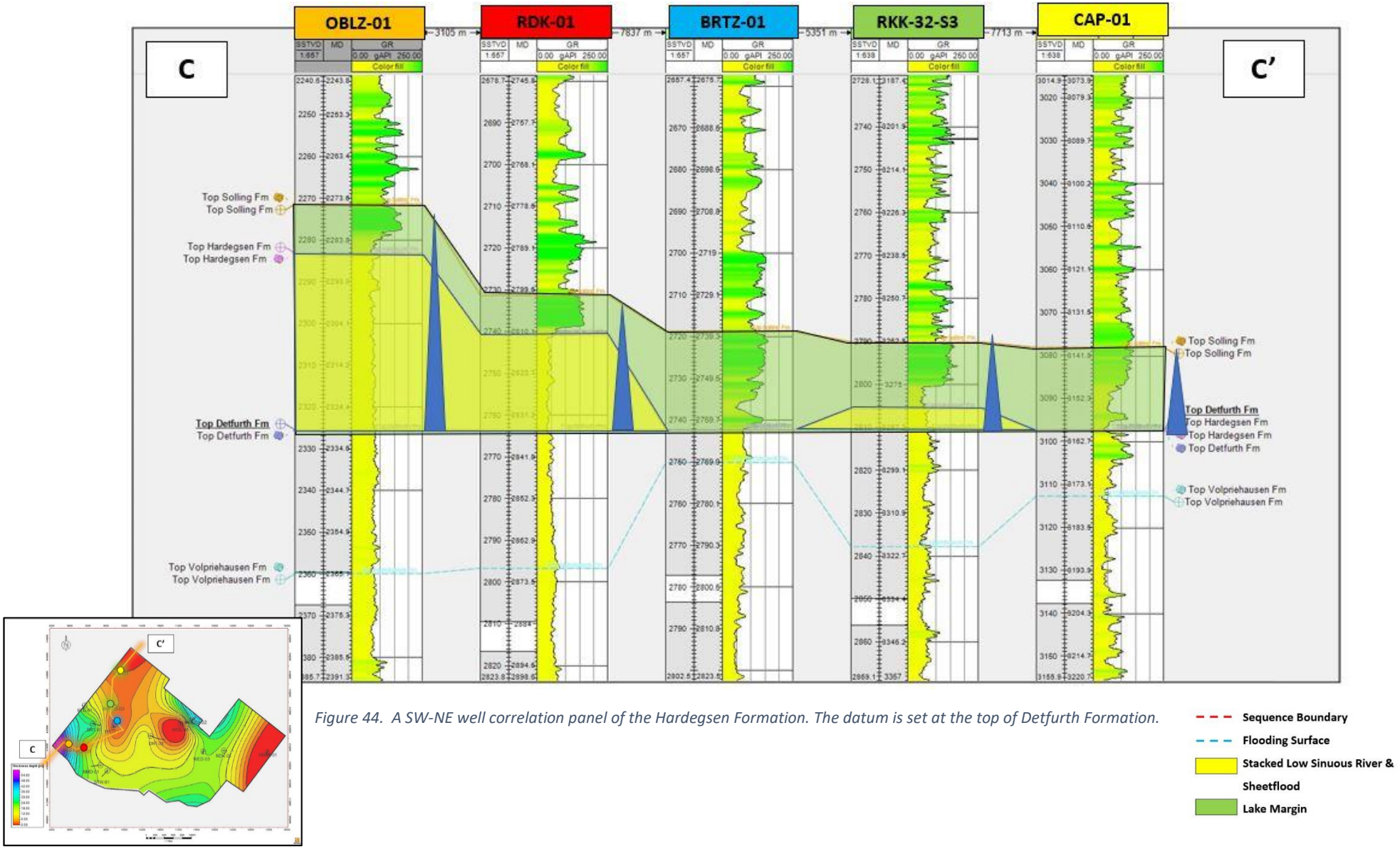

Figure 44. A SW-NE well correlation panel of the Hardegsen Formation. The datum is set at the top of Detfurth Formation.

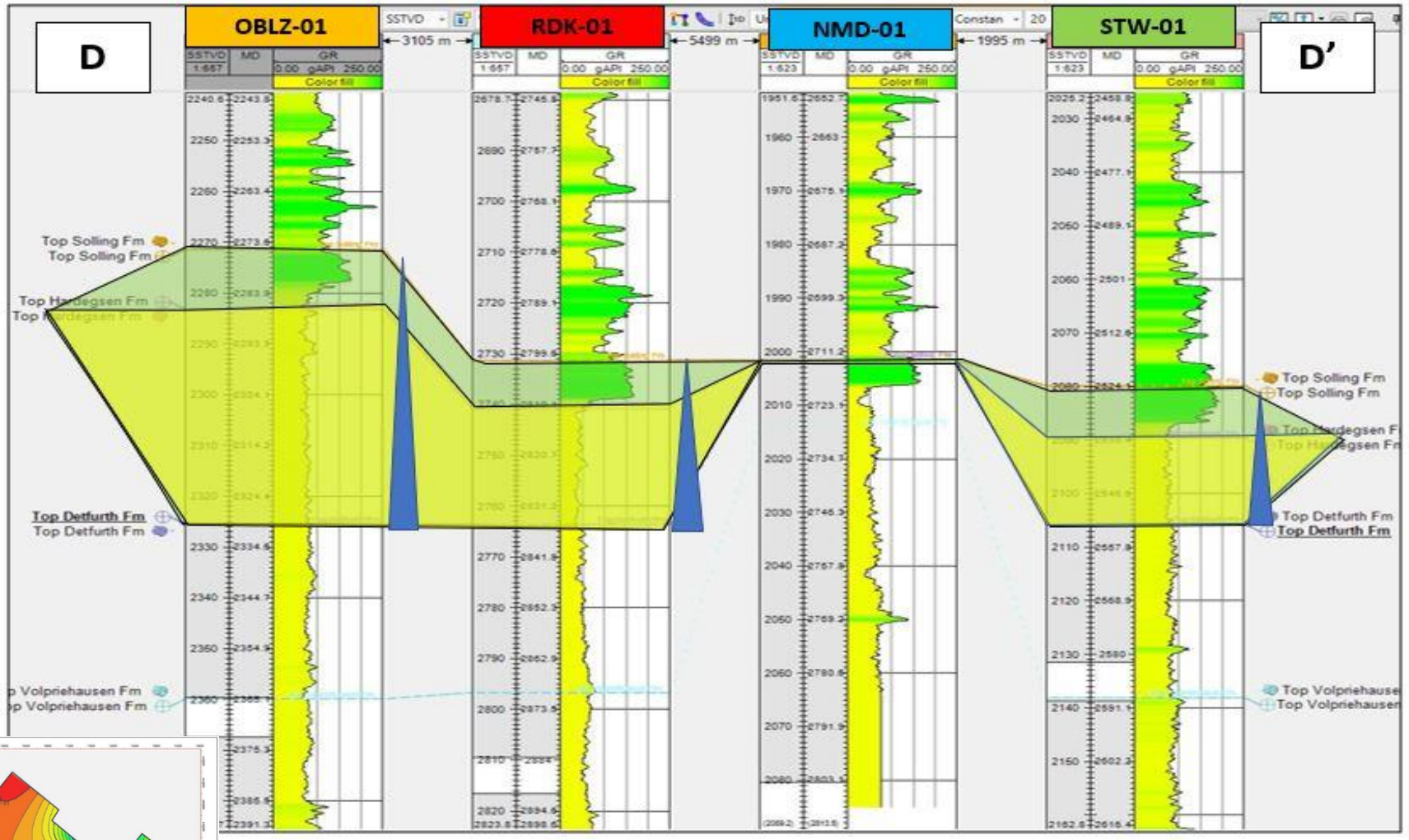

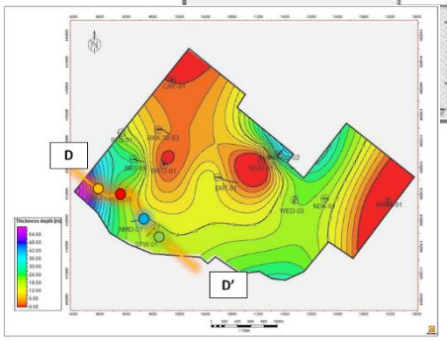

Figure 45. A SE-NW well correlation panel of the Hardegsen Formation. The datum is set at the top of Detfurth Formation.

4.2.4. Lithofacies Analysis of the Detfurth and Volpriehausen Formations

Since no core description is performed in this interval, therefore the lithofacies interpretation is mainly based on the gamma-ray response only. Two well correlation panels in the SE-NW and SW-NE orientations are made to investigate the continuity of the sandstone bodies within these two formations as presented in Figure 46 and 47.

Based on the correlation results, a relatively low gamma-ray value range is observed within these two formations. Several coarsening upward sequences are spotted to dominate the Volpriehausen and Detfurth interval. At a period where the relative base level increase, a higher gamma-ray value is observed and shows a fining upward trend. According to the lithofacies interpretation for the Hardegsen Formation in the previous section, this variation in gamma-ray pattern might indicate an alternation of a sheet flood and low sinuous river deposit. A lake deposit is probably absent in this interval as the high gamma-ray value is still much lower compared to the one in the Röt Formation.

This variation in the gamma-ray pattern is used to interpret the sequence boundaries and flooding surfaces in order to correlate the sand bodies. Some thickness variations within the Detfurth and Volpriehausen Formation are observed in both correlation panels. However, based on that it can be clearly seen that the Volpriehausen Formation has much thicker succession than the Detfurth Formation.

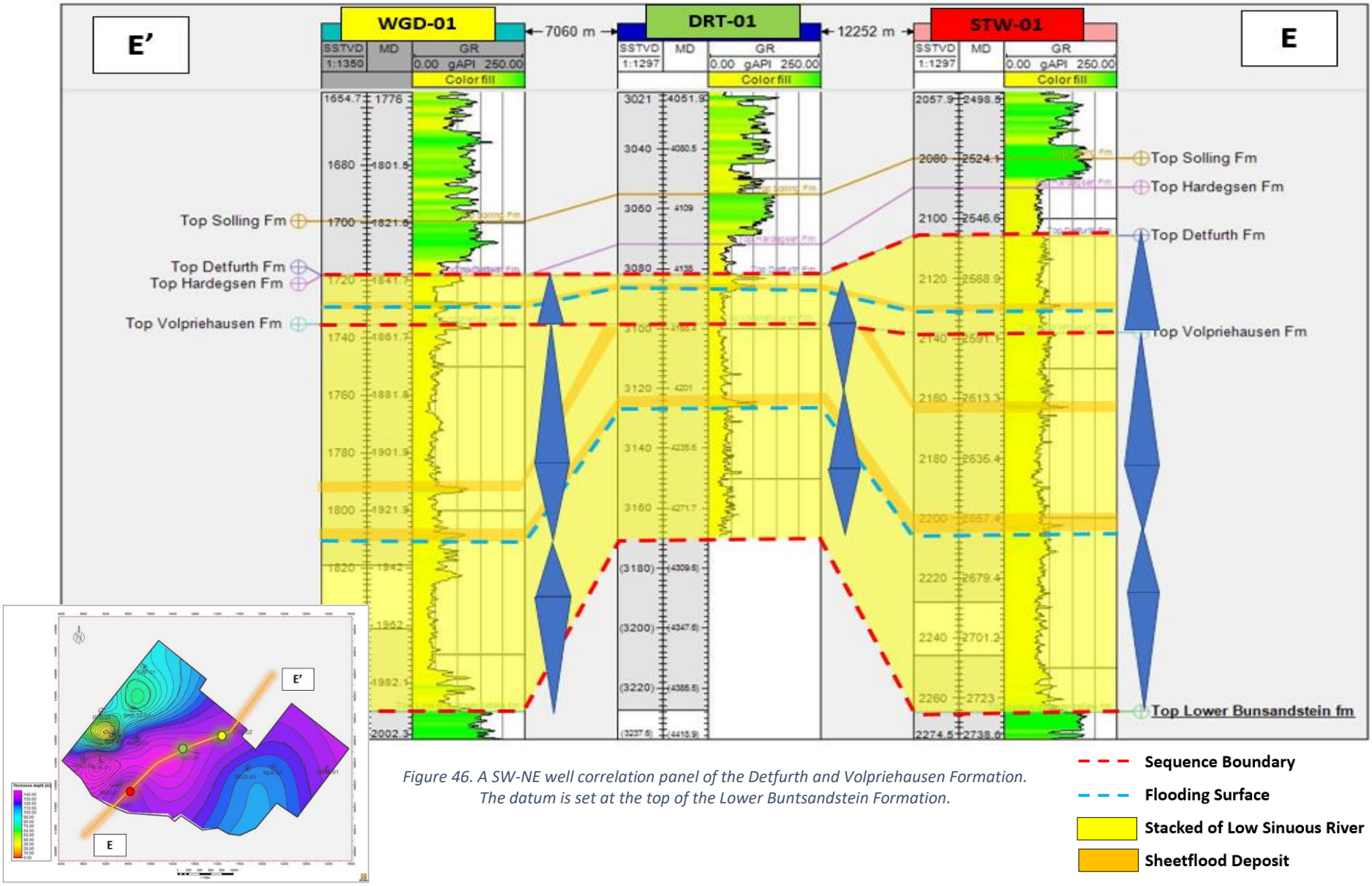

Figure 46. A SW-NE well correlation panel of the Detfurth and Volpriehausen Formation. The datum is set at the top of the Lower Buntsandstein Formation.

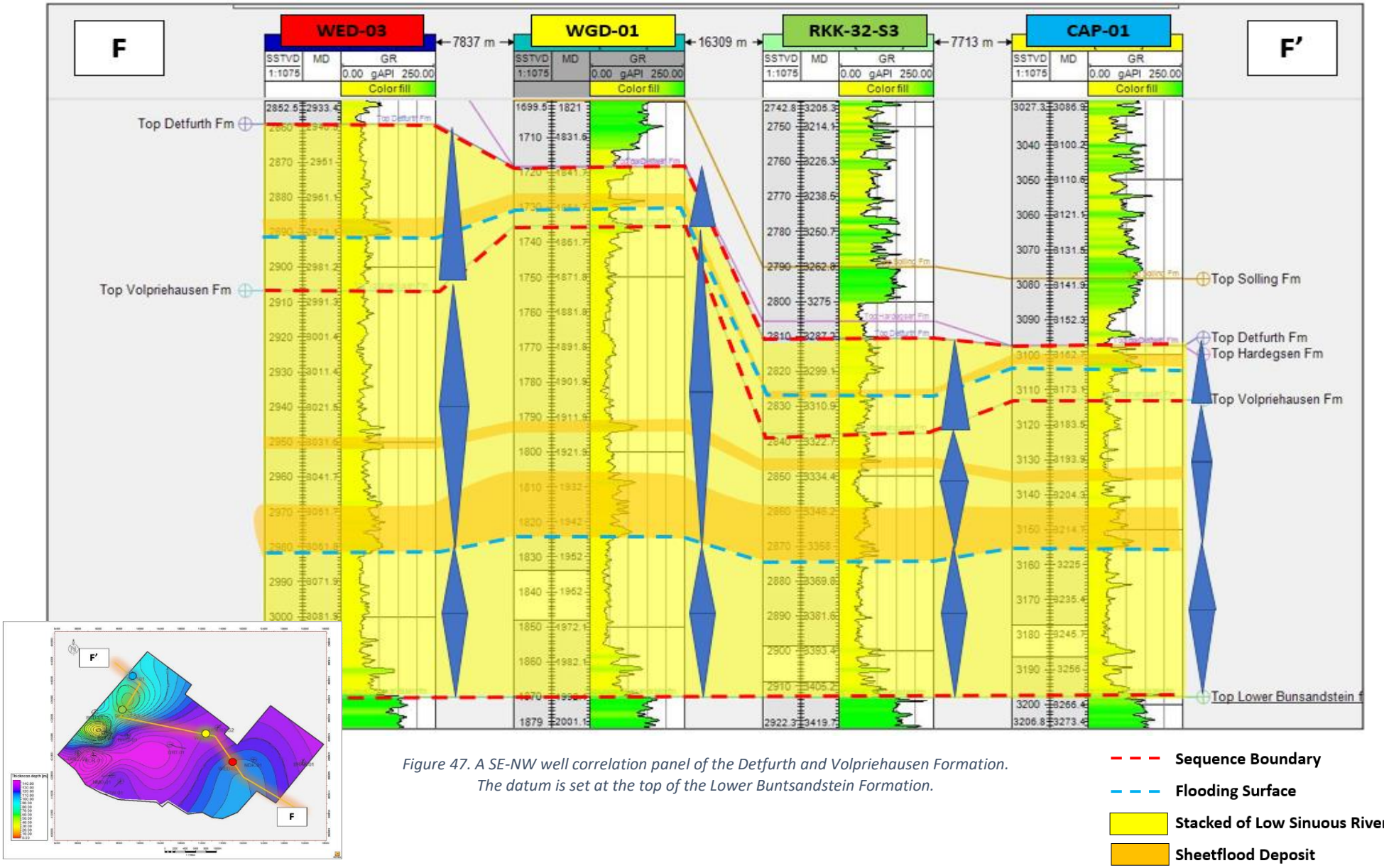

Figure 47. A SE-NW well correlation panel of the Detfurth and Volpriehausen Formation. The datum is set at the top of the Lower Buntsandstein Formation.

4.3. Petrophysical Evaluation

Eight wells within the study area have been selected for petrophysical evaluation. Well data from BRAK-01, BRTZ-01, MOL-02-S2, OBLZ-01, RDK-01, STW-01, WED-03 and WGD-01 are selected for the evaluation based on several criteria as listed below:

- Sufficient well logs data;
- Availability of core data, and;
- Location in the study area.

The objective of this analysis is to investigate the reservoir properties of each target formation within the Triassic successions. Several log processing steps are performed to determine the reservoir properties for each formation. All of the steps are done in Petrel 2014 and Microsoft Excel software. The detailed explanation can be found in below subchapters.

4.3.1. The volume of Shale Calculation

The first step of the analysis is the volume of shale (Vshale) calculation. The Gamma Ray (GR) method is used during the calculation by following below formula:

$$Vsh\_GR = \frac{(GR_{log} - GR_{min})}{(GR_{max} - GR_{min})} \quad (2)$$

The value of GR_{max} and GR_{min} respectively are determined from the shale and sandstone base line by analyzing the overall GR log response in the Triassic successions interval. Next, both values will be used to subtract the GR log response from each depth to estimate the shale volume within the rock interval.

4.3.2. Porosity Calculation

Porosity calculation is performed by applying the combination of density and neutron logs method. Firstly, the density method is utilized by following the below formula:

$$\Phi_{Density} = \frac{(\rho_{ma} - \rho_b)}{(\rho_{ma} - \rho_{fl})} \quad (3)$$

The petrophysical evaluation is performed in predominantly sandstone intervals, thus the ρ_{ma} value of 2.65 g/cc is used. While, the ρ_{fl} value depends on the fluid content which occurred in the investigated interval. This is done by analysing the resistivity and density-neutron logs response and from the well report. In the water zone interval ρ_{fl}= 1 g/cc is used while in the gas and oil-bearing interval ρ_{fl} of 0.8 and 0.25 g/cc are applied respectively.

However, the application of the density method is sometimes considered too simplistic and error-prone, since a uniform ρ_{ma} value is used during the calculation. Therefore, the neutron-density method is implemented by combining the response from neutron log ($\Phi_{Neutron}$) and the porosity estimation result ($\Phi_{Density}$) from density method as presented in formula below:

$$\Phi_{ND} = \sqrt{\frac{\Phi_{Neutron}{}^2 + \Phi_{Density}{}^2}{2}} \quad (4)$$

At the end of the process, the estimated porosity is compared to the core porosity measurement for quality control. Overall, a good alignment between both data is observed. Hence, it provides a good confidence level for porosity determination part.

4.3.3. Permeability Estimation

In this part of the analysis, a permeability estimation is done by applying a porosity-permeability relation based on the core data measurement. All of the available core data within the study area are compiled and classified based on its formation interval to construct a porosity-permeability cross-plot.

The application of Swanson Mean regression method is applied during the process to generate low (K90), medium (K50) and high scenarios (K10). According to Betts (2017), This method is best to be applied in large datasets (>200 plugs) as several possibility scenarios can be obtained. Firstly, the core data within each formation is split into several porosity classes in which the Swanson Mean is calculated within each class by applying below formula:

$$Swanson\ Mean = 0.3P10 + 0.4P50 + 0.3P90 \quad (5)$$

The value of P10, P50 and P90 are calculated from the 10th, 50th and 90th percentiles of the porosity data within one class. The result from above formula will be the medium scenario while the low and high scenario can be estimated from below formula:

$$Low\ Scenario = 0.5P10 + 0.4P50 + 0.1P90 \quad (6)$$

$$High\ Scenario = 0.1P10 + 0.4P50 + 0.5P90 \quad (7)$$

After the calculation for each scenario is completed, a trend line fit is applied to derive a porosity-permeability relation. The results of permeability-porosity relation are presented in Figure 48, 49 and 50. Note that, the porosity-permeability relation for the Detfurth and Volpriehausen Formation are combined together as these intervals have similar relation and characteristic. The obtained porosity-permeability relations are as follows:

Röt Formation

K90(mD)	= -59.423 $\Phi_{ND}{}^2$ + 36.011Φ_{ND} – 2.5184	R² = 0.9987
K50(mD)	= -65.895 $\Phi_{ND}{}^2$ + 37.415 Φ_{ND} - 2.2366	R² = 0.9981
K10(mD)	= -68.041 $\Phi_{ND}{}^2$ + 37.877 Φ_{ND} - 2.0677	R² = 0.9979

Hardegsen Formation

K90(mD)	= 5.5935 $\Phi_{ND}{}^2$ + 12.036 Φ_{ND} – 0.2577	R² = 0.9990
K50(mD)	= 8.3068 $\Phi_{ND}{}^2$ + 9.6916 Φ_{ND} + 0.3381	R² = 0.9902
K10(mD)	= 9.1798 $\Phi_{ND}{}^2$ + 8.8945 Φ_{ND} + 0.6116	R² = 0.9817

Detfurth-Volpriehausen Formation

K90(mD)	= 5.7596 $\Phi_{ND}{}^2$ + 20.016 Φ_{ND} - 2.1457	R² = 0.9899
K50(mD)	= -0.3867 $\Phi_{ND}{}^2$ + 21.442 Φ_{ND} – 1.9082	R² = 0.9854
K10(mD)	= -2.3634 $\Phi_{ND}{}^2$ + 21.894 Φ_{ND} – 1.7524	R² = 0.9836

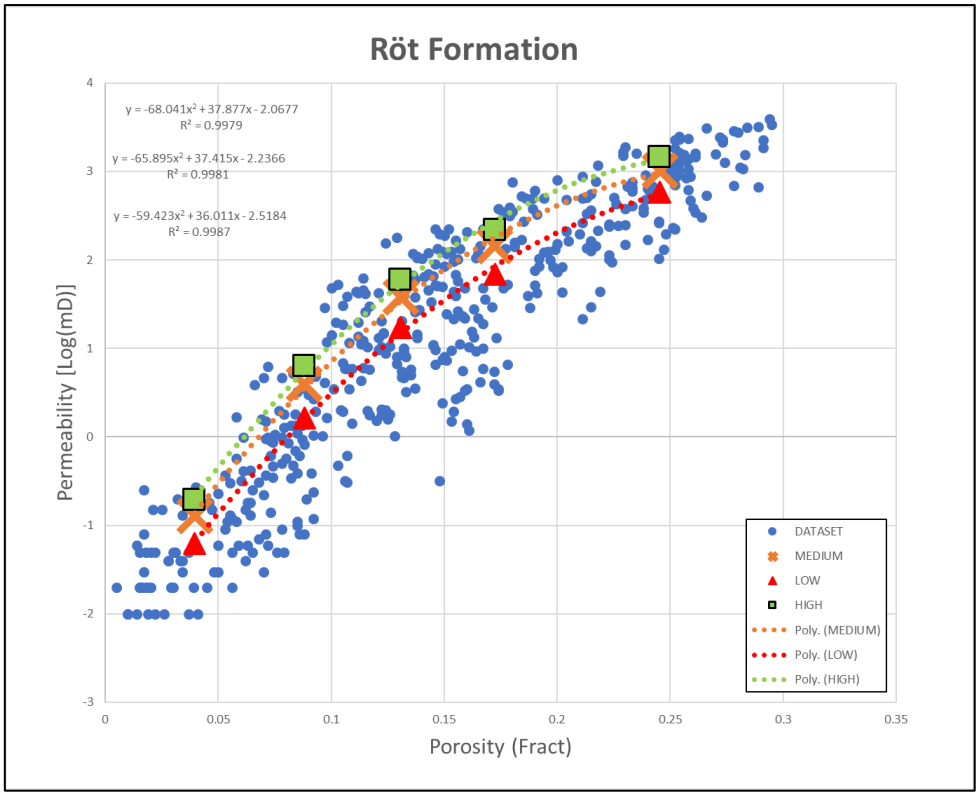

Figure 48. Porosity-permeability relation of the Röt Formation.

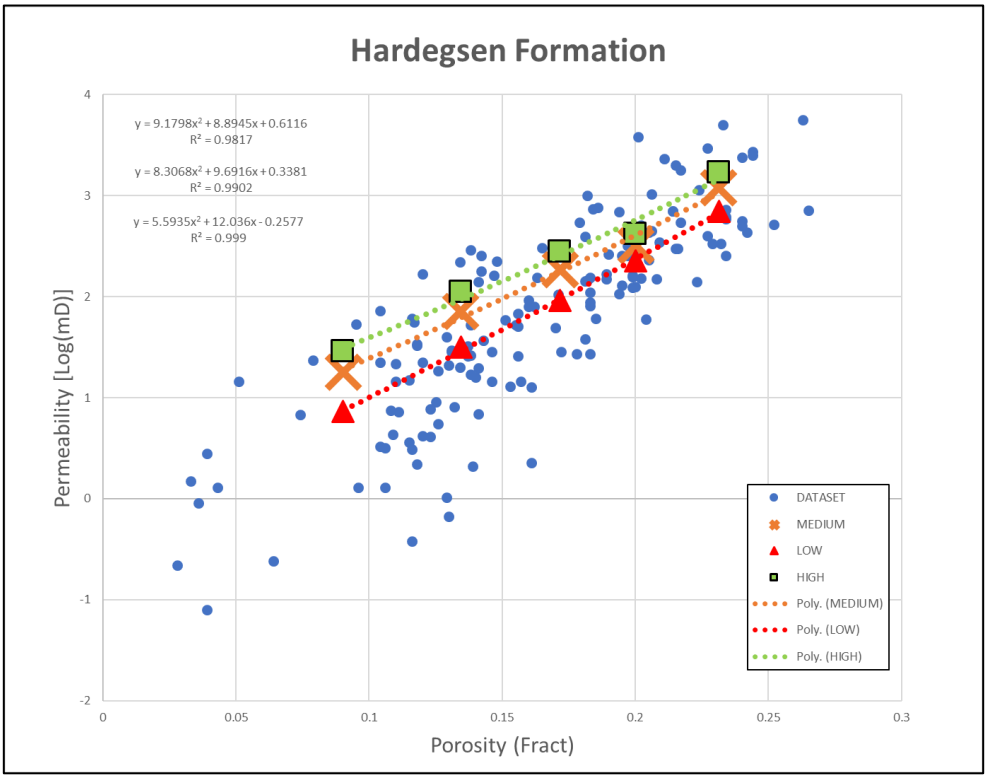

Figure 49. Porosity-permeability relation of the Hardegsen Formation.

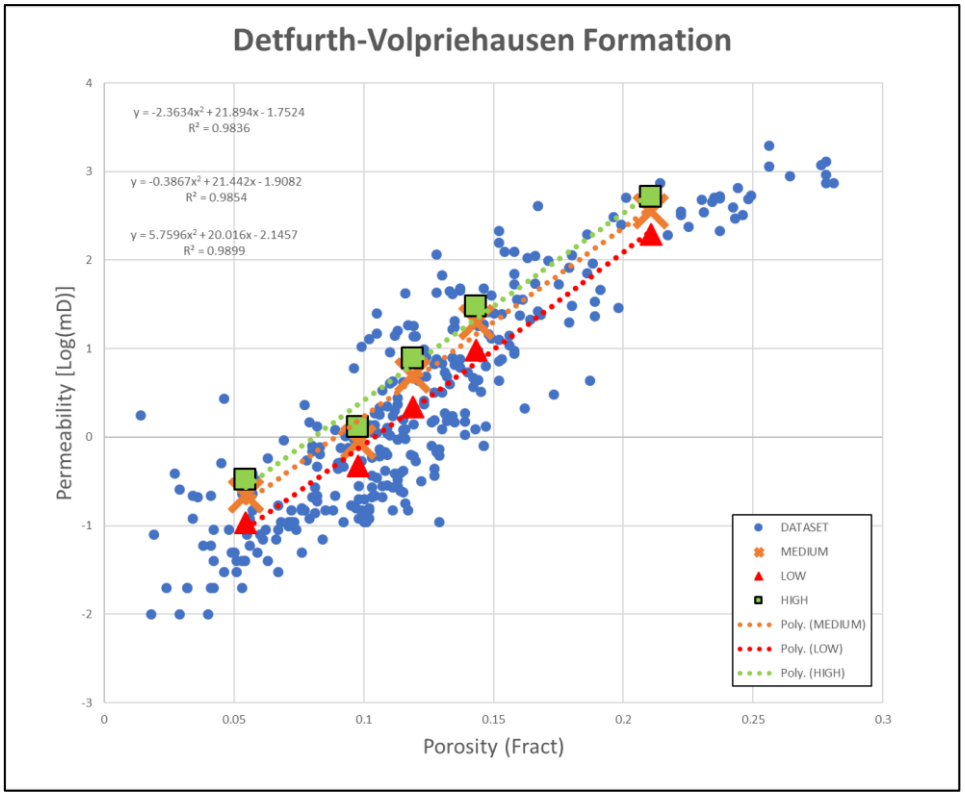

Figure 50. Porosity-permeability relation of the Detfurth and Volpriehausen Formation.

4.3.4. Petrophysical Averages

The result from the log processing steps in the previous sub-chapters is summarized in this part. The petrophysical evaluation results for the Röt, Hardegsen, Detfurth and Volpriehausen Formations are presented in the form of reservoir properties averages as shown in Table 4.

Appropriate cut offs of Vshale and permeability are applied to determine the net reservoir interval. The net reservoir is defined as an interval which has less than 50% of Vshale and a permeability of more than 1 mD. These cut offs are implemented to give a quick look evaluation for a clean sand interval in which a significant flow of a fluid can occur. The obtained net reservoir interval can be used to estimate N/G ratio for each formation. The result of petrophysical evaluation for each well is compiled in one well-section as presented in Figure 51 for STW-01 well. The result for the other wells and its utilized petrophysical parameters can be found in Appendix.E.

Based on the evaluation result, various N/G ratio, porosity and permeability averages are observed within the same formation interval at the different well location. This might correspond to its depth difference due to some compaction during and after deposition since the Triassic successions are influenced by several rifting episodes as mentioned in previous sub-chapters. More detailed analysis regarding the result will be discussed in the next chapter.

Table 4. Petrophysical averages summary for each target formations per well.

Formation	Unit	Well	TVD		MD		Gross Thickness (m)	Net Thickness (m)	N/G (%)	Average Porosity (%)	Average Permeability (md)		
			Top (m)	Base (m)	Top (m)	Base (m)					LOW	MED	HIGH
Rot Fm	Unit-3	BRAK-01	2219.6	2249.6	2313	2345	32	3	9	10.09	3.73	8.48	12.44
	Unit-3	WED-03	2710.9	2726.9	2790	2807	17	0	2	9.81	2.77	6.31	9.86
	Unit-3	WGD-01	1586.3	1614	1707	1735	28	6	23	9.96	4.42	9.40	14.66
	Unit-3	MOL-02-S2	2564.6	2558.2	2647	2673	26	0	0	0.00	0.00	0.00	0.00
	Unit-3	STW-01	1998.3	2016.3	2425	2448	23	11	46	22.67	410.30	722.47	1036.48
	Unit-3	OBLZ-01	2197.5	2217.2	2200	2220	20	0	2	0.00	43.73	90.89	137.68
	Unit-3	RDK-01	2651.2	2673.1	2717	2740	23	9	39	10.56	7.01	14.15	21.40
	Unit-3	BRTZ-01	2633	2659.7	2651	2678	27	3	10	10.05	4.65	9.27	14.00
	Unit-2	BRAK-01	2249.7	2293.7	2345	2392	47	17	36	8.18	1.79	2.79	3.78
	Unit-2	WED-03	2726.9	2785.5	2807	2866	59	24	40	8.91	3.31	5.33	7.79
	Unit-2	WGD-01	1614.1	1668.6	1735	1790	55	33	60	18.78	196.68	378.94	559.92
	Unit-2	MOL-02-S2	2558.3	2603.5	2673	2690	17	3	19	7.38	2.89	1.79	2.05
	Unit-2	STW-01	2016.6	2060.8	2448	2502	54	47	87	19.80	267.40	486.73	706.09
	Unit-2	OBLZ-01	2217.3	2251.7	2220	2255	35	23	65	17.12	114.22	233.20	351.15
	Unit-2	RDK-01	2673.2	2717	2740	2786	46	30	65	11.49	11.95	24.13	35.80
	Unit-2	BRTZ-01	2659.8	2699	2678	2718	40	22	54	12.22	18.88	38.29	58.02
	Unit-1	BRAK-01	2293.8	2326	2392	2427	35	0	0	0.00	0.00	0.00	1.14
	Unit-1	WED-03	2785.6	2818.4	2866	2899	33	1	4	8.01	1.65	2.48	3.67
	Unit-1	WGD-01	1668.7	1699	1790	1821	31	3	10	13.14	21.81	48.59	75.30
	Unit-1	MOL-02-S2	2603.6	2625	2690	2714	24	16	66	9.75	4.55	8.38	12.38
	Unit-1	STW-01	2060.9	2089.5	2502	2524	22	9	42	19.68	219.72	424.75	628.12
	Unit-1	OBLZ-01	2251.8	2271.4	2255	2275	20	4	18	15.09	63.97	135.24	205.98
	Unit-1	RDK-01	2717.1	2731.3	2786	2801	15	2	11	10.00	0.00	8.24	12.19
	Unit-1	BRTZ-01	2699.1	2718.7	2718	2738	20	1	7	8.43	1.89	3.26	4.37
Hardegsen Fm	Unit-1	WED-03	2838.2	2859.1	2919	2940	21	8	80	7.15	5.91	15.01	24.34
	Unit-1	MOL-02-S2	2646.6	2681.8	2738	2777	39	36	100	9.87	11.81	27.74	43.67
	Unit-1	STW-01	2089.6	2553	2535	2553	18	18	100	18.74	169.48	298.61	424.61
	Unit-1	OBLZ-01	2328.4	2350.1	2287	2330	43	43	99	17.52	123.75	223.43	320.56
	Unit-1	RDK-01	2740.8	2763.6	2811	2835	24	24	100	9.66	10.01	24.25	38.56
Detfurth Fm	Unit-1	BRAK-01	2377.2	2384.5	2483	2491	8	4	52	10.39	1.36	2.23	3.17
	Unit-1	WED-03	2859.2	2906.7	2940	2988	48	34	71	14.36	14.85	26.28	36.46
	Unit-1	WGD-01	1718.4	1735.3	1840	1857	17	12	73	16.81	36.42	69.79	102.19
	Unit-1	MOL-02-S2	2699.9	2710.8	2797	2809	12	0	0	0.00	0.00	0.00	0.00
	Unit-1	STW-01	2105.7	2138.1	2553	2589	36	36	100	17.49	110.63	199.13	288.08
	Unit-1	OBLZ-01	2329.2	2363.5	2330	2365	35	35	99	17.08	52.00	99.43	146.68
	Unit-1	RDK-01	2763.6	2796.7	2835	2870	35	34	98	12.72	7.65	11.63	16.72
	Unit-1	BRTZ-01	2742.3	2750	2762	2770	8	7	84	12.64	3.68	7.31	11.08
Volpriehausen Fm	Unit-1	BRAK-01	2384.6	2516.6	2491	2637	146	26	18	9.85	1.64	1.77	2.07
	Unit-1	WED-03	2906.8	3022.9	2988	3105	117	7	6	10.14	2.04	2.19	2.62
	Unit-1	WGD-01	1735.4	1869.9	1857	1992	135	124	92	15.28	18.80	36.47	54.14
	Unit-1	MOL-02-S2	2710.9	2815.7	2809	2925	116	0	0	0.00	0.00	0.00	0.00
	Unit-1	STW-01	2138.2	2264.7	2589	2728	139	138	99	16.17	31.19	60.58	89.80
	Unit-1	OBLZ-01	2363.6	2499.9	2365	2508	143	132	92	14.89	17.55	34.14	50.76
	Unit-1	RDK-01	2796.8	2961.7	2870	3043	173	65	37	11.70	8.93	11.60	14.22
	Unit-1	BRTZ-01	2750.1	2876.4	2770	2899	129	66	51	10.96	2.82	3.88	5.18

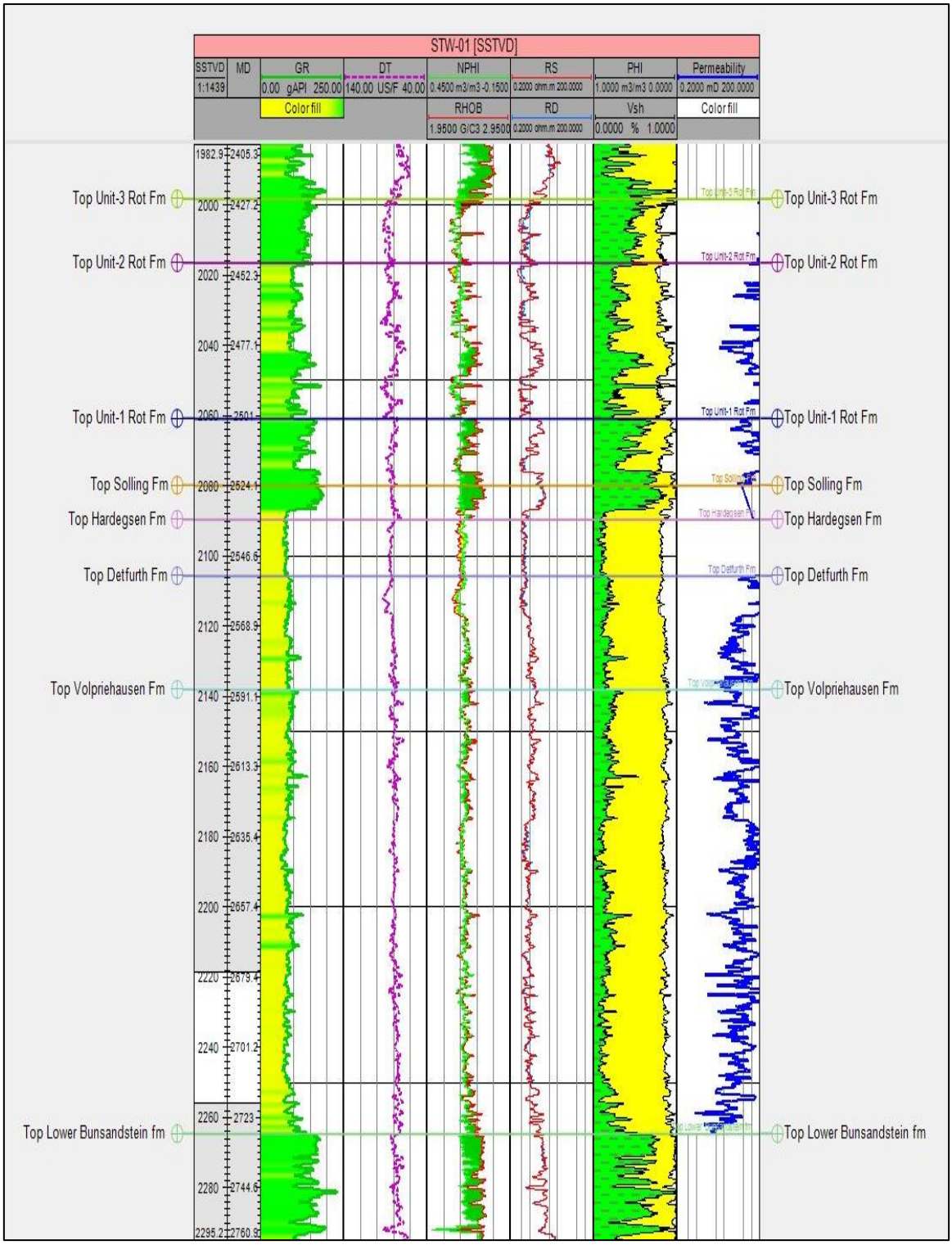

Figure 51. Petrophysical evaluation of STW-01 well.

5 Discussion

In this chapter, the results from the previous chapter are combined to determine the most suitable area for deployment of a geothermal doublet. This is done by considering the size, shape, spatial distribution and connectivity (reservoir architecture) of the Triassic Sandstones and their reservoir properties distribution. More detailed discussion regarding these subjects are presented in below sub-chapter.

5.1. Reservoir Architecture Model of Triassic Sandstones

The interpretation of lithofacies and regional well correlation in the reservoir sedimentology sub-chapter have allowed a sedimentological model to be constructed in this part. General distribution of depositional settings in the study area is summarized in Figure 52. Based on the analysis result, mainly the successions within the target formations are constituted of an alluvial fan to lacustrine deposits.

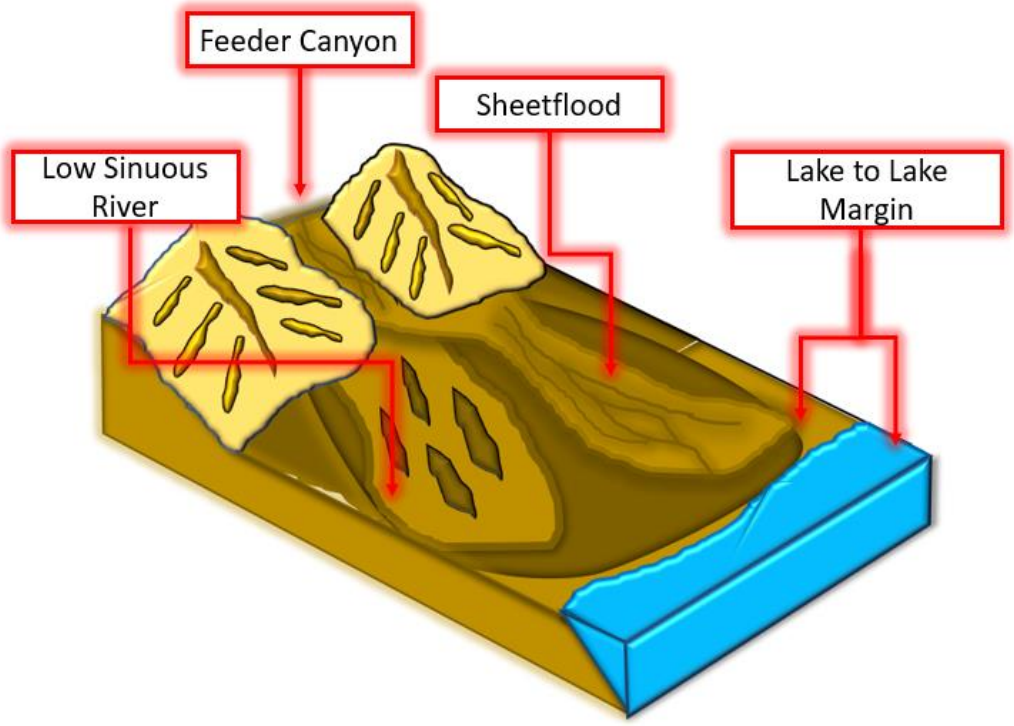

Figure 52. The sedimentological model of the study area.

In general, there are two types of alluvial fan deposit can be observed in the study area which are a sheet flood and stream channel deposits (Figure 52). A sheet flood deposit is interpreted as sheet geometry beds with some sedimentary couplets, while a stream channel deposit has

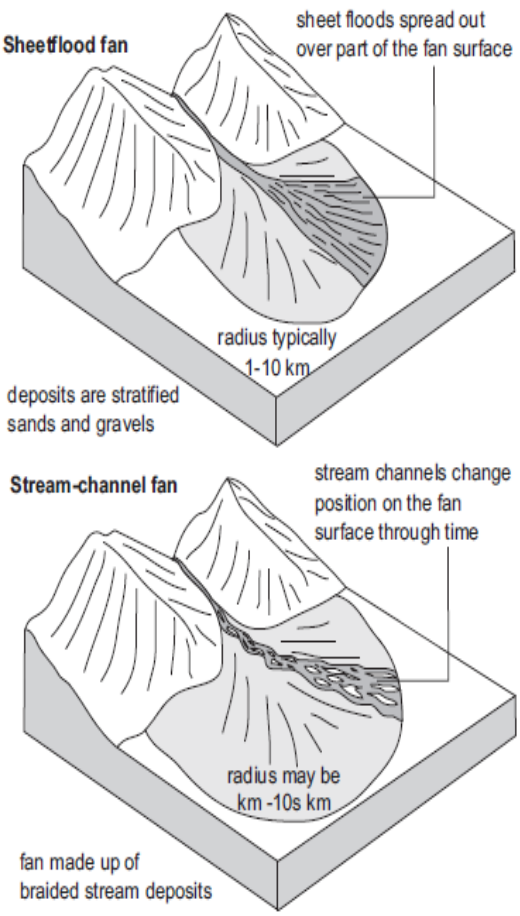

Figure 53. Types of alluvial fan deposit which might occur in the study area. Note that both types of deposit might reach several km in radius distance (Nichols, 2009)

thicker beds with some mud clasts are observed. According to Nichols (2009), mainly the deposition process in these settings is determined by the availability of water, the amount and type of sediment being carried from the feeder canyon and gradient on the fan surface. Therefore, the tectonic activity and climate condition play a big role in here. In arid-semi arid condition, the rainy period is not very frequent. Thus, it also affects different types and amount of the carried sediment. Whilst, the tectonic activity might give influence in controlling the gradient of the slope. A sheet flood deposit occurs in an unconfined flow system during a heavy rainstorm period, in which the sediments are carried as a bedload and in suspension out on to the fan surface. While a stream channel deposit occurs in a more confined type of flow as the emerging river from feeder canyon continue to flow as a channel (Nichols, 2009). Both types of deposit can reach the radius up to 10 Km (Figure 53) and hence increase the connectivity chance of the sandstones interval regionally, as shown in the correlation results. A lacustrine environment is estimated to be located at the distal part of this alluvial plain setting. It is characterized by a claystone deposit in some of the target intervals. In the continental setting where a marine influence is limited, the relative base level variation is referred to its water level. Hence, it also controls the available accommodation space for the deposition process.

The study area is bounded by two structural highs of the London-Brabant Massif and the Rhenish Massif in the southern part. These two highs are separated by the RVG which is estimated to act as a feeder canyon during the deposition of the Volpriehausen, Detfurth, Hardegsen and Röt Formation. Regional well correlation in the previous part suggests that the sediment supply was carried in SE-NW overall trend and might confirm the feeder system of the RVG.

The above interpretations are in line with the regional facies distribution of Triassic Successions (Figure 54-56) by Geluk (2005). Based on these schematic interpretations, the study area was mainly covered by an alluvial plain setting which fringing into lake-lake margin environment. The sediment supply was mainly derived from the SE and transported towards NE direction. Several transgression and regression periods can be observed in the study area and resulted into an alternation of alluvial plain and lacustrine deposits within the Triassic successions. Since only three core data are used during the reservoir sedimentology part, an additional core data analysis is recommended for further study to improve the quality of lithofacies Interpretation.

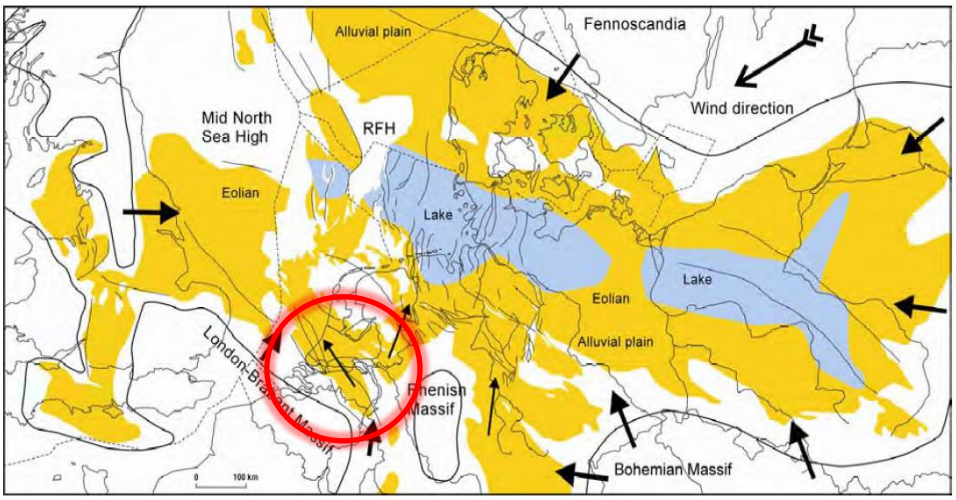

Figure 54. Present day and facies distribution of the Main Buntsandsetin Sub-Group (Geluk, 2005)*. The study area is highlighted by a red circle.*

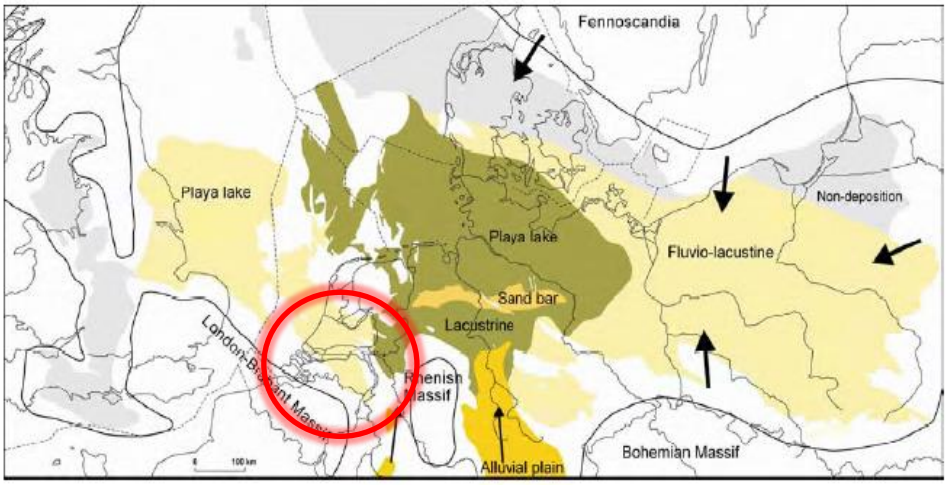

Figure 55. Present day and facies distribution of the Solling Formation (Geluk, 2005)*. The study area is highlighted by a red circle.*

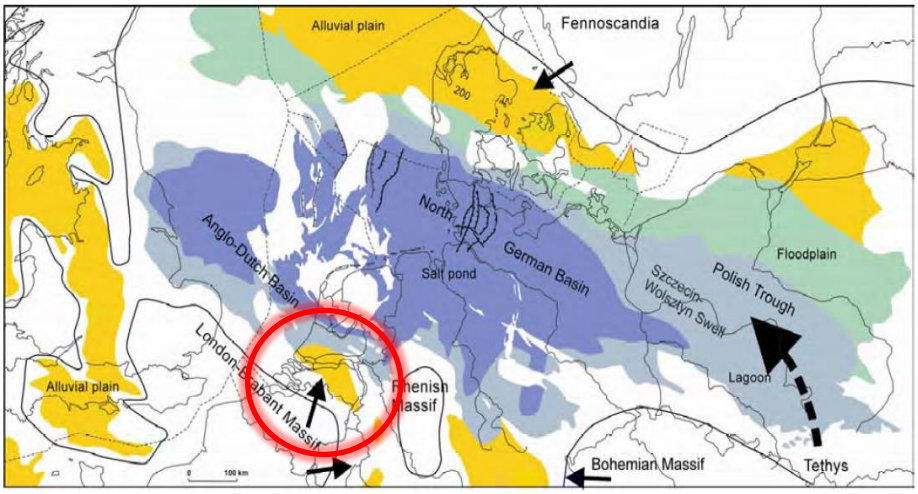

Figure 56. Present day and facies distribution of the Röt Formation (Geluk, 2005)*. The study area is highlighted by a red circle.*

5.2. Reservoir Properties Distribution

The result from petrophysical evaluation in the previous part shows some variation in the reservoir properties within the same target formation at the different well location. Figure 57 displays several plots of various average porosities as a function of depth per well for different target formation. Note that for the Röt Formation, only the unit-2 is plotted as it has higher N/G ratio compare to the other units.

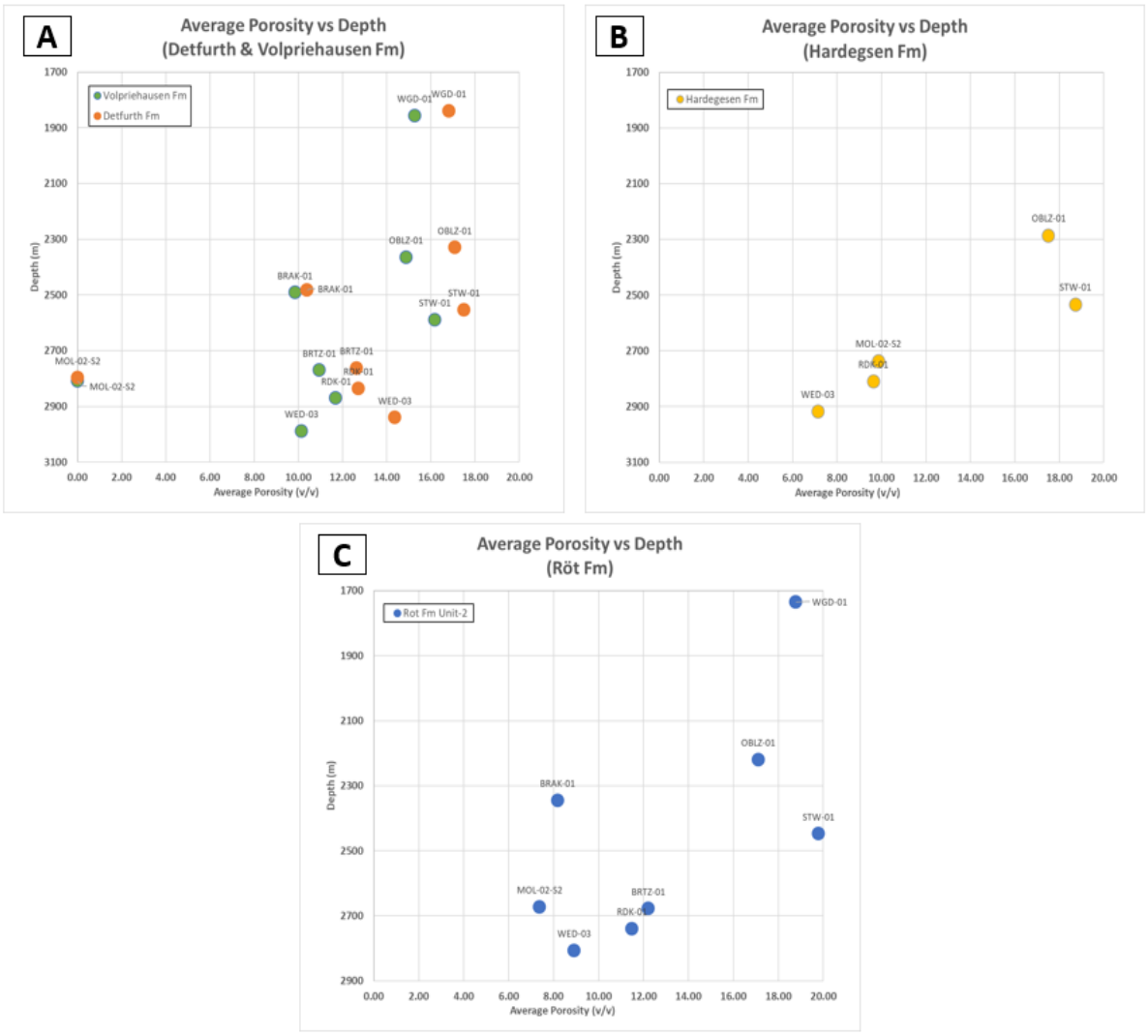

Figure 57. Cross-plot of average porosity vs depth per well for (A) the Detfurth and Volpriehausen Formation, (B) the Hardegsen Formation, and (C) the Röt Formation.

Based on Figure 57, it can be observed that the average porosities at the deeper level are lower than the shallower depth. This relation can be seen at each formation and suggests an inverse relation between the porosity value and depth. This might highlight the compaction effect as it increases with depth and thus decreases the porosity value. However, the relation is quite distorted in the study area, in which a non-linear trend is observed. According to Geluk (2007), the Triassic deposit was influenced by an extensional and inversion tectonic episode which resulted to some differentiated subsidence and uplift movement in the most areas in the Netherlands and therefore affected its reservoir properties. Several examples of differentiated subsidence and uplift can be observed in the wells MOL-02-S2 and WGD-01, where both of wells have a lower porosity compared to other wells which located in the same or deeper level. According to seismic interpretation result, a relatively major uplift and subsidence are

observed in the east flank of the area where the wells MOL-02-S2, WGD-01, WED-03, and BRAK-01 are located. Unlike in the east side, a relatively minor uplift and subsidence are detected in the west side of the area.

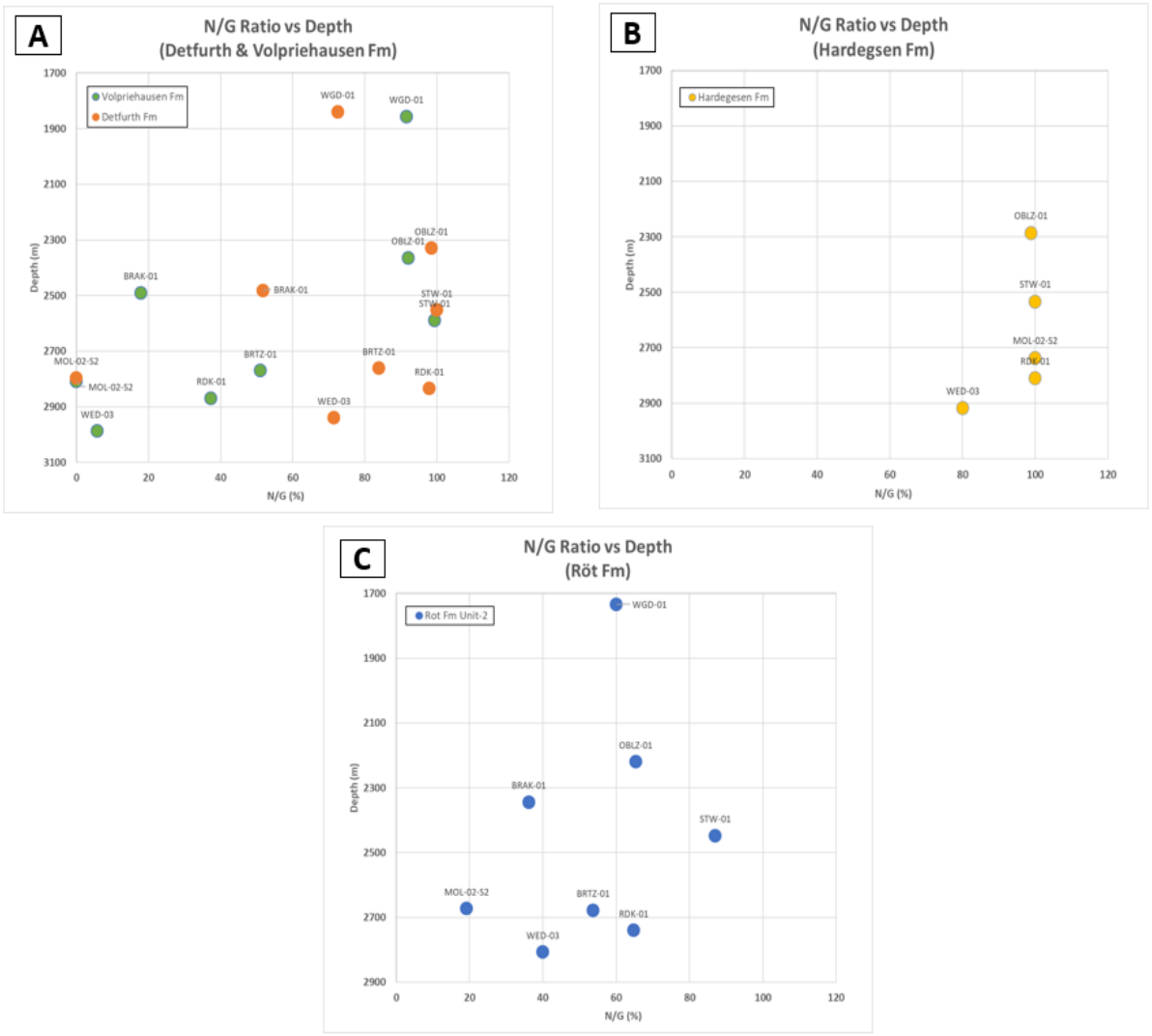

Figure 58. Cross-plot of N/G ratio vs depth per well for (A) the Detfurth and Volpriehausen Formation, (B) the Hardegsen Formation, and (C) the Röt Formation.

The implemented cut-offs of vshale and permeability in the previous analysis are performed to investigate the net reservoir interval. Figure 58 shows the plot of N/G ratio in function of depth per well for each formation. Based on this plot, a quite similar trend with porosity plot (Figure 57) can be recognized here. In general, a relatively higher N/G ratio is discovered at the shallower level and vice versa. This is logical as the permeability value is estimated from porosity value. The N/G ratio in the shallower wells such as STW-01, OBLZ-01, and WGD-01 are higher than the deeper wells such as MOL-02-S2, WED-03, BRAK-01, RDK-01 and BRTZ-01. However, since the shale volume cut-off is also applied, thus the relation is also influenced by this factor. According to the plot result, it can be observed that the Hardegsen Formation has a higher N/G ratio compared to the other formations. This implies that a relatively clean sandstone interval is developed in this interval and indicate a potential target for this project.

The above analysis shows that the reservoir properties are affected by the compaction effect. Since the focus of this study is to determine the most suitable area for geothermal application,

hence this effect has to be considered despite the expected temperature that will be encountered. Moreover, as the study area was majorly influenced by extensional and inversion episodes, a maximum burial history study is recommended to be performed to investigate the impact of uplifting and burial to the reservoir properties distribution.

5.3. Proposed Doublet Location

Two doublet locations in the study area are determined in this part based on the analysis results which are conducted in the previous chapter. In general, the ideal reservoir for geothermal application has a temperature >70°C, a relatively good permeability (>30 mD) and a thickness of preferably >30 m (Lokhorst & Wong, 2007). Therefore, the selection of the doublet location is performed by considering the aforementioned conditions. The distance between the producer and injector well is set to be 1500 m. The proposed doublet locations within the study area are presented in Figure 59. The Röt Formation depth structural map is used in this evaluation as it sits at a shallower level. The X and Y coordinates for both proposed doublets are presented in Table 5.

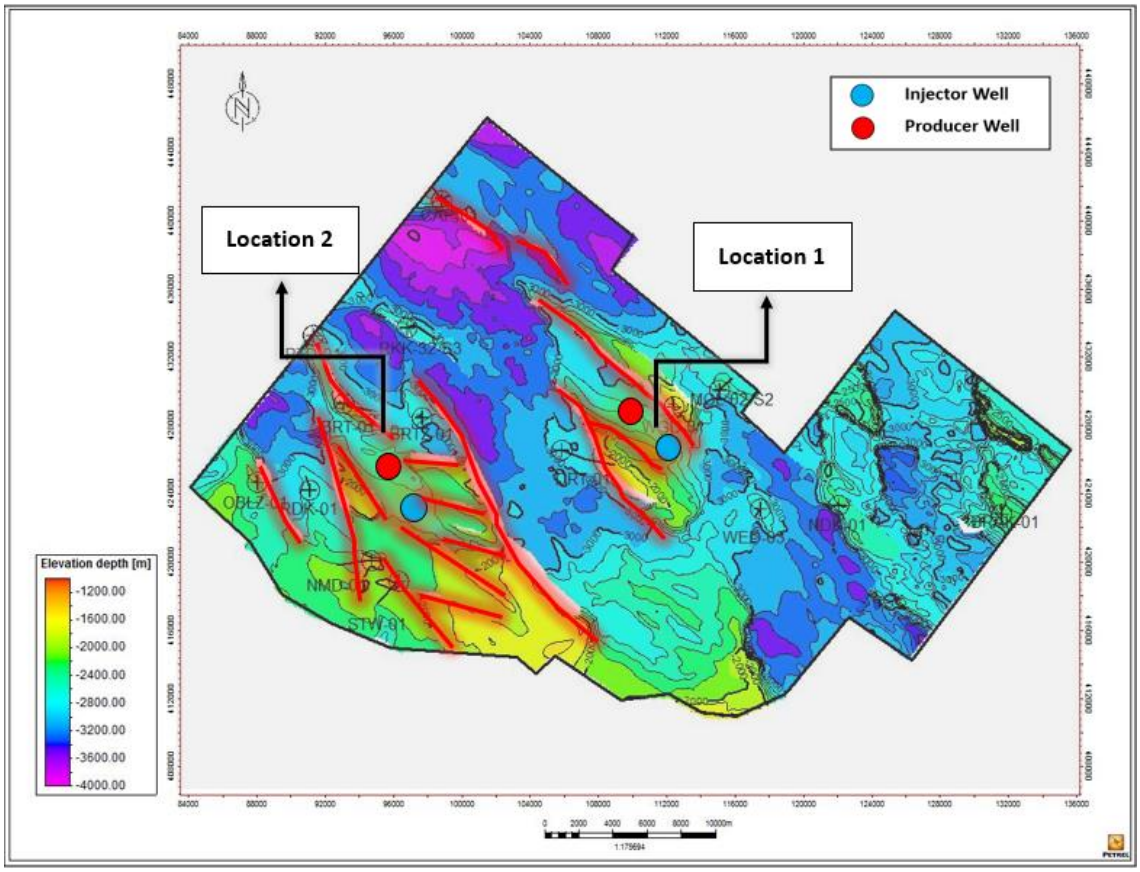

Figure 59. The proposed doublet locations within the study area. Note that the well symbols represent the surface location of the well.

Table 5. The X and Y coordinates for both of the proposed doublet locations.

Info	Well	X (RD)	Y (RD)
Location-1	Injector	110982.10	427109.65
	Producer	109589.5	427940.19
Location-2	Injector	96319.52	95784.01
	Producer	423963.4	425149.51

The first location is on the east flank of the study area. Based on the generated isopach maps in the sub-chapter 4.1, the estimated thickness for the Röt (Unit-2), Detfurth, and Volpriehausen Formation in this location are around 50, 10 and 135 m respectively. The Hardegsen Formation is absent in this area. The doublet is estimated to encounter the Röt, Detfurth, and Volpriehausen Formations at a depth of around 2400-2500 m, 2590-2600 and 2600-2800 m respectively. Thus, the average porosity for each formation can be inferred from the well STW-01 as it encountered the target formations within the quite similar depth range of the proposed doublet (Table 4).

In order to make sensitivity analysis of the estimated reservoir properties, various scenarios from low to high cases are generated for each parameter. The value for the low, medium and high case of expected thickness and N/G are estimated from 10th, 50th and 90th percentiles from the calculated petrophysical averages for different reservoir targets as presented in Table. 4. An exception is made for the expected thickness value in medium case which is estimated from the corresponding formation isopach map. The estimated average porosity value is obtained from the well STW-01. While for the estimated permeability for each case are calculated form a relation between average porosity and various average permeability (low, medium and high) in Table.4. The relation of average porosity vs average permeability for each case are presented in Figure 60. The reservoir properties of each target formation for doublet location-1 are summarized in Table 6, 7 and 8.

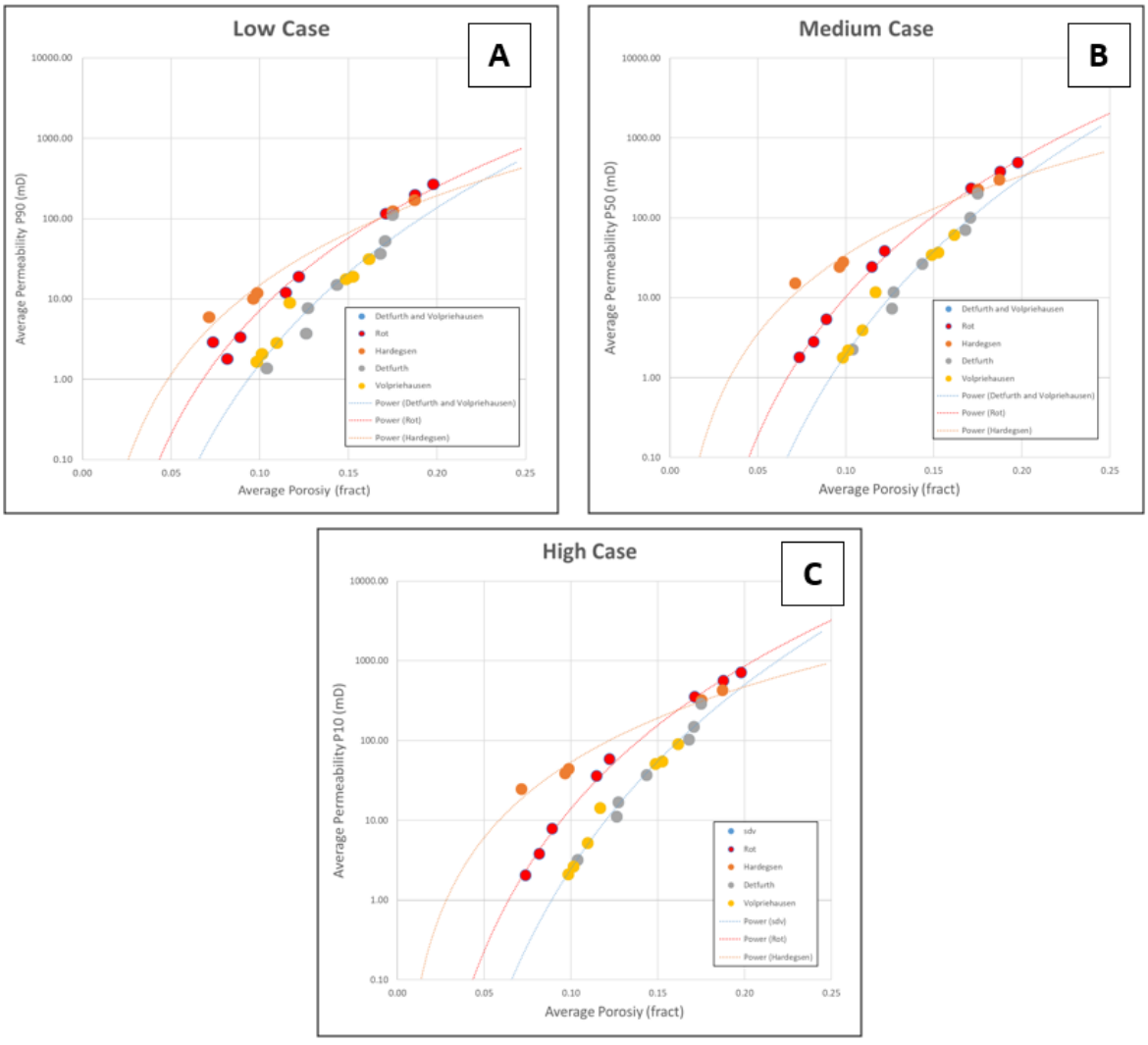

Figure 60. The average porosity-permeability relation for (A) low case, (B) medium case, and (C) High case.

Table 6. The expected reservoir properties of the Röt Formation for doublet location-1.

Röt Formation			
Reservoir Properties	**Low**	**Medium**	**High**
Expected Thickness (m)	30	50	70
N/G (%)	31	57	72
Expected Porosity (fract)	0.20	0.20	0.20
Expected Permeability (mD)	249.99	554.60	718.75

Table 7. The expected reservoir properties of the Detfurth Formation for doublet location-1.

Detfurth Formation			
Reservoir Properties	**Low**	**Medium**	**High**
Expected Thickness (m)	8	10	41
N/G (%)	64	84	99
Expected Porosity (fract)	0.17	0.17	0.17
Expected Permeability (mD)	53.04	90.00	129.97

Table 8. The expected reservoir properties of the Volpriehausen Formation for doublet location-1.

Volpriehausen Formation			
Reservoir Properties	**Low**	**Medium**	**High**
Expected Thickness (m)	124	135	157
N/G (%)	13	51	95
Expected Porosity (fract)	0.16	0.16	0.16
Expected Permeability (mD)	35.84	57.68	81.75

The second location is on the west flank of the study area. The estimated thickness for the Röt (Unit-2), Hardegsen, Detfurth, and Volpriehausen are around 40, 15, 30 and 140 m respectively. The doublet is encountered the same depth range as STW-01 in which the Röt Formation is located in depth 2400-2600 m. Hence, the analog average porosity can also be estimated from it as well. The estimated parameters for each case are generated using the same approach as the previous explanation. The summarized reservoir properties of each formation target for doublet location-2 are presented in Table 9, 10, 11, and 12.

Table 9. The expected reservoir properties of the Röt Formation for doublet location-2.

Röt Formation			
Reservoir Properties	**Low**	**Medium**	**High**
Expected Thickness (m)	30	40	70
N/G (%)	31	57	72
Expected Porosity (fract)	0.20	0.20	0.20
Expected Permeability (mD)	249.99	554.60	718.75

Table 10. The expected reservoir properties of the Hardegsen Formation for doublet location-2.

Hardegsen Formation			
Reservoir Properties	**Low**	**Medium**	**High**
Expected Thickness (m)	8	15	41
N/G (%)	88	93	100
Expected Porosity (fract)	0.19	0.19	0.19
Expected Permeability (mD)	159.97	282.43	401.81

Table 11. The expected reservoir properties of the Detfurth Formation for doublet location-2.

Detfurth Formation			
Reservoir Properties	**Low**	**Medium**	**High**
Expected Thickness (m)	8	30	41
N/G (%)	64	84	99
Expected Porosity (fract)	0.17	0.17	0.17
Expected Permeability (mD)	53.04	90.00	129.97

Table 12. The expected reservoir properties of the Volpriehausen Formation for doublet location-2.

Volpriehausen Formation			
Reservoir Properties	**Low**	**Medium**	**High**
Expected Thickness (m)	124	140	157
N/G (%)	13	51	95
Expected Porosity (fract)	0.16	0.16	0.16
Expected Permeability (mD)	35.84	57.68	81.75

A rough estimation of temperature distribution in doublet location is performed by applying the average thermal gradient of 31°C/km with an additional surface temperature of 10°C (Van Dalfsen, 1981). The result of temperature distribution for Base Altena (Top Triassic) in the study area is presented in Figure 61. The result displays that the proposed locations have sufficient estimated temperature which is >70°C. However, a more advanced temperature estimation is recommended to obtain more precise gradient temperature at doublet location prior to the drilling execution. Since the temperature gradient may vary at a different location of the study area.

In order to maintain the pressure communication between the injector and producer well, both of the proposed doublets are designed to follow the SE-NW overall trend of the deposition. This is done with the objective to reduce the risk of connectivity loss of the targeted reservoir. Moreover, this orientation is also parallel with the main fault trend and will minimize the presence of faults chance in between the two wells. The injector is proposed to be located at the shallower level than the producer to allow for gravity-driven flow propagation (Donselaar, Groenenberg, & Gilding, 2015). Since the area is highly faulted, a fault seal analysis study is recommended to assess the sealing capacity of the surrounding faults. The seismic cross-sections for both proposed doublet locations are presented in Figure 62-67.

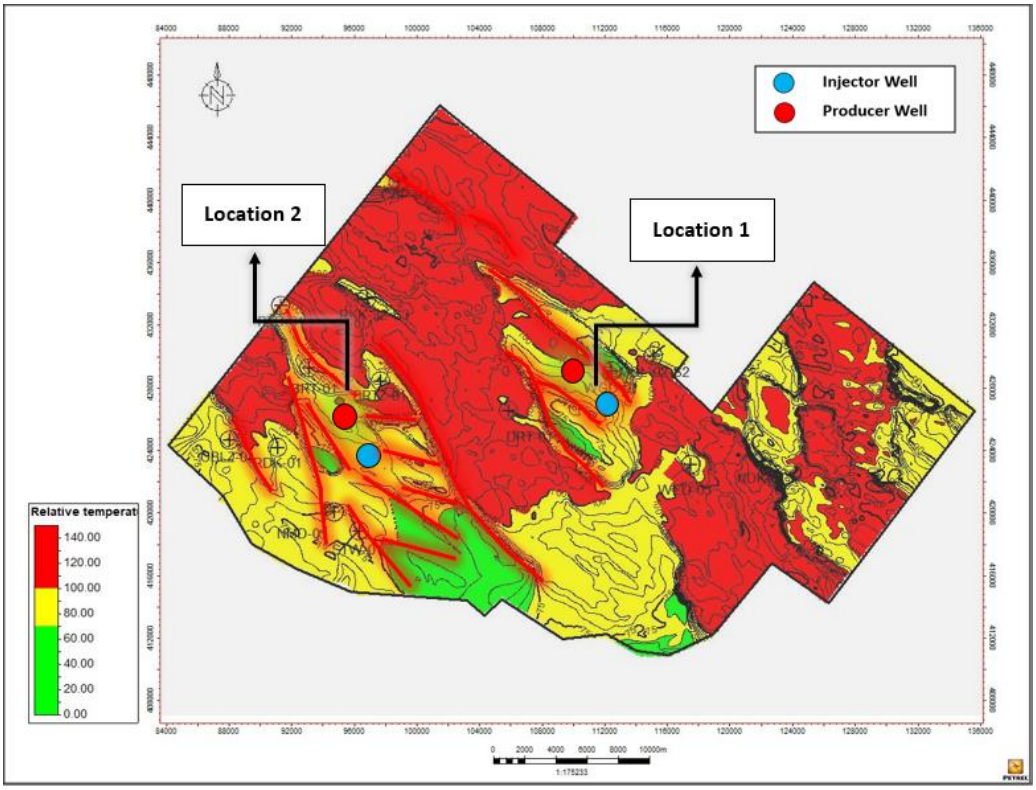

Figure 61. The estimated temperature distribution map of the study area.

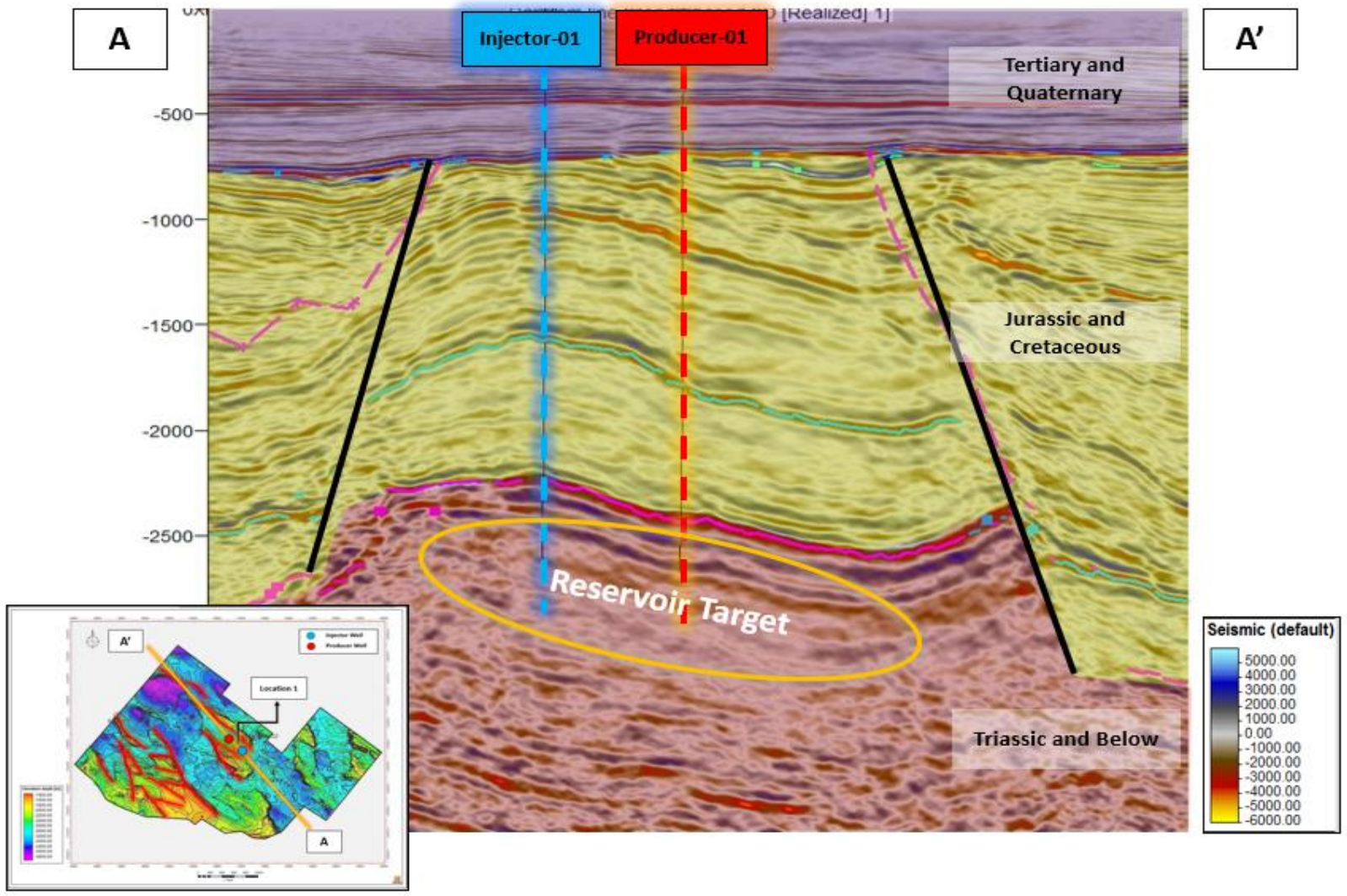

Figure 62. A SE-NW seismic cross-section for the injector (Blue) and producer (Red) wells for the proposed location-1. Note that the dashed line for each well does not represent the true well trajectory.

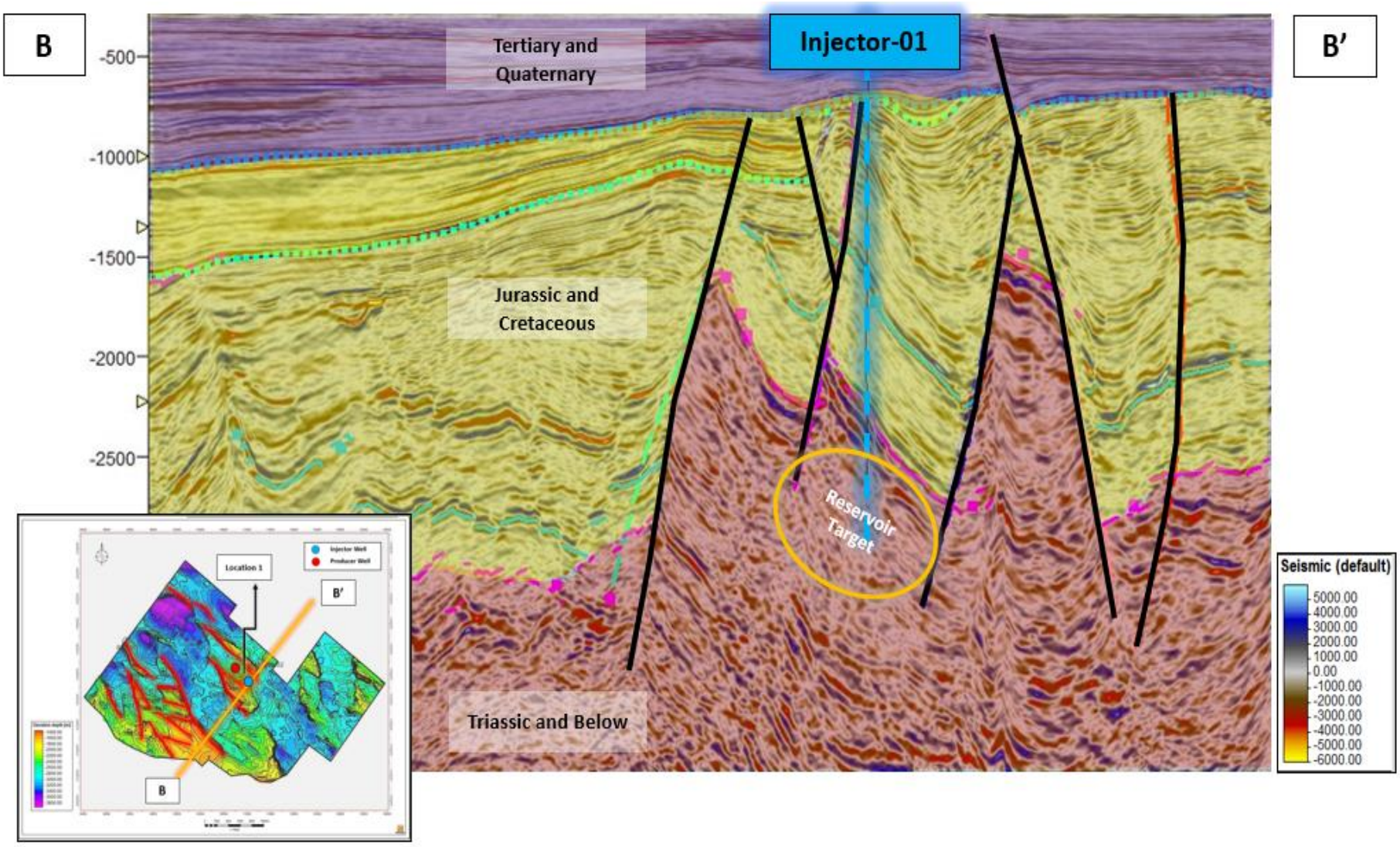

Figure 63. A seismic cross-section from IL-4405 for the injector (Blue) well of the proposed location-1. Note that the dashed line for each well does not represent the true well trajectory.

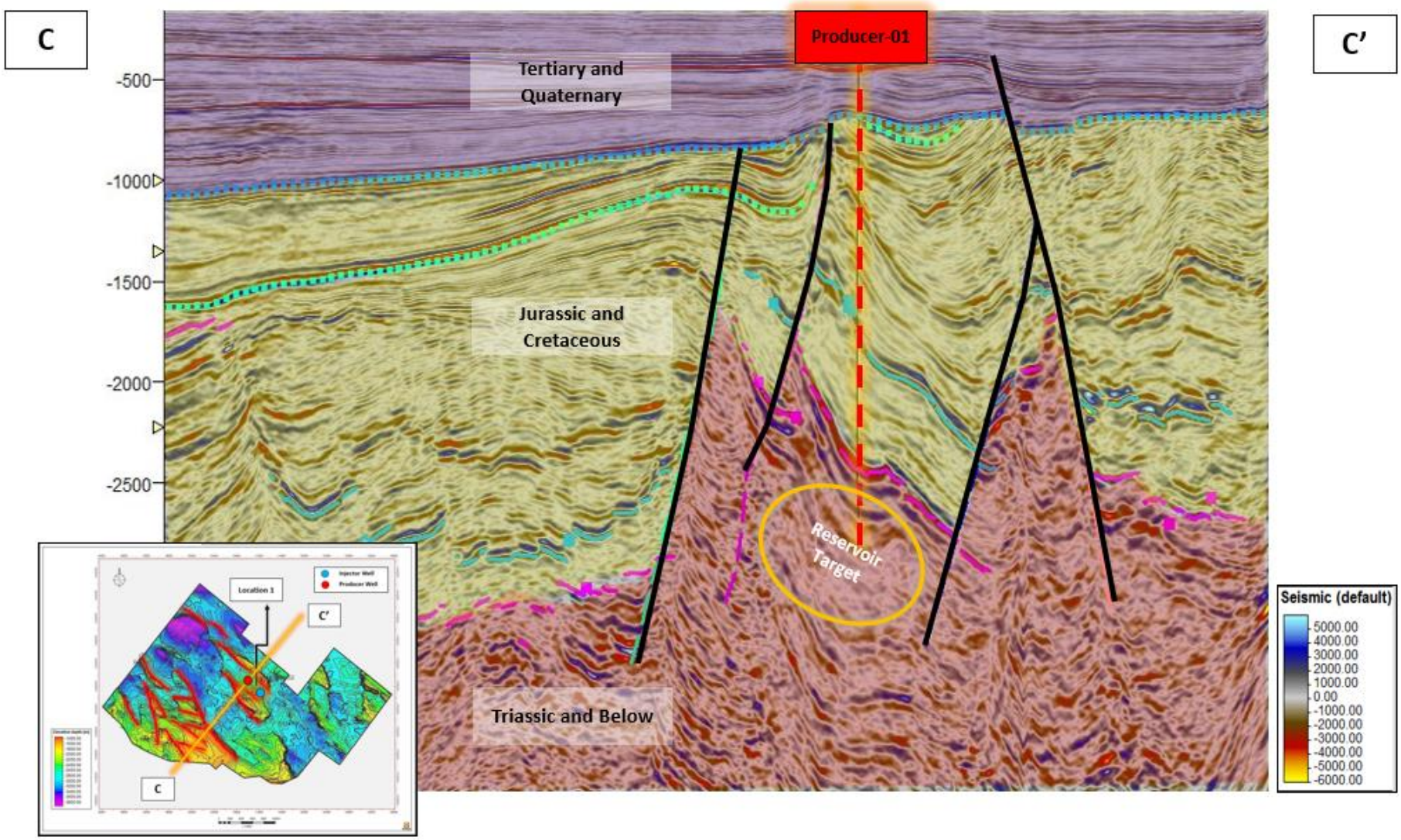

Figure 64. A seismic cross-section from IL-3933 for the producer (red) well of the proposed location-1. Note that the dashed line for each well does not represent the true well trajectory.

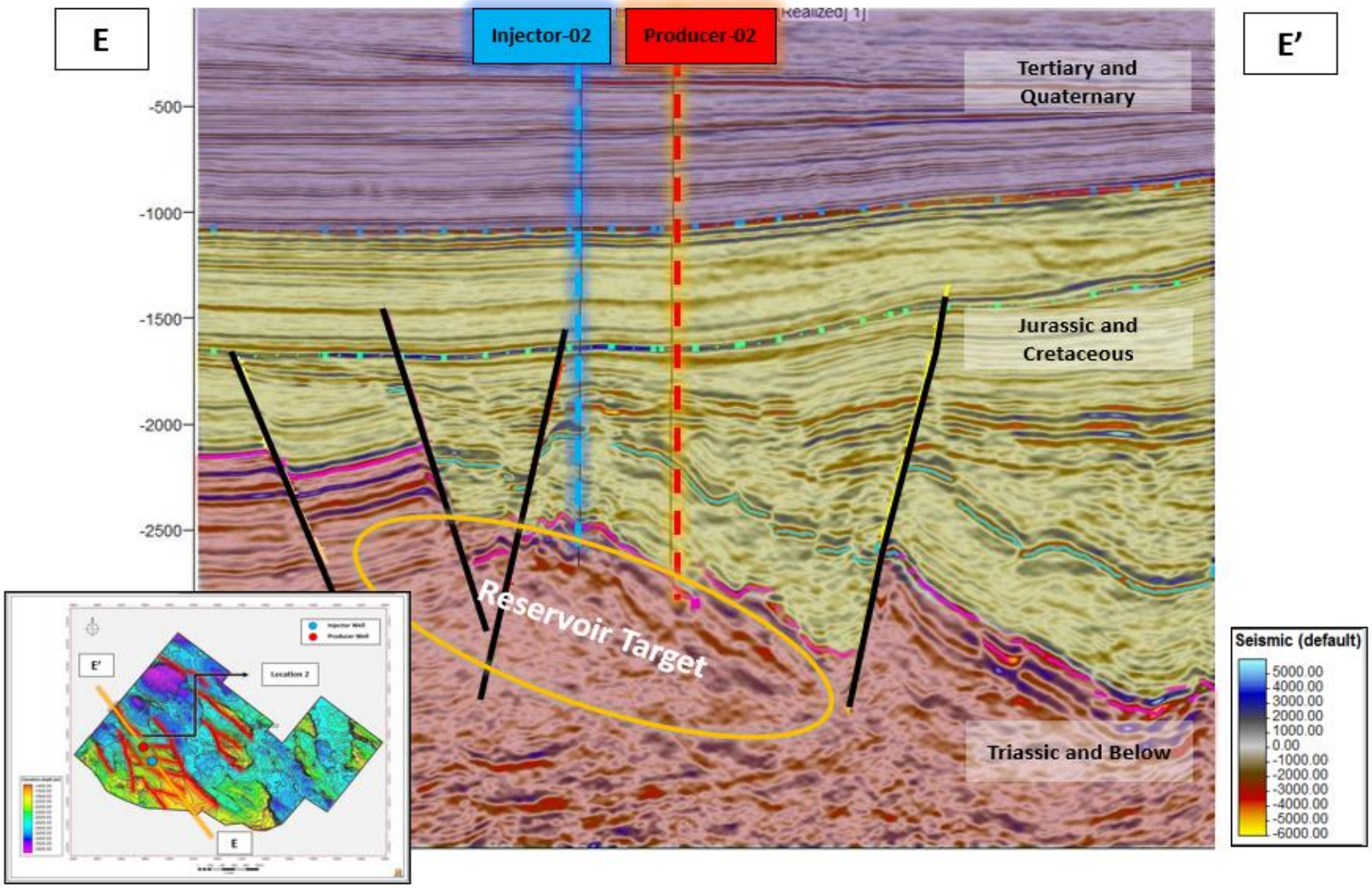

Figure 65. A SE-NW seismic cross-section for the injector (Blue) and producer (Red) wells for the proposed location-2. Note that the dashed line for each well does not represent the true well trajectory.

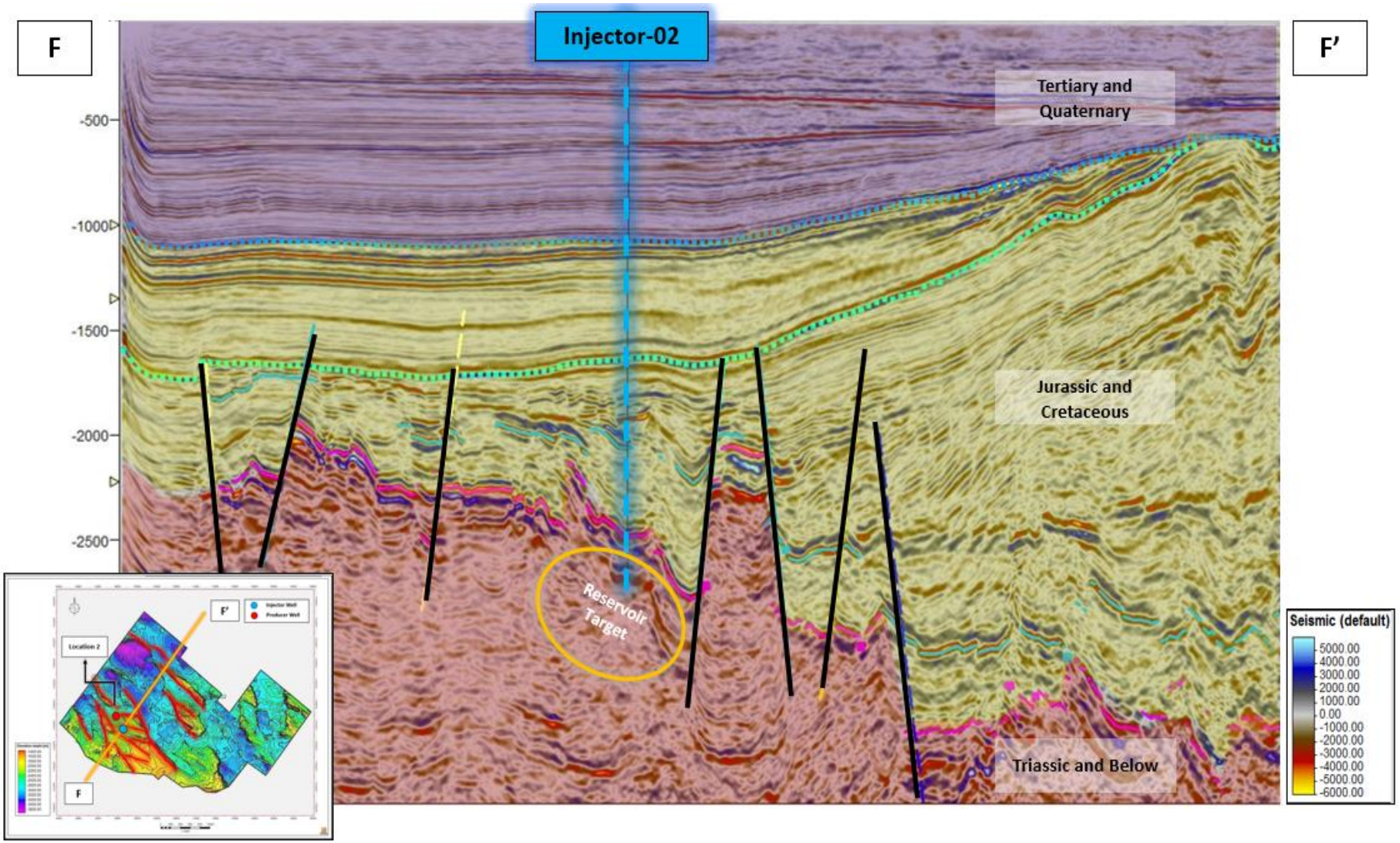

Figure 66. A seismic cross-section from IL-4235 for the injector (Blue) well of the proposed location-2. Note that the dashed line for each well does not represent the true well trajectory.

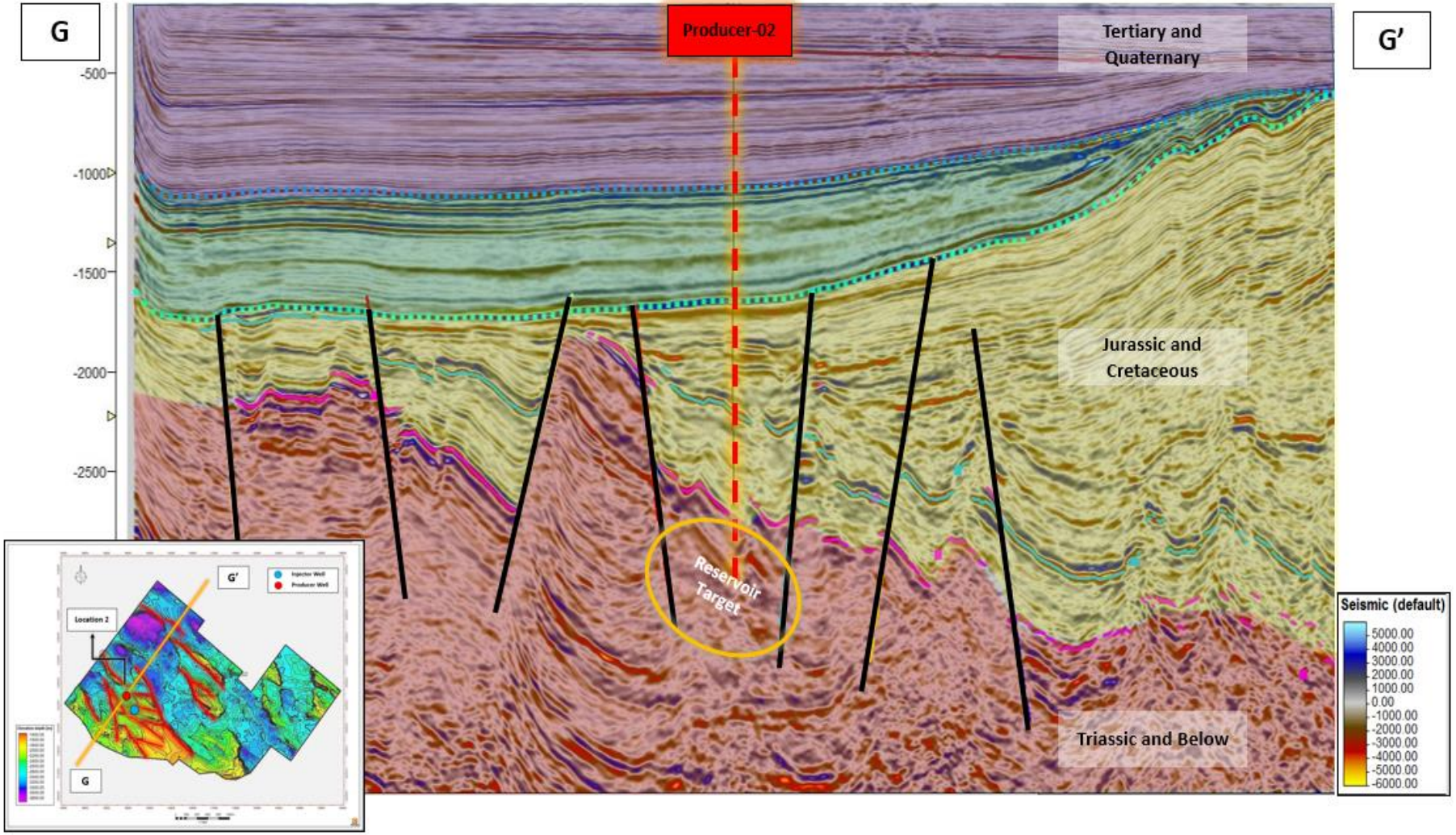

Figure 67. A seismic cross-section from IL-3853 for the producer (red) well of the proposed location-2. Note that the dashed line for each well does not represent the true well trajectory

6 Conclusions and Recommendations

In this research, the Triassic successions within the Drechtsteden area in the WNB are evaluated for its potential for geothermal energy production. A reservoir characterization approach is implemented during the process to determine the most suitable area for deployment of doublet applications. Several points can be concluded based on the results of this study:

- From the regional geology and literature study result show that sandstone intervals within the Triassic successions occur in the Röt-, Hardegsen-, Detfurth- and Volpriehausen Formation.
- Seismic interpretation is performed in the study area to investigate the geometry and structural features of the targeted reservoirs. The result shows that the top of the Triassic successions (Base Altena) still can be traced in some parts of the area despite its position in the deeper level of the subsurface. However, the individual formations within the Triassic successions are not clearly visible in most part of the area. Thus, the interpretation on that levels are completed by using the isopach maps which are generated from the available well tops with Base Altena horizon as a reference.
- Based on the fault interpretation result, the study area is characterized by NW-SE major faults trending in which dissected the study area into the tilted fault block. The interpreted faults divide the area into three compartments where the Triassic level sits deeper in the middle section. Pronounced syn-rift and inversion features such as half-graben structures and reactivation of the existing fault can be seen in some parts of the area.
- The generated isopach maps show a different trend of thickness distribution for each formation. The result shows that some of the targeted formations such as the Hardegsen and Detfurth Formation are subjected to uplift and erosional periods as the thickness of these formations vary significantly from location to locations.
- Reservoir sedimentology analysis is conducted by utilizing the available well logs data and three core data from the Röt and Hardegsen intervals of wells OBLZ-01 and WGD-01. The analysis result shows that the sandstone intervals within the Triassic successions are composed of the stacked of low sinuous river and sheet flood deposits with some interbedded lake to lake margin deposits.
- The regional correlation suggests that the sand bodies within each formation can be correlated over distances of kilometers, hence increase the connectivity chance of the sandstones interval regionally.
- The interpretation of lithofacies and regional well correlation in the reservoir sedimentology sub-chapter have allowed a sedimentological model to be constructed. The result shows that the study area is mainly covered by an alluvial plain setting which fringing into lake-lake margin environment. The sediment supply was mainly derived from the SE and transported towards NE direction which might confirm the feeder

system of the RVG. Several transgression and regression periods were estimated to occur in the study area and resulted into an alternation of alluvial plain and lacustrine deposits within the Triassic successions.

- Since only three core data are used during the reservoir sedimentology part, an additional core data analysis is recommended for further study to improve the quality of lithofacies Interpretation.
- In order to evaluate the reservoir properties, a petrophysical evaluation is conducted. The result displays some variation in reservoir properties (N/G, average porosity, and permeability) at a different location within the study area.
- A notable decrease in reservoir properties (porosity and permeability) at greater depths are observed. This might indicate that compaction with the increasing depth plays a large role. However, the relation is quite distorted in the study area as a response to differentiated subsidence and uplift movement due to an extensional and inversion tectonic episode. A maximum burial history study is recommended to be performed to investigate the impact of uplifting and burial to the reservoir properties distribution.
- Two doublet locations in the study area are determined based on the analysis results in the previous chapter. the selection of the doublet location is performed by considering several parameters such as the required temperature of >70°C, a relatively good permeability (>30 mD) and a thickness of preferably >30 m.
- The first location is on the east flank of the area and the second on the west side of it. The distance between the producer and injector well is set to be 1500 m. Both of the proposed doublets are designed to follow the SE-NW overall trend of the deposition to maintain the pressure communication between the doublet. Moreover, this orientation is also parallel with the main fault trend and will minimize the presence of faults chance in between the two wells. The injector is designed to be located at the shallower level than the producer to allow for gravity-driven flow propagation. Fault seal analysis is proposed to evaluate the sealing capacity of the available faults. As the area is characterized by numerous faults with varying offsets.
- A rough estimation of temperature distribution in doublet location is done by applying the average thermal gradient of 31°C/km with an additional surface temperature of 10°C. The result displays that the proposed locations have sufficient estimated temperature which is >70°C. Since the temperature gradient may vary at a different location of the study area, a more advanced temperature estimation using Borehole Temperature (BHT) gradient analysis is recommended to obtain more precise gradient temperature at doublet location prior to the drilling execution.
- The expected reservoir properties at the proposed doublet locations are estimated from the depth range of penetrated doublet, the generated isopach maps, and petrophysical averages on the evaluated wells within the study area by a statistical approach. In order to make sensitivity analysis of the estimated reservoir properties, various scenarios from low to high cases are generated for each parameter.

Bibliography

Ames, R., & Farfan, P. F. (1996). The environments of deposition of the Triassic Main Buntsandstein Formation in the P and Q quadrants, offshore the Netherlands. In H. E. Rondeel, D. A. J. Batjes, & W. H. Nieuwenhuijs (Eds.), Geology of Gas and Oil under the Netherlands (pp. 167–178). Kluwer Academic Publishers.

Heekeren, van, V., & Bakema, G. (2015). The Netherlands Country Update on Geothermal Energy. Proceedings World Geothermal Congress 2015, Melbourne, Australia, 19-25 April, 2013(April), 2–7.

Betts, P. (2017). Permeability Prediction. Lecture presented at Field Development Project in TU Delft, Delft.

Cecil, C. B. (2003). The concept of autocyclic and allocyclic controls on sedimentation and stratigraphy, emphasizing the climatic variable.

De Jager, J., Doyle, M. A., Grantham, P. J., & Mabillard, J. E. (1996). Hydrocarbon habitat of the West Netherlands Basin. In H. E. Rondeel, D. A. J. Batjes, & W. H. Nieuwenhuijs (Eds.), Geology of Gas and Oil under the Netherlands (p. 1996). Dordrecht: Kluwer Academic Publishers. https://doi.org/10.1002/ecy.1501

De Jager, J. (2003). Inverted basins in the Netherlands, similarities and differences. Geologie En Mijnbouw/Netherlands Journal of Geosciences, 82(4), 355–366. https://doi.org/10.1017/S0016774600020175

De Jager, J. (2007). Geological development. Geology of the Netherlands, 5-26.

DeVault, B., & Jeremiah, J. (2002). Tectonostratigraphy of the Nieuwerkerk Formation (delfland subgroup), West Netherlands Basin. AAPG Bulletin, 86(10), 1679–1707. https://doi.org/10.1306/61EEDD50-173E-11D7-8645000102C1865D

Donselaar, M. E., Groenenberg, R. M., & Gilding, D. T. (2015). Reservoir Geology and Geothermal Potential of the Delft Sandstone Member in the West Netherlands Basin. *World Geothermal Congress 2015*, *1*(April), 9.

Geluk, M. C., & Röhling, H. G. (1997). High-resolution sequence stratigraphy of the Lower Triassic 'Buntsandstein'in the Netherlands and northwestern Germany. Geologie en Mijnbouw, 76(3), 227-246.

Geluk, M. (2005). *Stratigraphy and tectonics of Permo-Triassic basins in the Netherlands and surrounding areas*. *Faculty of Geosciences*. Universiteit Utrecht.

Geluk, M. C. (2007). Triassic. *Geology of the Netherlands Edited by Th.E.Wong, D.A.J. Batjes & J. de Jager Royal Netherlands Academy of Arts and Sciences, 2007*, 85–106. https://doi.org/10.1038/232604a0

Geluk, M. C., Plomp, A., & van Doorn, T. H. M. (1996). Development of the Permo-Triassic succession in the basin fringe area, southern Netherlands. *Geology of Gas and Oil under the Netherlands*, (January 1993), 57–78. https://doi.org/10.1007/978-94-009-0121-6_7

Kramers, L., van Wees, J.-D., Pluymaekers, M. P. D., Kronimus, A., & Boxem, T. (2012). Direct heat resource assessment and subsurface information systems for geothermal aquifers; the Dutch perspective. *Netherlands Journal of Geosciences*, *91*(4), 637–649. https://doi.org/10.1017/S0016774600000421

Lokhorst, A., & Wong, T. E. (2007). Geothermal Energy. Geology of the Netherlands, 341–

346. https://doi.org/10.1016/0375-6505(70)90089-1

Nichols, G. (2009). Sedimentology and stratigraphy. John Wiley & Sons.

Racero-Baena, A., & Drake, S. J. (1996). Structural style and reservoir development in the West Netherlands oil province. Geology of Gas and Oil under the Netherlands, 211–227. https://doi.org/10.1007/978-94-009-0121-6

Rondeel, H. E., Batjes, D. A. J., & Nieuwenhuijs, W. H. (1996). Geology of Gas and Oil under the Netherlands.

Sanner, B., Ria, K., Land, A., & Mutka, K. (2011). *Common Vision for the Renewable Heating & Cooling sector in Europe*. *RHC-Platform*. https://doi.org/10.2788/20474

Van Adrichem Boogaert, H. A., & Kouwe, W. F. (1997). Stratigraphic Nomenclature of the Netherlands, Revision and Update by RGD and NOGEPA, Meded. *Rijks Geol. Dienst*, *50*.

Van Dalfsen, W. (1981). *The shallow subsurface temperature field in The Netherlands*. Groundwater Survey TNO.

Appendixes

A. Seismic Data

In this appendix, the configuration of utilized seismic data is presented. The first one is the header of the 3D PSDM dataset in the depth domain. The second is the header of the 3D Post-Stack Time Migration dataset in the time domain.

A.1 3D PSDM Dataset

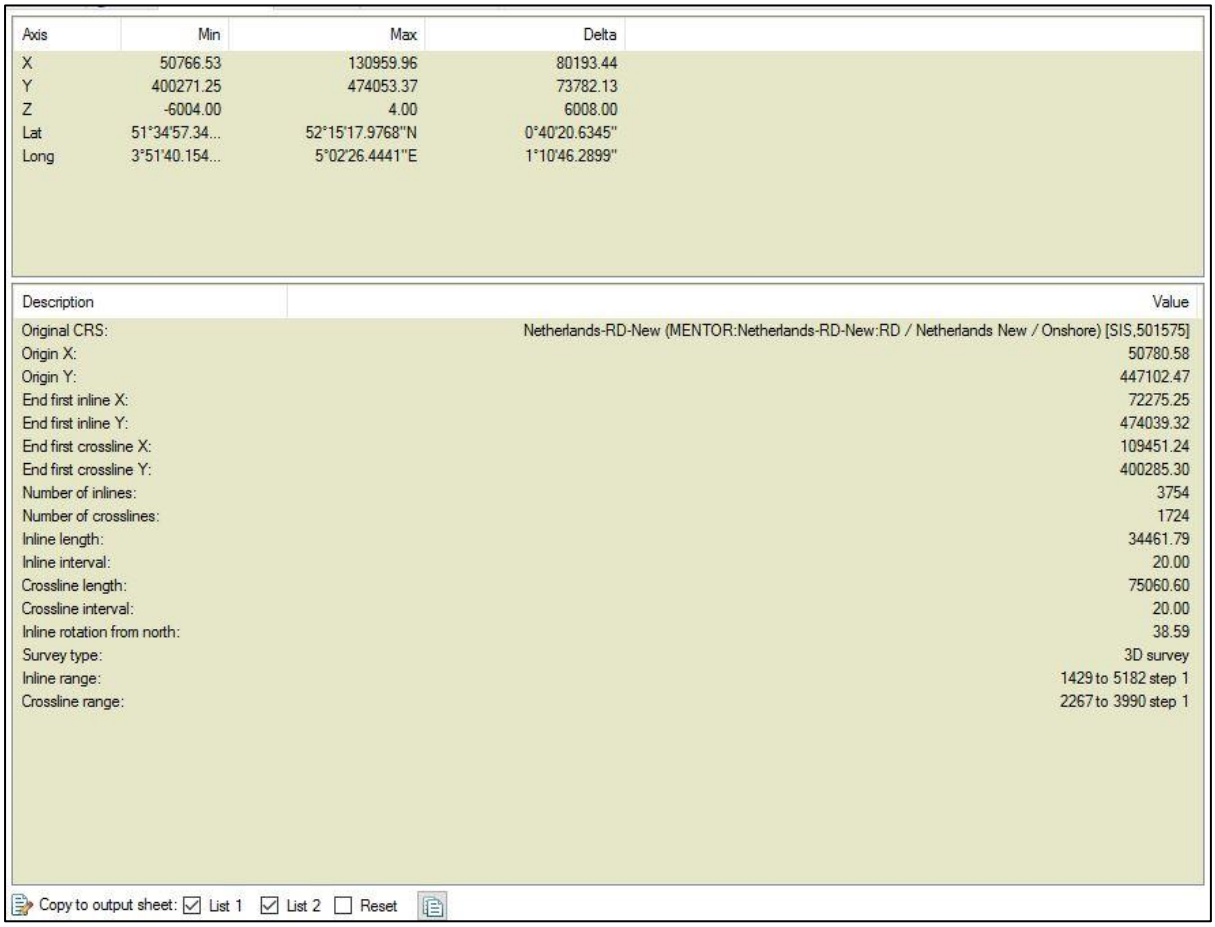

Axis	Min	Max	Delta
X	50766.53	130959.96	80193.44
Y	400271.25	474053.37	73782.13
Z	-6004.00	4.00	6008.00
Lat	51°34'57.34...	52°15'17.9768"N	0°40'20.6345"
Long	3°51'40.154...	5°02'26.4441"E	1°10'46.2899"

Description	Value
Original CRS:	Netherlands-RD-New (MENTOR:Netherlands-RD-New:RD / Netherlands New / Onshore) [SIS,501575]
Origin X:	50780.58
Origin Y:	447102.47
End first inline X:	72275.25
End first inline Y:	474039.32
End first crossline X:	109451.24
End first crossline Y:	400285.30
Number of inlines:	3754
Number of crosslines:	1724
Inline length:	34461.79
Inline interval:	20.00
Crossline length:	75060.60
Crossline interval:	20.00
Inline rotation from north:	38.59
Survey type:	3D survey
Inline range:	1429 to 5182 step 1
Crossline range:	2267 to 3990 step 1

Copy to output sheet: ☑ List 1 ☑ List 2 ☐ Reset

Figure 68. 3D PSDM configuration

A.2 3D Post-Stack Time Migration Dataset

Axis	Min	Max	Delta
X	115793.40	133790.74	17997.35
Y	415941.39	434735.79	18794.41
Z	-4998.00	2.00	5000.00
Lat	51°43'54.34...	51°54'6.065...	0°10'11.716...
Long	4°49'4.4377...	5°04'50.087...	0°15'45.649...

Description	Value
Original CRS:	Netherlands-RD-New (MENTOR:Netherlands-RD-New:RD / Netherlands New / Onshore) [SIS,501575]
Origin X:	115807.45
Origin Y:	422543.31
End first inline X:	125494.59
End first inline Y:	434721.74
End first crossline X:	124089.55
End first crossline Y:	415955.44
Number of inlines:	530
Number of crosslines:	779
Inline length:	15561.33
Inline interval:	20.01
Crossline length:	10582.68
Crossline interval:	20.00
Inline rotation from north:	38.50
Survey type:	3D survey
Inline range:	1105 to 1634 step 1
Crossline range:	730 to 1508 step 1

Figure 69. 3D Post-Stack Time Migration dataset configuration.

B. Well Data

The appendix consists of a well database which lists the available well logs, well-seismic match result for seismic interpretation phase in 3D Post-Stack Time Migration dataset, and well logs for the remaining of the available well.

B.1 Well Database

Table 13. Well database.

Well	Depth From	Depth Until	Cretaceous	Jurassic	Triassic	Info	GR	Porosity	Density	Sonic	Resistivity	Well Shot	Core data
MOL-02-S2	2426	3287				Core desc, analysis, photoghraps and Dip Log Available, Core interval determined from report							2685-2688
NDK-01	0	2677				DLIS, VSP Report available,							
NMD-01	0	2804				DLIS Format							
OAS-01	0	2177				Res-Lateral,long-short, Palynology report, core interval undetermined							913-2128 ??
OBLZ-01	0	2745				DLIS, Core analysis, description and lab reports are available, Core interval determined from report							2202-2296
OBLZ-02	1289	4640				DLIS, Neutron and Res are available in different type of logs							
RDK-01	0	3053				DLIS, Core description, analysis, biostratigraphy reports and photos are available							2722-2735, 2800-2814, 2816-2825
RKK-32-S3	2115	3695				Core photograph available							3312-3329
STR-01	0	2779				No other well logs							
STW-01	0	3101				DLIS, Core Analysis available							2445-2455. 2546-2563
WED-02	0	3516				DLIS, Micro and iInduction log resistivity, SP Log, Core analysis available							2971-3488
WED-03	0	3125				DLIS, Core photos and por-perm analysis available							2821-2982
WGD-01	0	2394				DLIS, Core description and photos available, Wellshot file unidentified yet							1379-1775
BRTZ-01	10	3261				Core photo, desc and analysis available, dipmeter log							2664-2677; 2677-2895
BRT-01	36	3373				Core desc and analysis available, dipmeter log							1696-1704; 1930-1938.7; 1939-1948
BRT-02-S1	16.8	3183.3				VSP in SEGY file, core photos available						segy file	3006.1-3023.8
BRT-02-S2	0.7	3302.1											
BRAK-01	798.3	2694				Core desc and photos available							1154-1160; 2348.9-2369; 2452.52-2479.0
BRTZ-02-S3	1545	3307				VSP in SEGY file, DLIS format available						segy file	
BRTZ-04	5.4	2867.2											
BRTZ-04-S1	2481	3360											
DRT-01	6	4292				Dip log available							
BLK-01	2165	2258				no such logs data measured							
BRTZ-03	2736	3043											

B.2 Well-Seismic Match Result

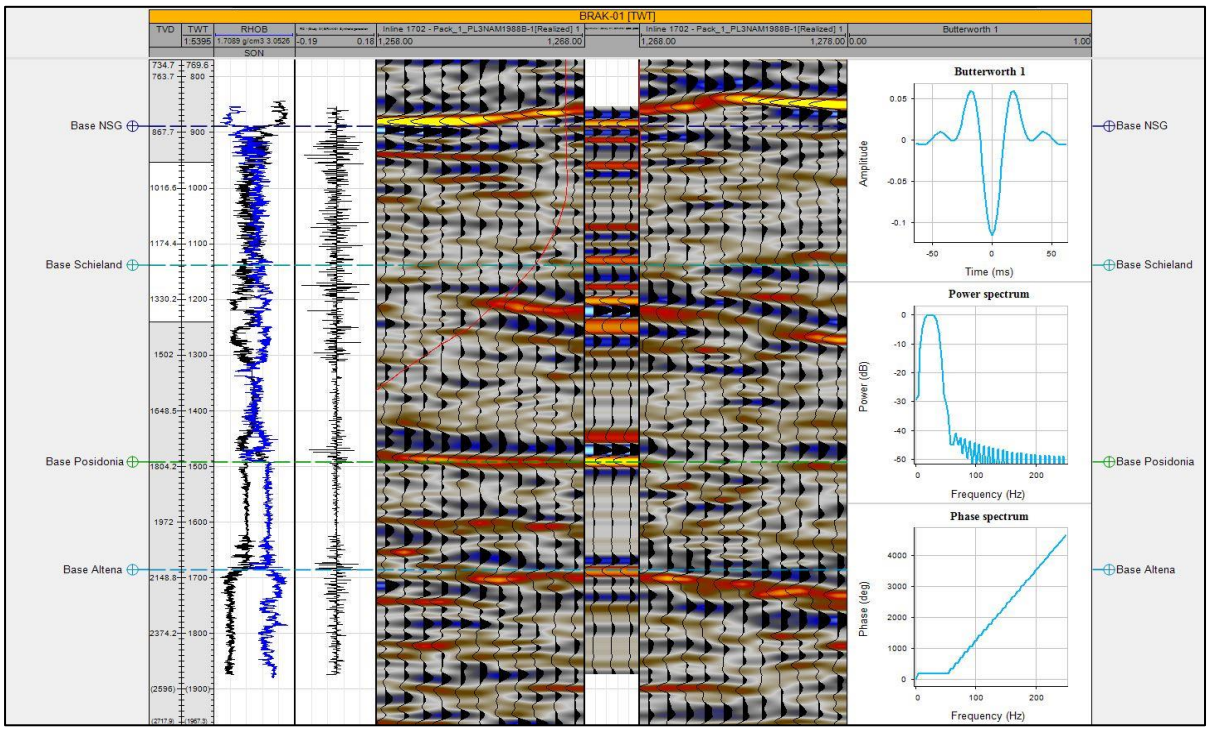

Figure 70. Well-seismic match result for BRAK-01 well.

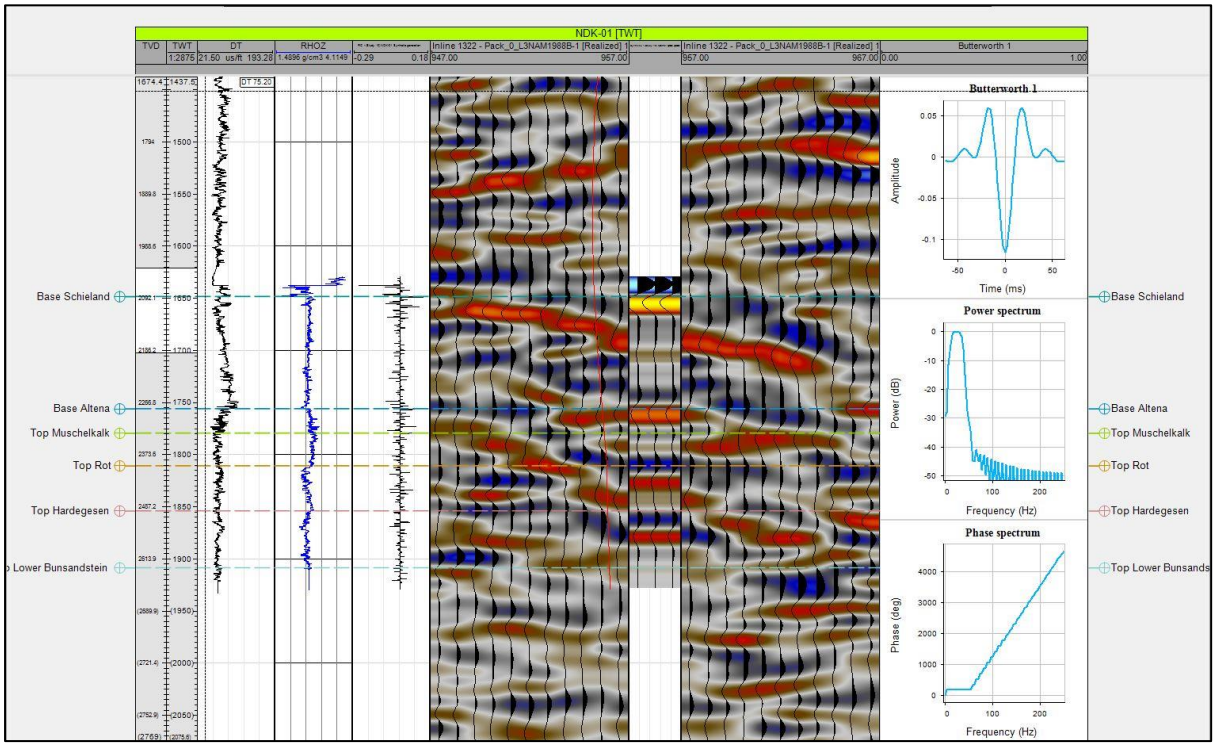

Figure 71. Well-seismic match result for NDK-01 well.

B.3 Well Logs Data

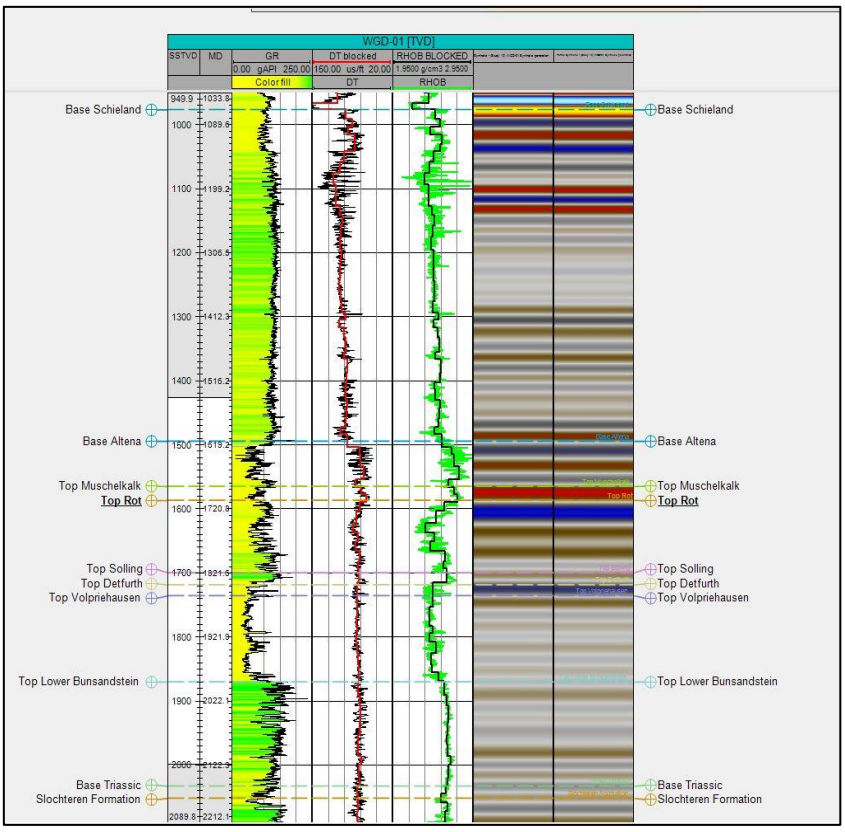

Figure 72. Well logs data of WGD-01 well.

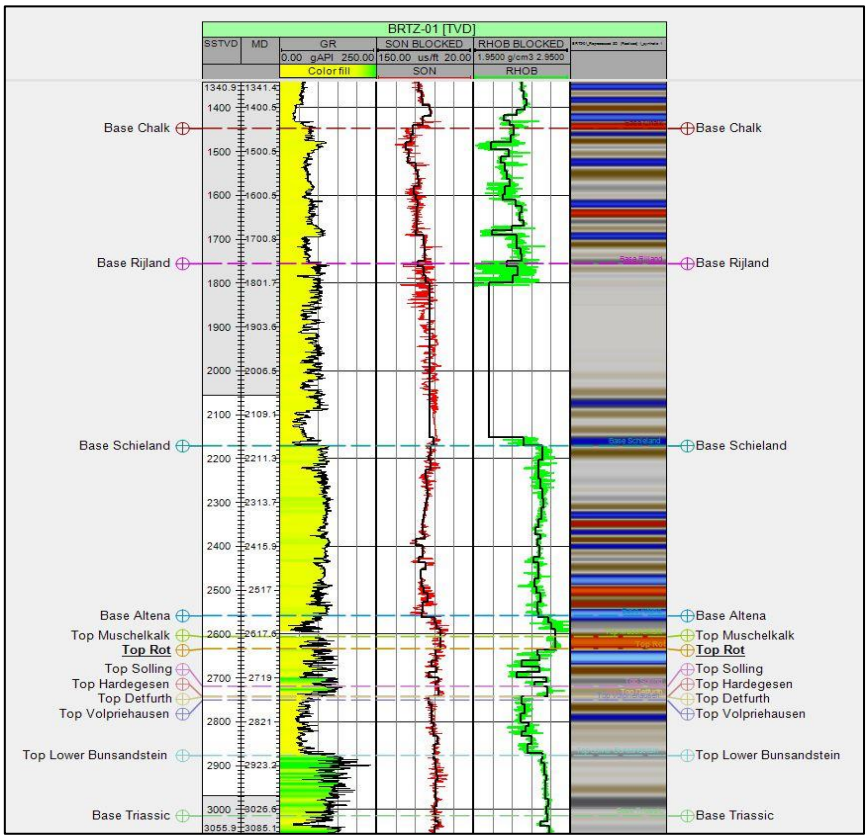

Figure 73. Well logs data of BRTZ-01 well.

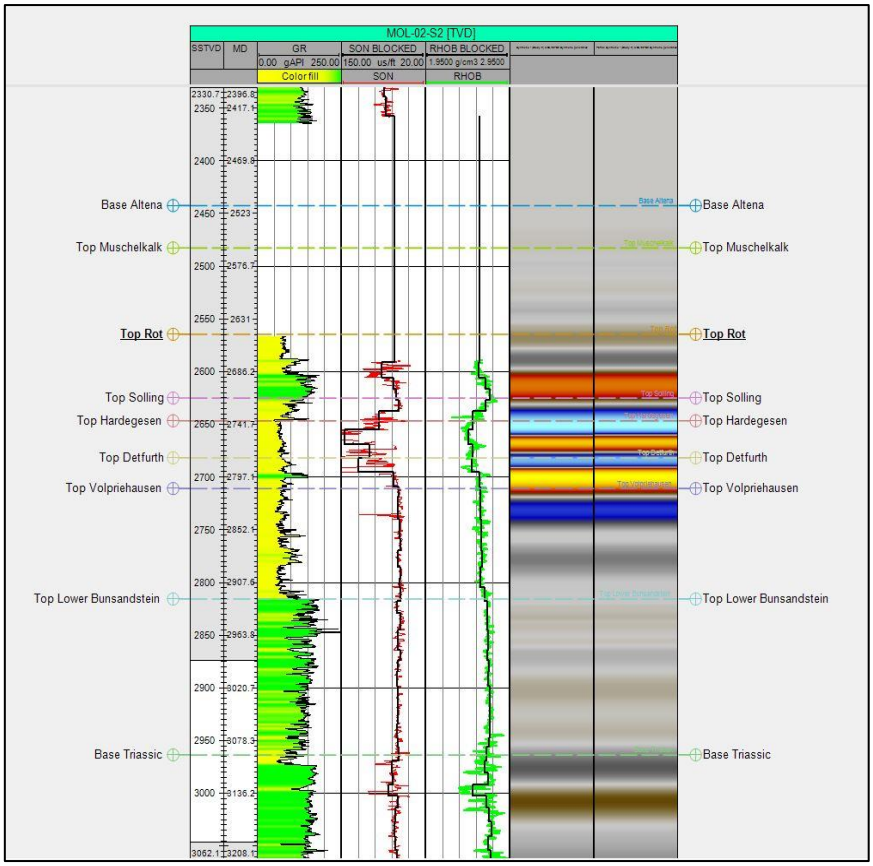

Figure 74. Well logs data of MOL-02-S2 well.

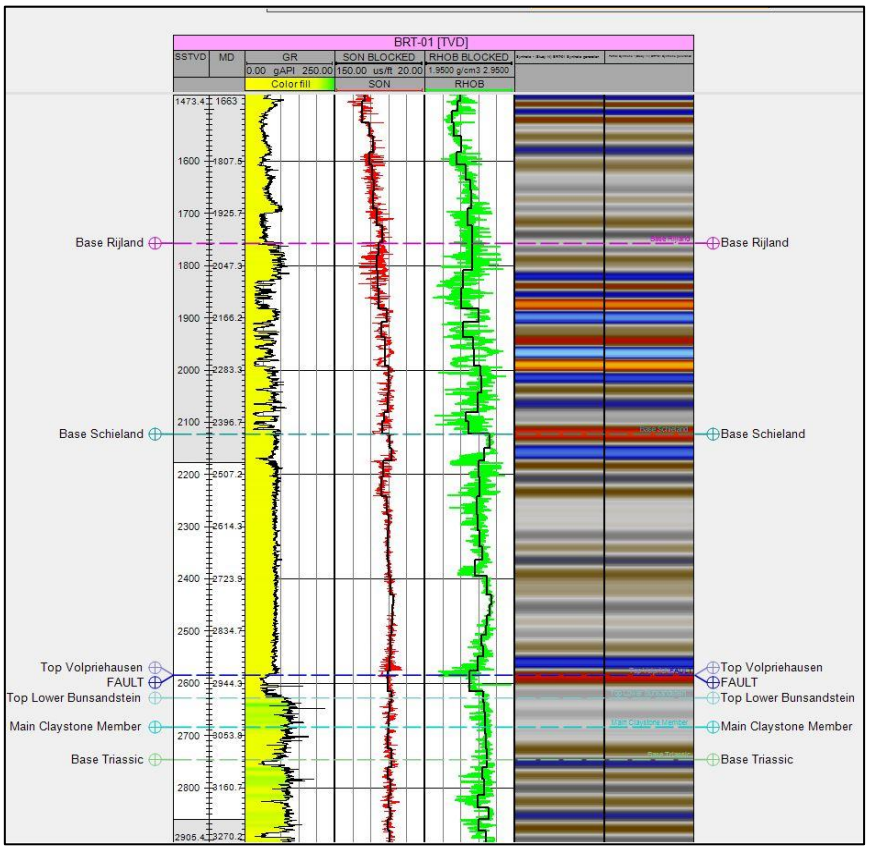

Figure 75. Well logs data of BRT-01 well.

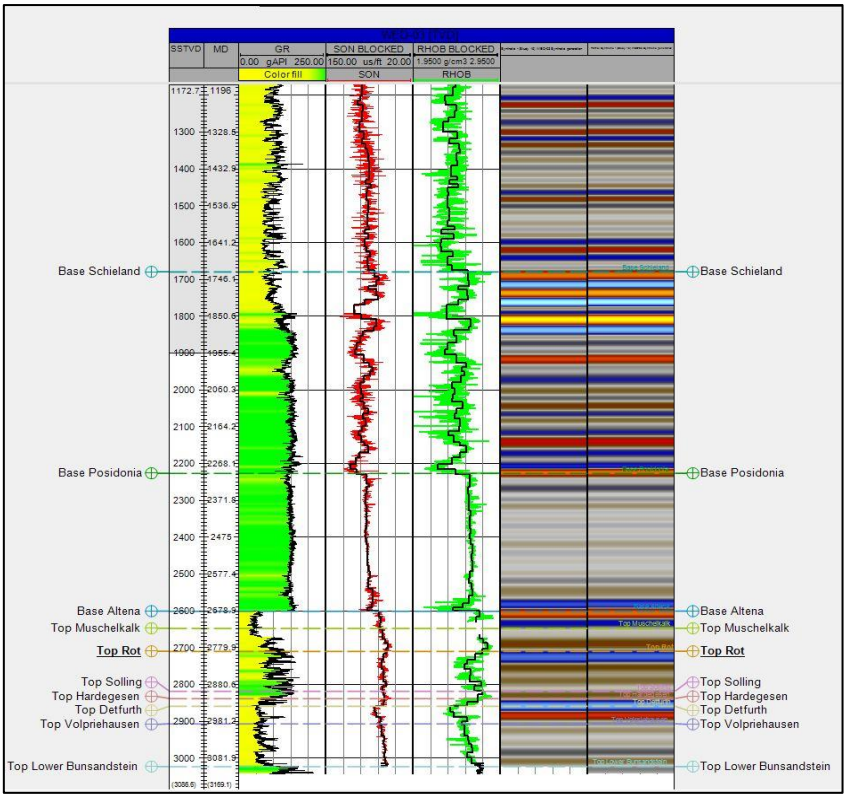

Figure 76. Well logs data of WED-03 well.

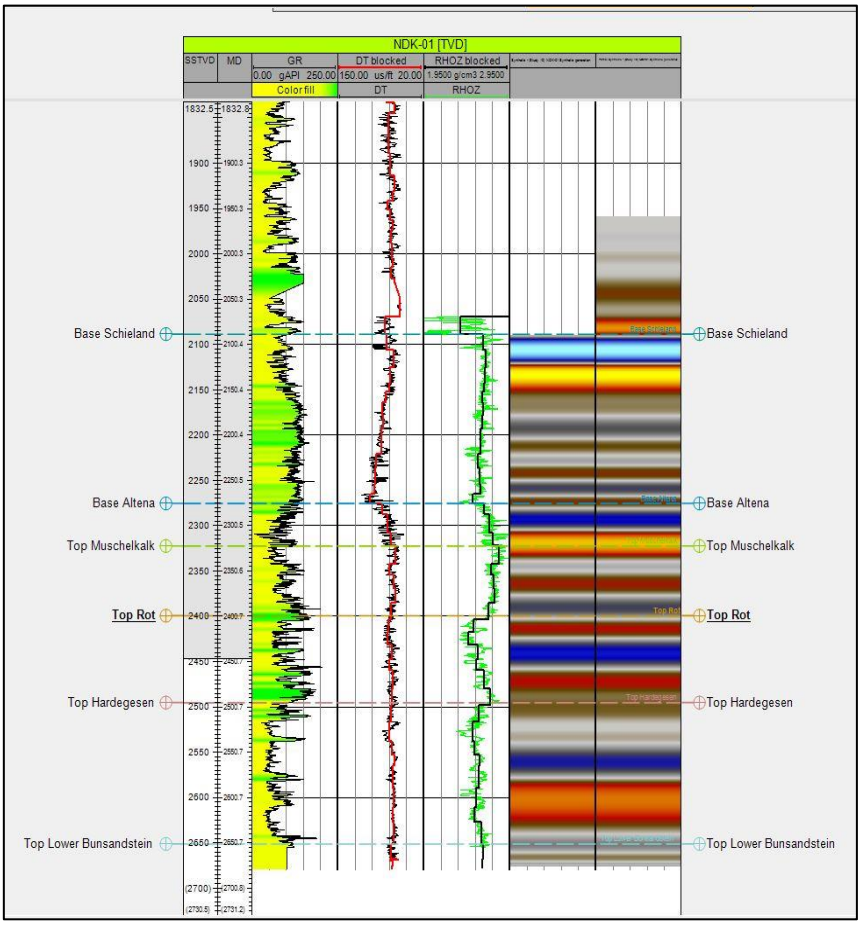

Figure 77. Well logs data of NDK-01 well.

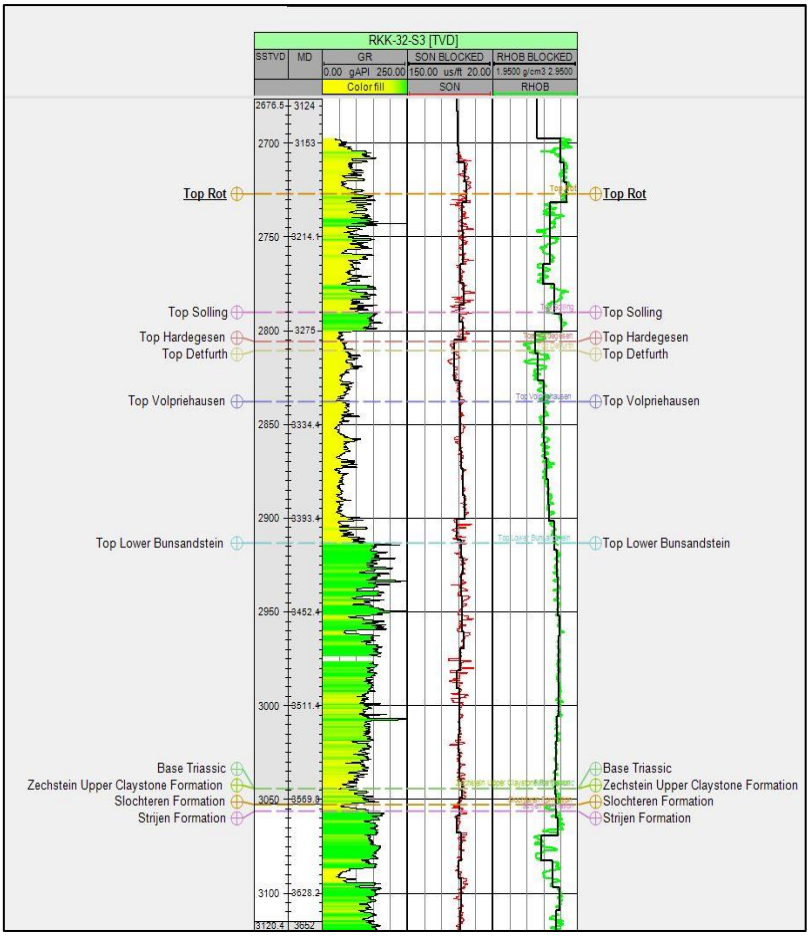

Figure 78. Well logs data of RKK-32-S3 well.

C. Seismic Interpretation

All of the interpreted horizons and isopach map of Base Posidonia and every formation within Triassic successions can be found in this appendix.

C.1 Time Structural Map (3D Post-Stack Time Migration Dataset)

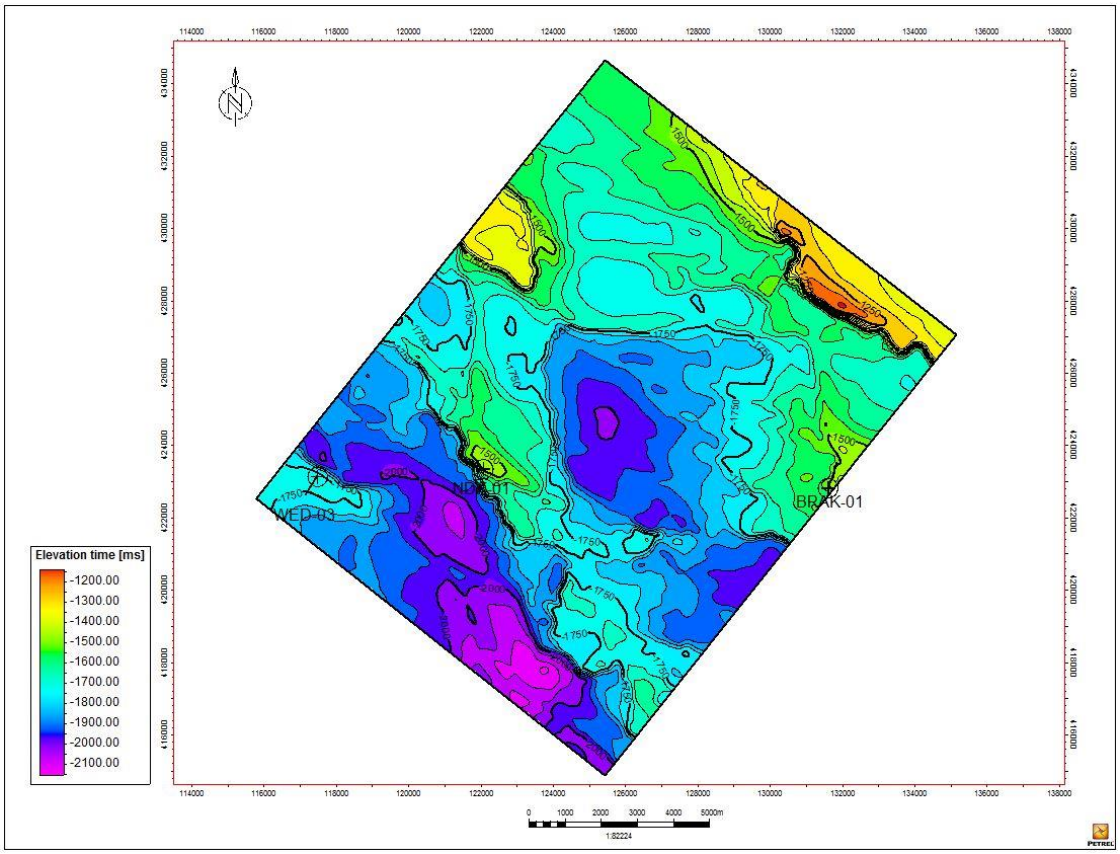

Figure 79. Time structural map of Base Posidonia.with 3D Post-Stack Time Migration dataset.

C.2 Depth Structural Map (3D PSDM and Post-Stack Time Migration Dataset)

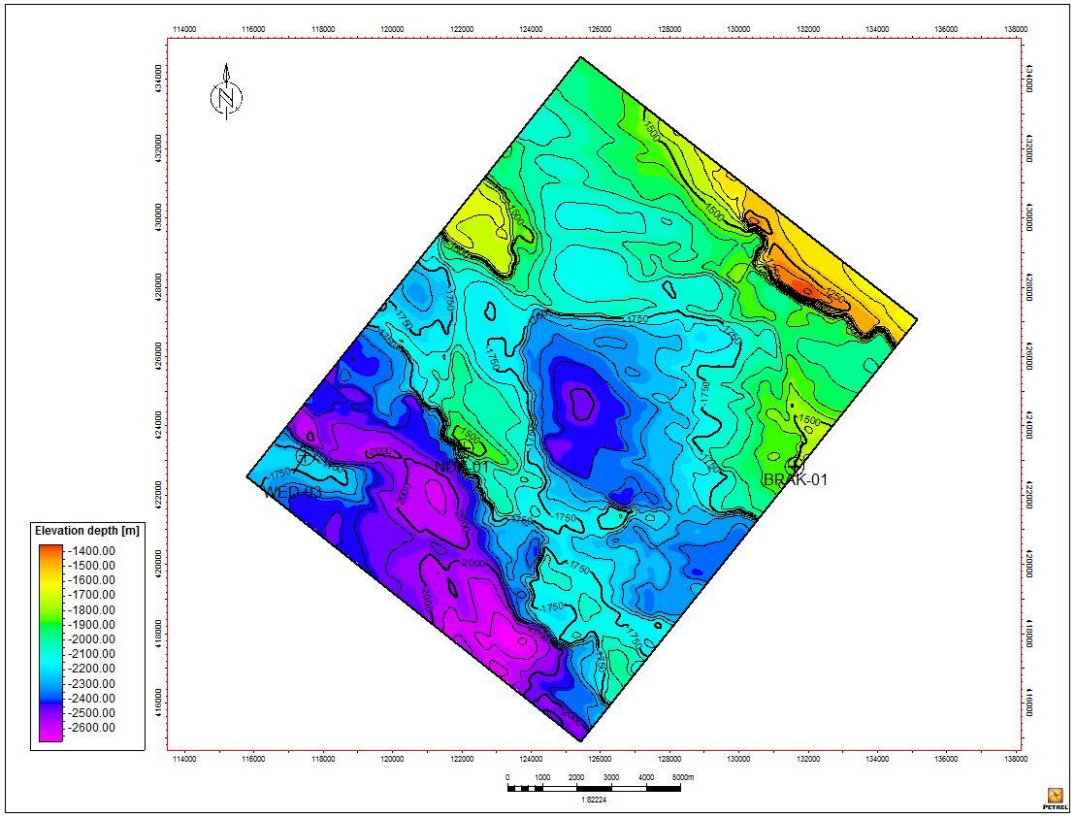

Figure 80. Depth structural map of Base Posidonia with 3D Post-Stack Time Migration dataset.

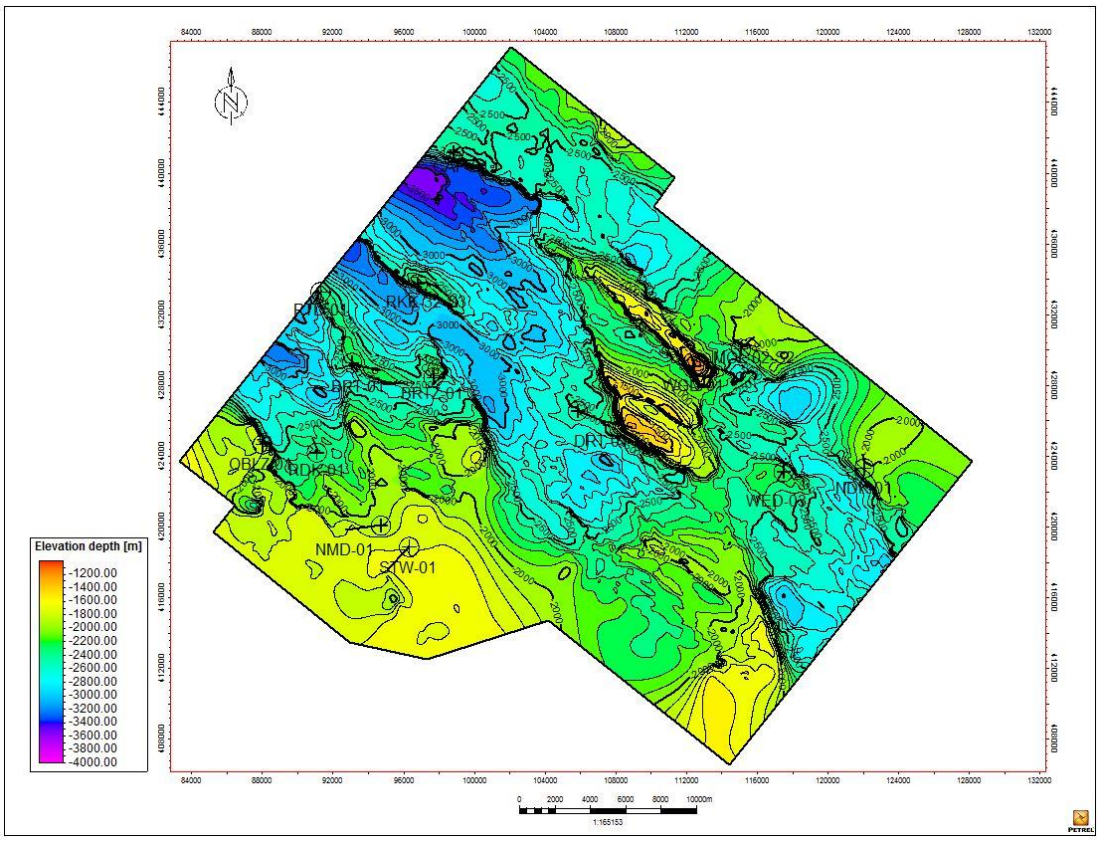

Figure 81. Depth structural map of Base Posidonia with 3D PSDM dataset.

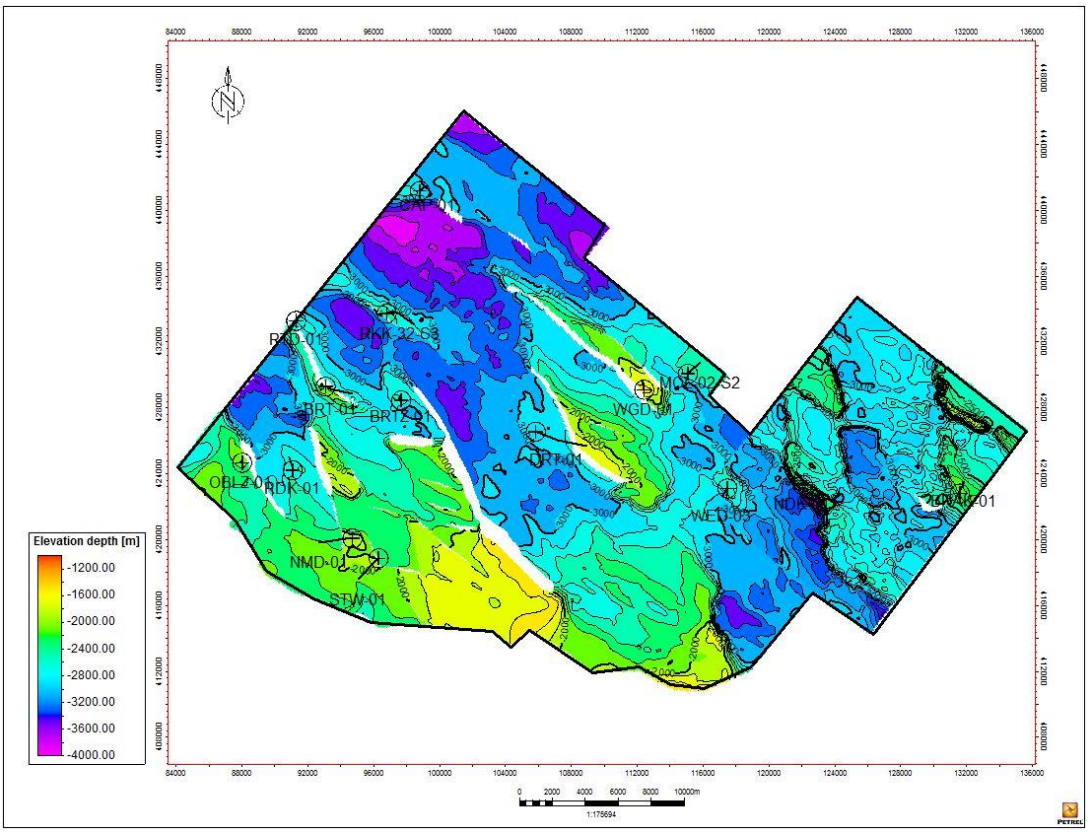

Figure 82. Depth structural map of Top Muschelkalk Formation with 3D Post-Stack Time Migration and PSDM dataset.

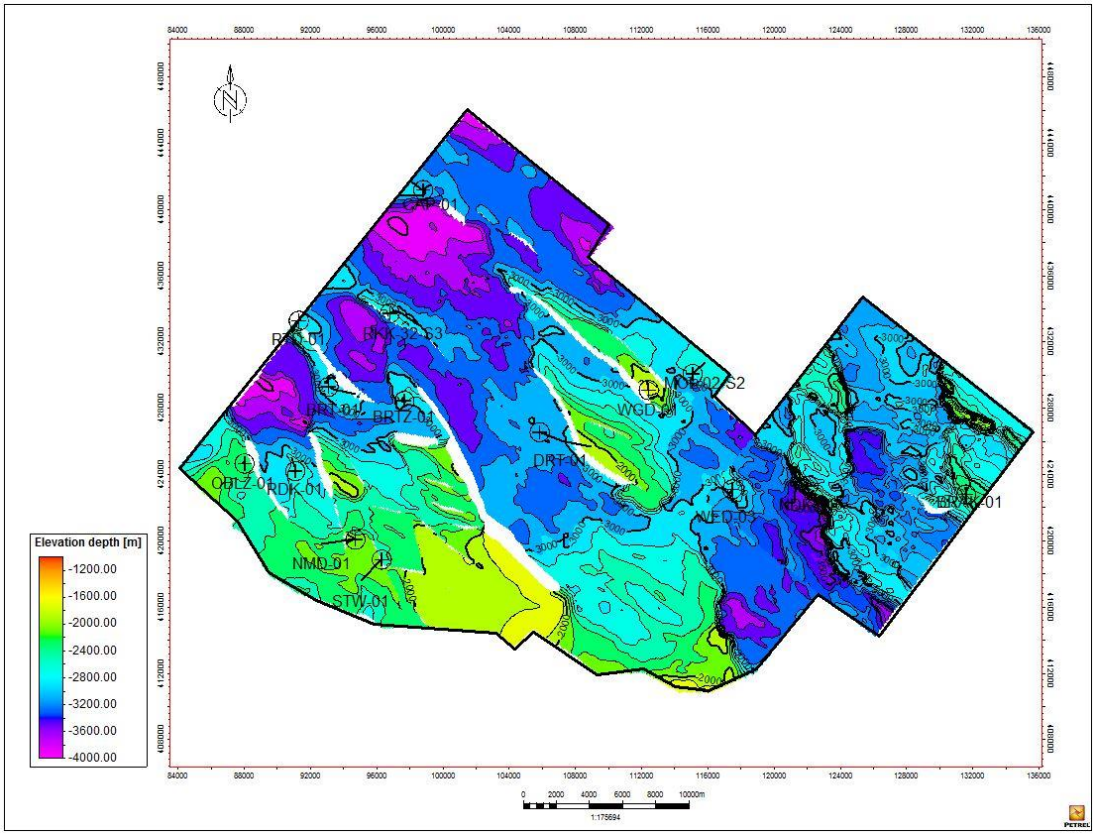

Figure 83. Depth structural map of Top Solling Formation with 3D Post-Stack Time Migration and PSDM dataset.

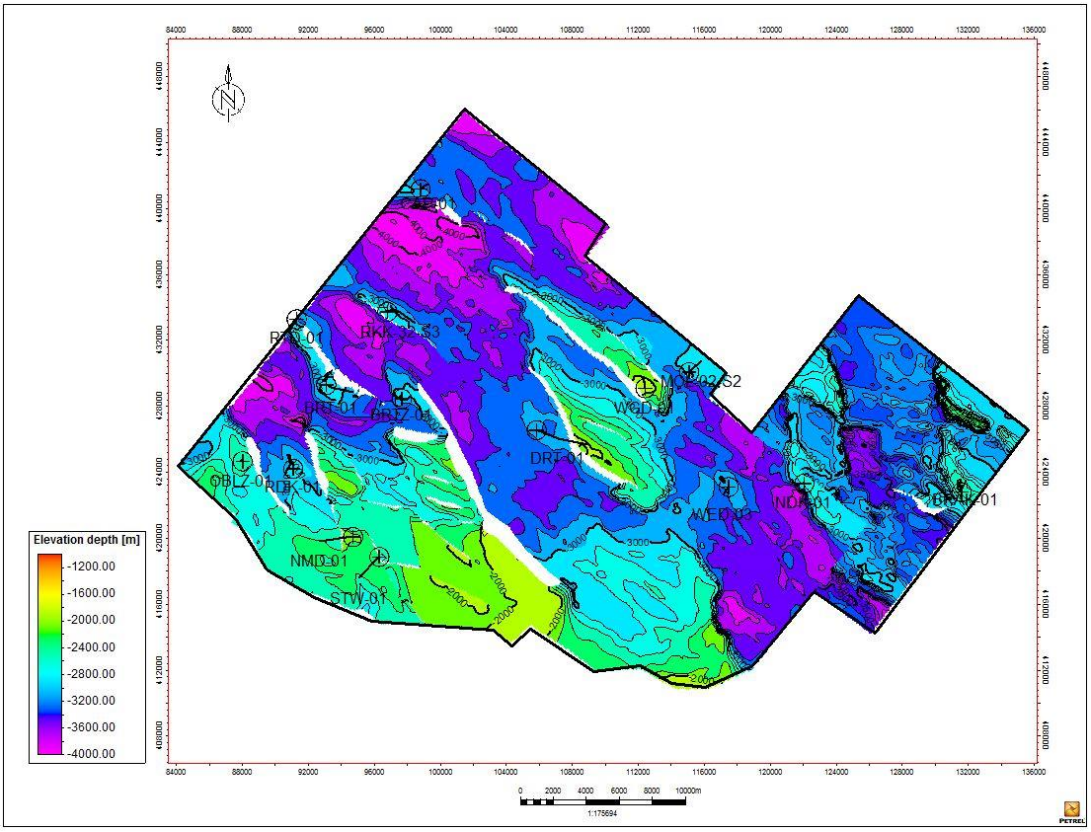

Figure 84. Depth structural map of Top Lower Bunsandstein Formation with 3D Post-Stack Time Migration and PSDM dataset.

C.3 Isopach Map

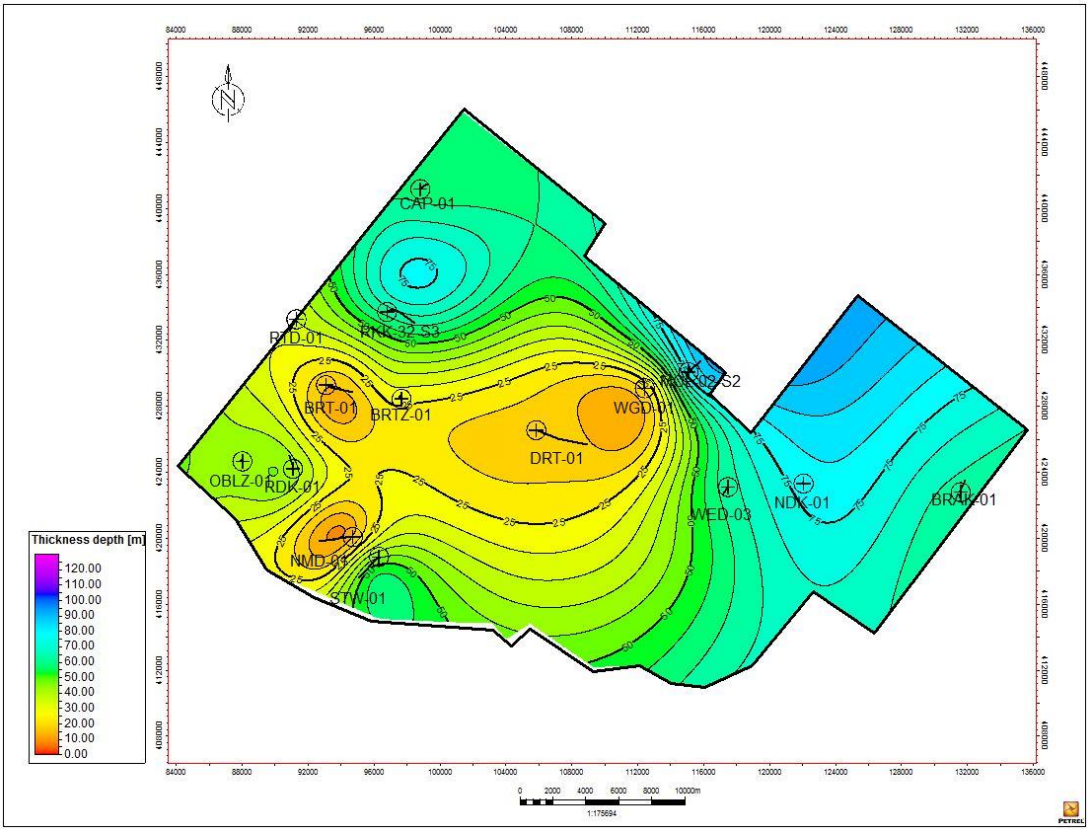

Figure 85. Isopach map of the Muschelkalk Formation.

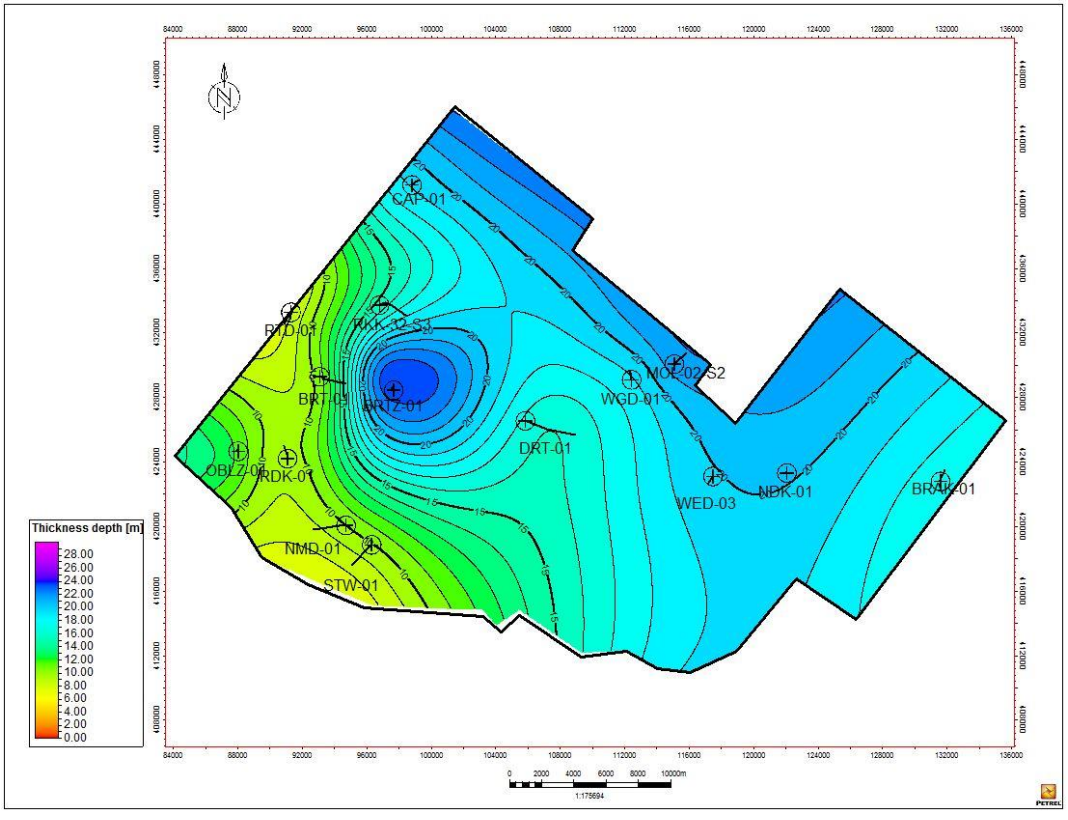

Figure 86. Isopach map of the Solling Formation.

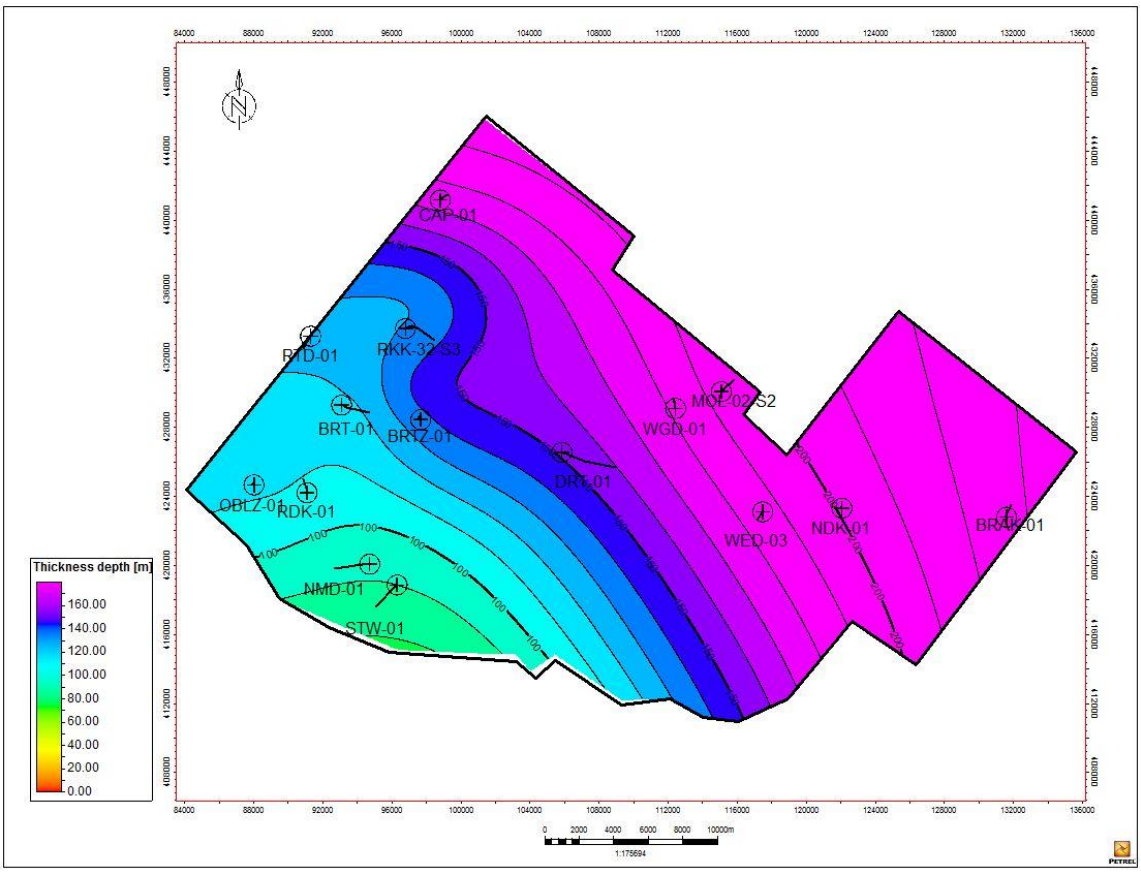

Figure 87. Isopach map of the Lower Buntsandstein Formation.

D. Core Description

In this appendix, the core database and full core description from the selected wells (OBLZ-01 and WGD-01) are presented. The subdivision is made based on the well name and cored Interval.

D.1 Core Database

Table 14. Core database within the study area.

Well	Company	Core Number	Core Interval (m AH)		Total Length (m)	Recovery (%)	Average Porosity (%)	Average Permeability (md)	Information
			Depth From	Depth Until					
OBLZ-01	NAM	Core-1	2202	2220.44	18.44	100	21.86	384.06	Upper Rot Fringe Claystone Member
		Core-2	2275	2300	25	87	17.05	607.88	Solling Claystone Member- Hardegesen Formation
RDK-01	NAM	Core-1	2722	2740	18	77	11.88	9.19	Upper Rot Fringe Claystone Member
		Core-2	2800	2816	16	91	6.70	15.51	Solling Claystone Member - Hardegesen Formation
		Core-3	2816.5	2835	18.5	48	13.16	233.79	Hardegesen Formation
STW-01	NAM	Core-1	2445	2456	11	98	22.01	993.83	Upper Rot Fringe Claystone Member - Rot Fringe Sandstone Member
		Core-2	2546	2565	19	94	22.12	424.31	Hardegesen Formation - Upper Detfurth Sandstone Member
WED-03	NAM	Core-1	2821.1	2827.7	6.6	100	10.20	53.78	Rot Fringe Sandstone Member
		Core-2	2827.7	2845.4	17.7	100	6.12	21.14	Rot Fringe Sandstone Member
		Core-3	2965	2983	18	100	9.11	0.59	Upper Detfurth Sandstone Member - Lower Detfurth Sandstone Member
BRT-02-S1	NAM	Core-1	3006.1	3023.8	17.7	Unknown	12.47	9.19	Lower Detfurth Sandstone Member
BRTZ-01	NAM	Core-1	2664	2677	13	Unknown	8.12	6.59	Upper Rot Fringe Claystone Member
		Core-2	2677	2695	18	Unknown	12.62	111.60	Rot Fringe Sandstone Member
		Core-3	2734	2734.1	0.1	Unknown	4.50	NA	Lower Rot Fringe Claystone Member
		Core-4	2736	2753	17	Unknown	4.57	0.31	Solling Claystone Member
		Core-5	2754	2770	16	Unknown	8.84	9.28	Basal Solling Sandstone Member - Lower Detfurth Sandstone Member
		Core-6	2772	2789	17	Unknown	12.65	32.92	Upper Volprihausen Sandstone Member
WED-02	NAM	Core-1	2971	2993	22	Unknown	7.28	0.46	Rot Fringe Sandstone Member
		Core-2	3150	3158	8	Unknown	NA	NA	Lower Bunsandstein Formation
BRAK-01	NAM	Core-2	2348.9	2369	20.1	100	6.73	3.02	Rot Fringe Sandstone Member
		Core-3	2452.52	2479	26.48	98	6.96	1.19	Defurth Claystone Member
MOL-02-S2	NAM	Core-1	2684	2688.5	4.5	Unknown	4.04	NA	Rot Fringe Sandstone Member
WGD-01	NAM	Core-1	1739.5	1775.5	36	Unknown	19.23	570.17	Rot Fringe Sandstone Member

D.2 Core Description of OBLZ-01 Well – Core No.1

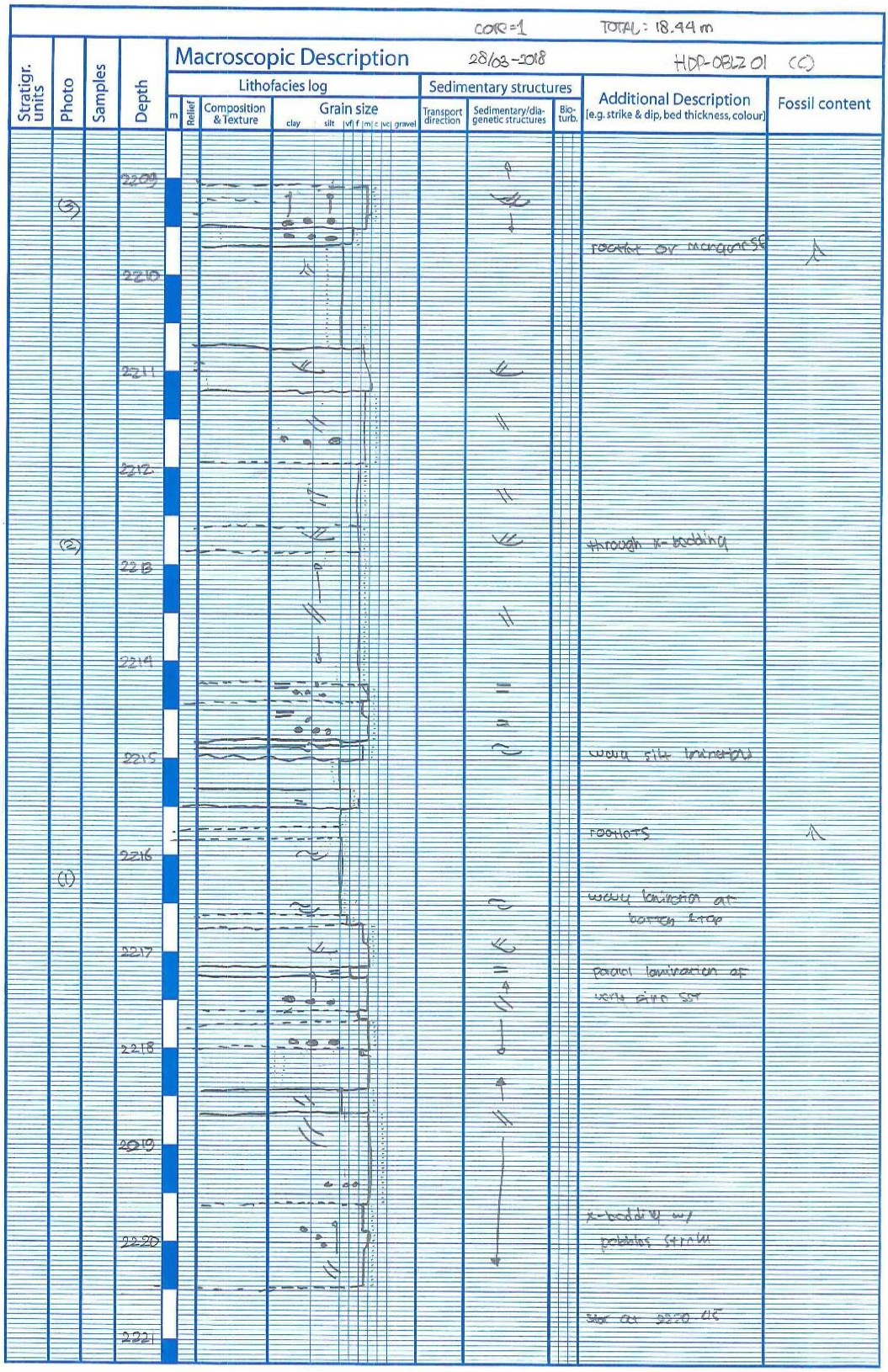

Figure 88. Core description of core no.1 from OBLZ-01 (2220.55-2209 m).

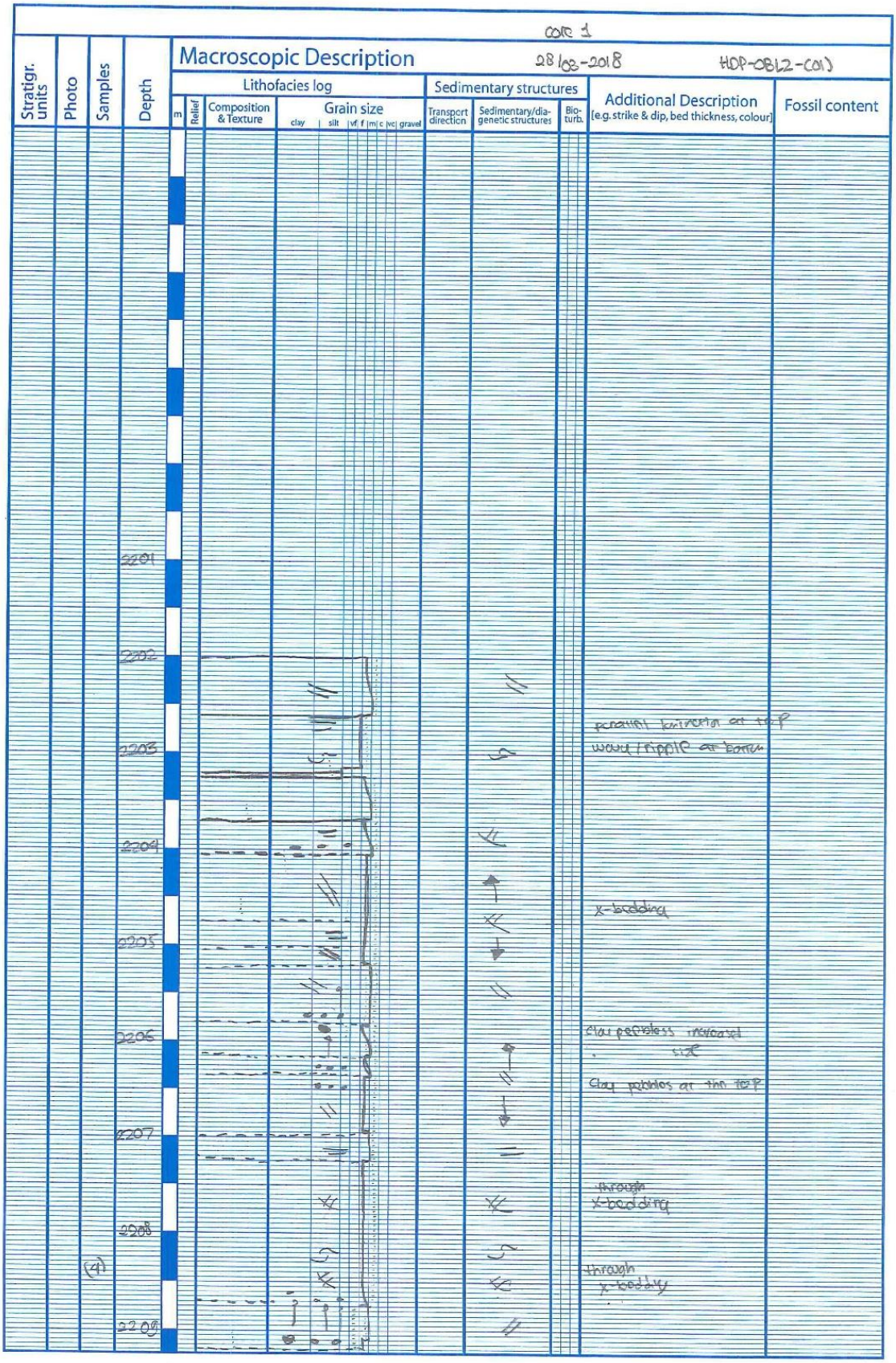

Figure 89. Core description of core no.1 from OBLZ-01 (2209 -2202 m)

D.3 Core Description of OBLZ-01 Well – Core No.2

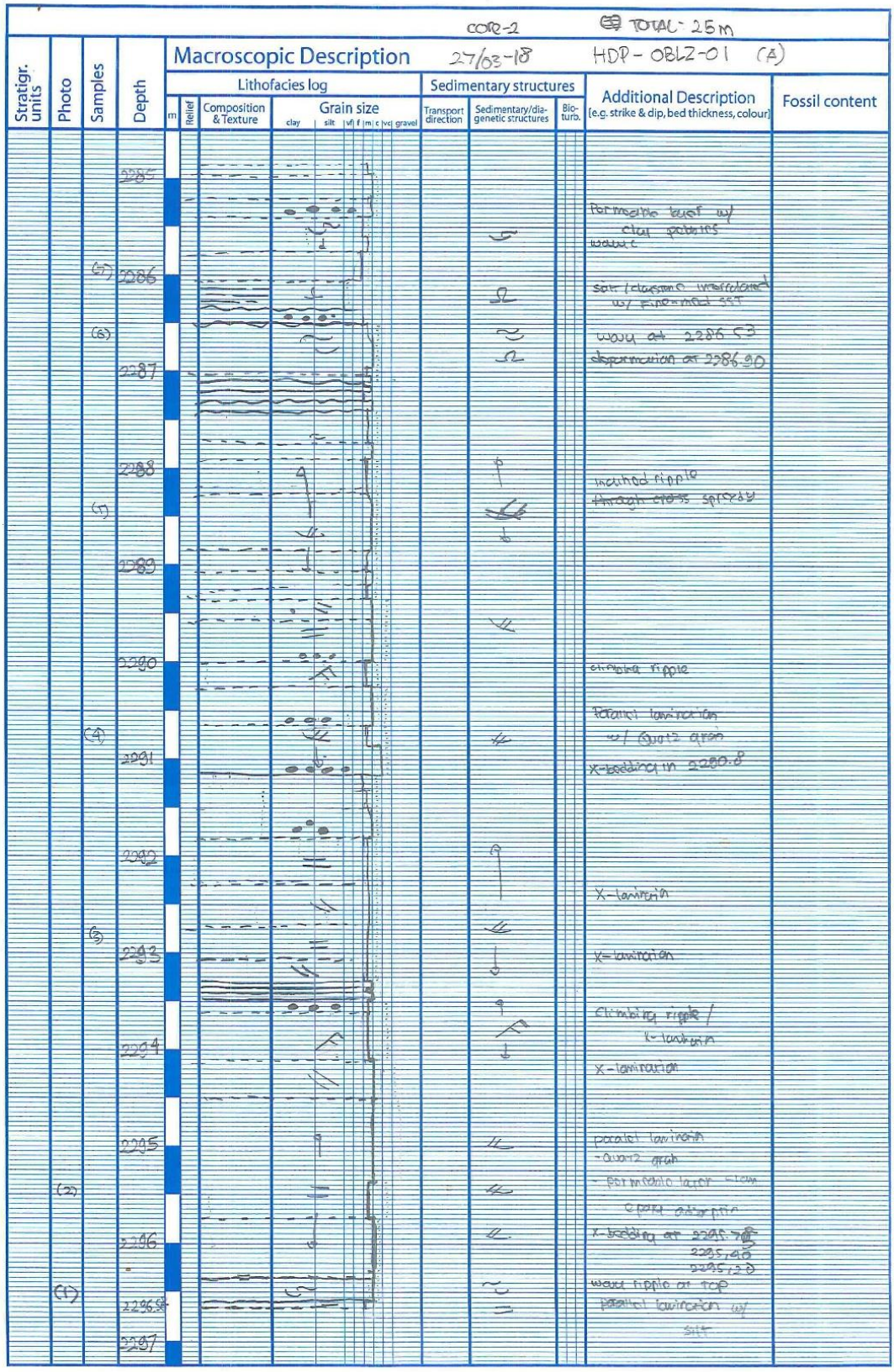

Figure 90. Core description of core no.2 from OBLZ-01 (2296.58-2284.83 m)

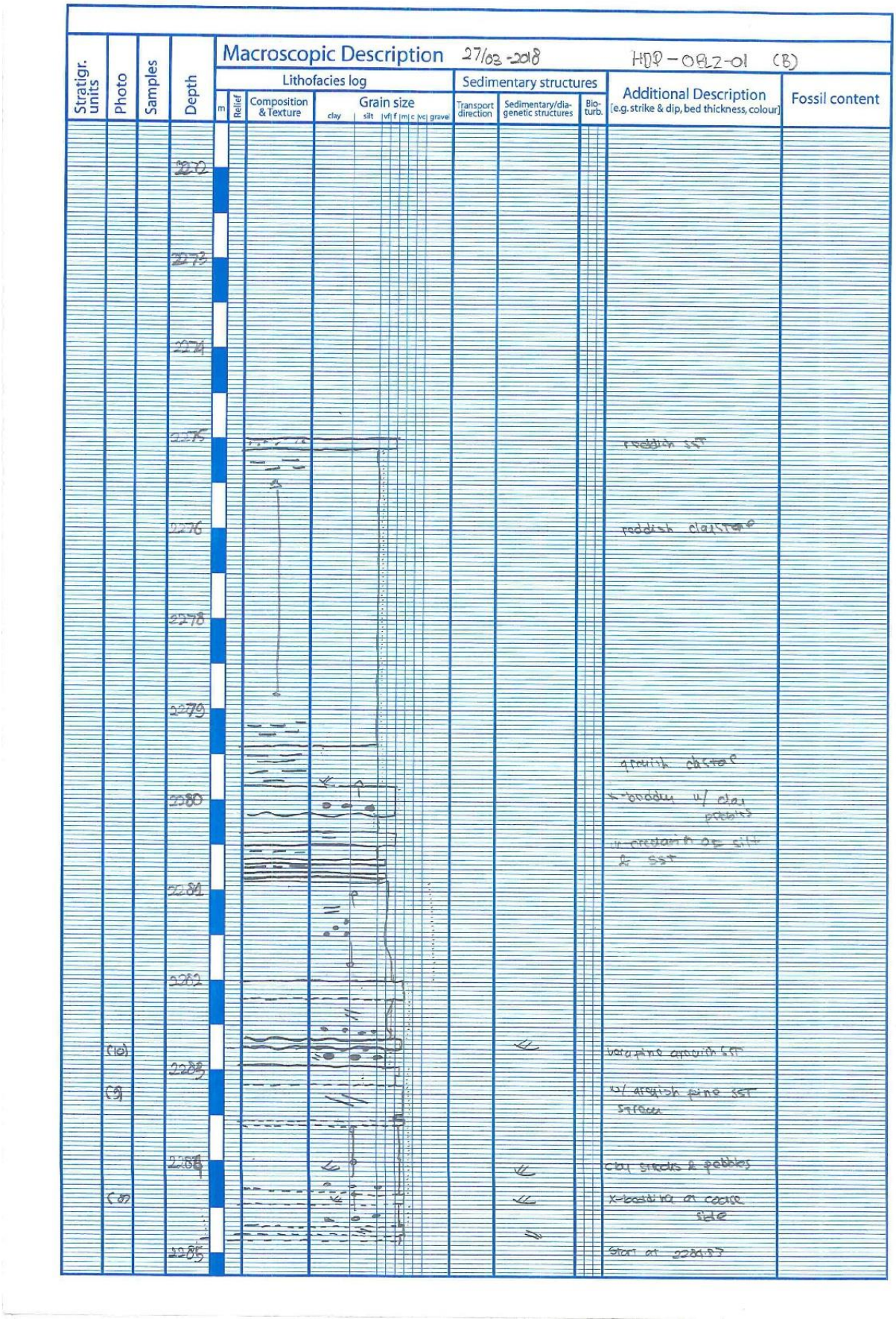

Figure 91. Core description of core no.2 from OBLZ-01 (2284.83-2275 m)

D.4 Core Description of WGD-01 Well – Core No.1

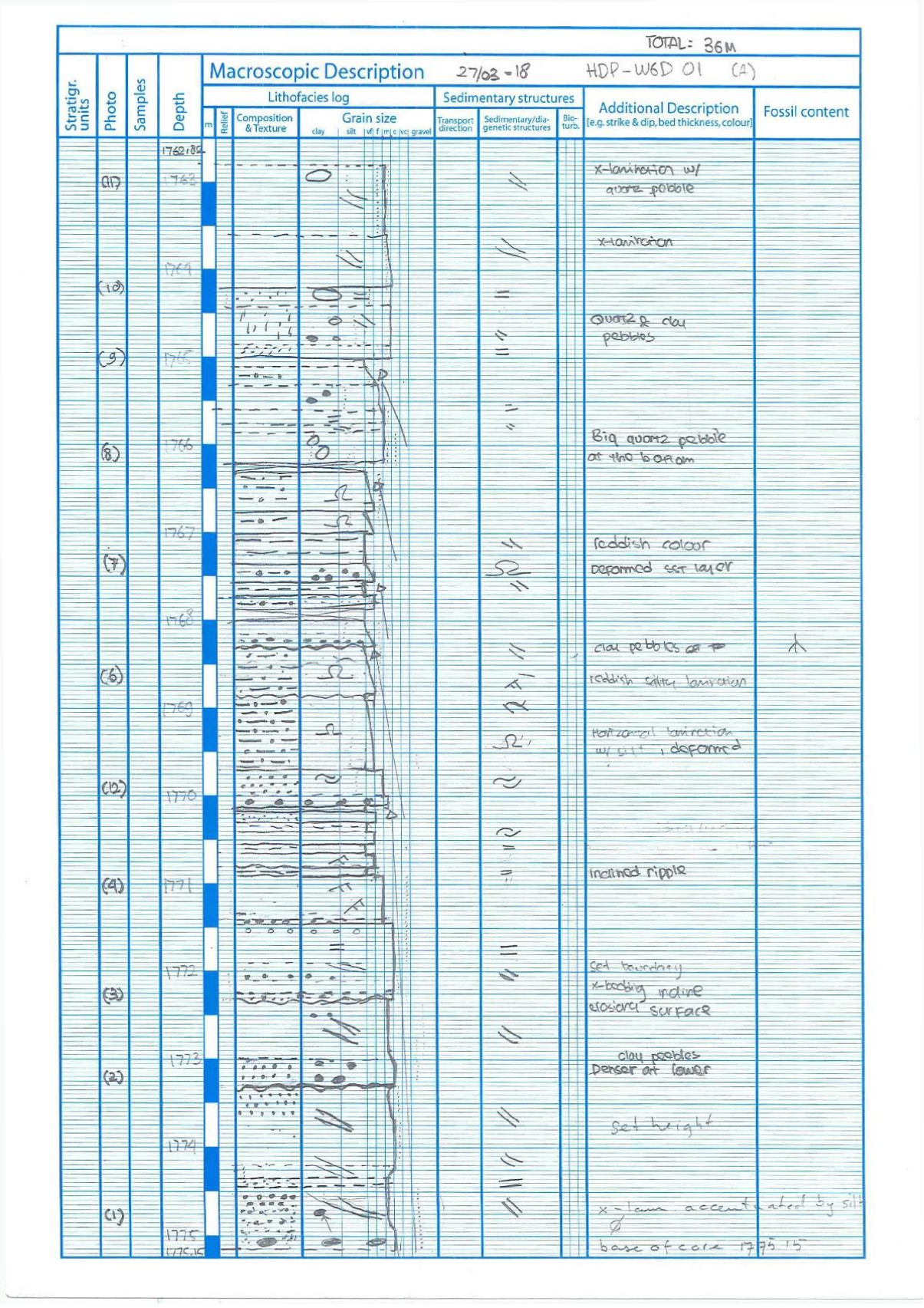

Figure 92. Core description of core no.1 from WGD-01 (1775.75-1762.82 m)

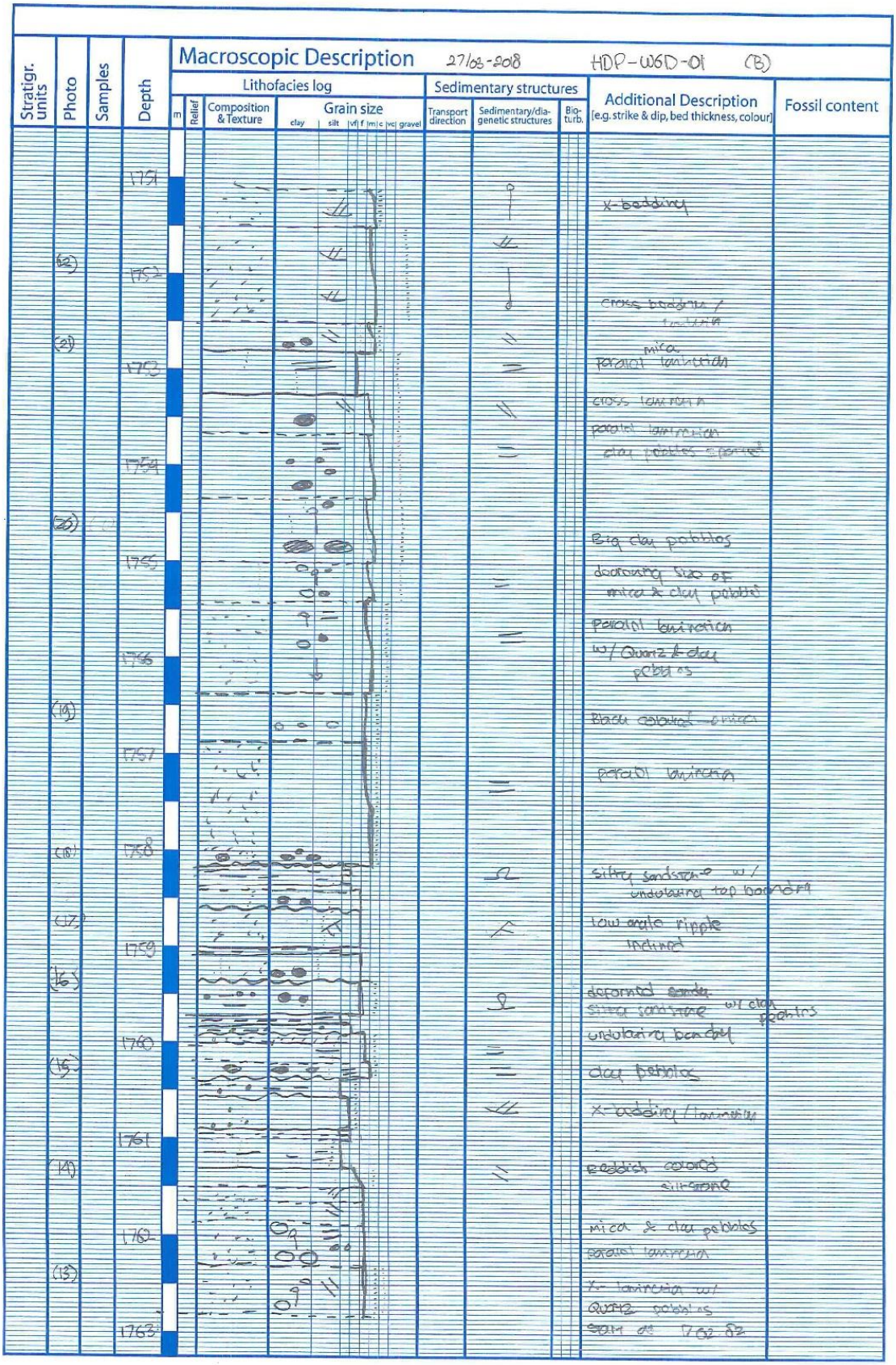

Figure 93. Core description of core no.1 from WGD-01 (1762.82-1751.4 m)

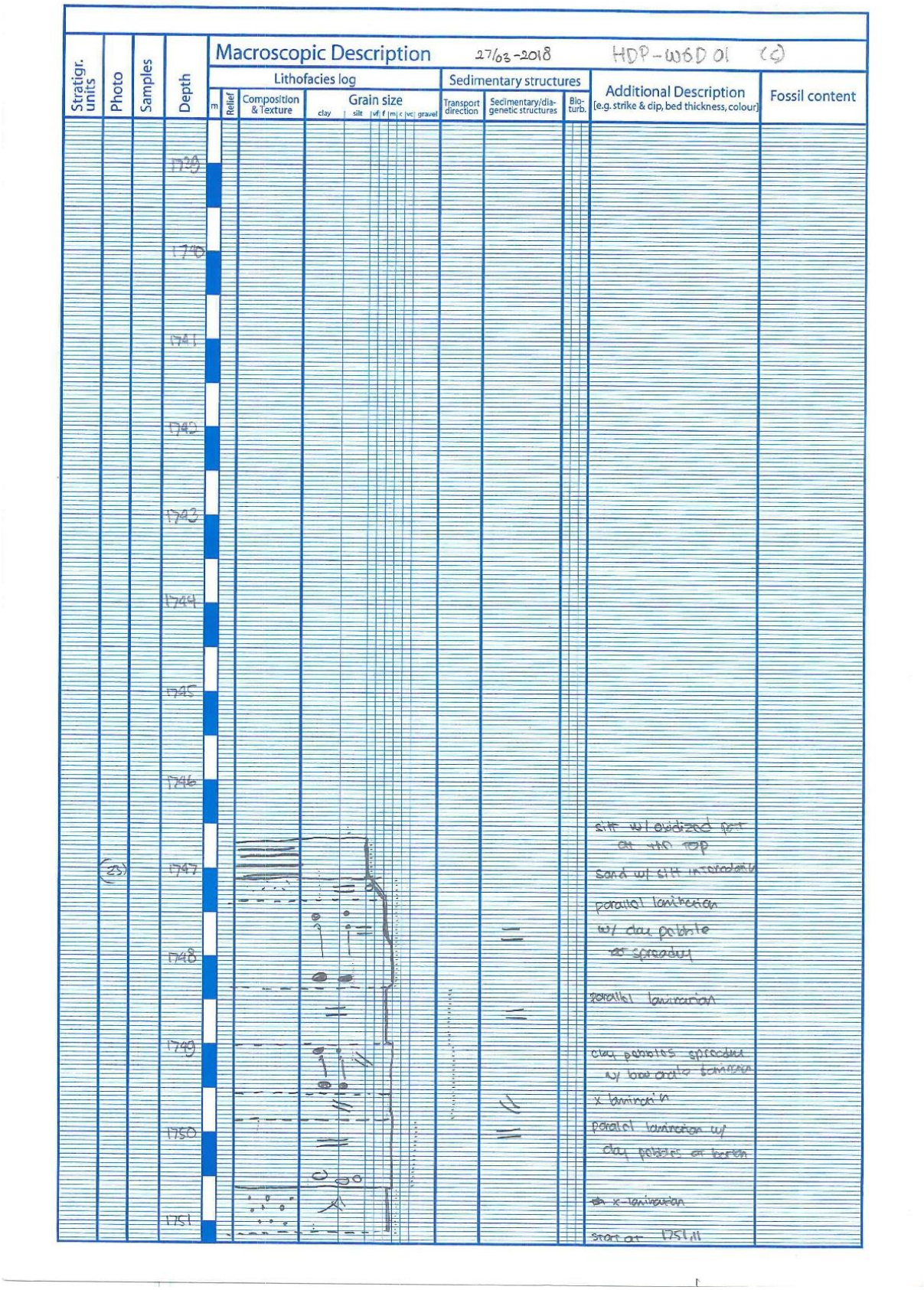

Figure 94. Core description of core no.1 from WGD-01 (1751.4-1746.65 m)

E. Petrophysical Evaluation

The result of petrophysical evaluation and used parameters during the analysis process for each well are presented in this Appendix.

E.1 Petrophysical Evaluation of BRAK-01 Well

GR Max : 180

GR Min : 40

Rho Matrix : 2.65 g/cc

Rho water : 1 g/cc

Rho oil : 0.8 g/cc

Rho gas : 0.25 g/cc

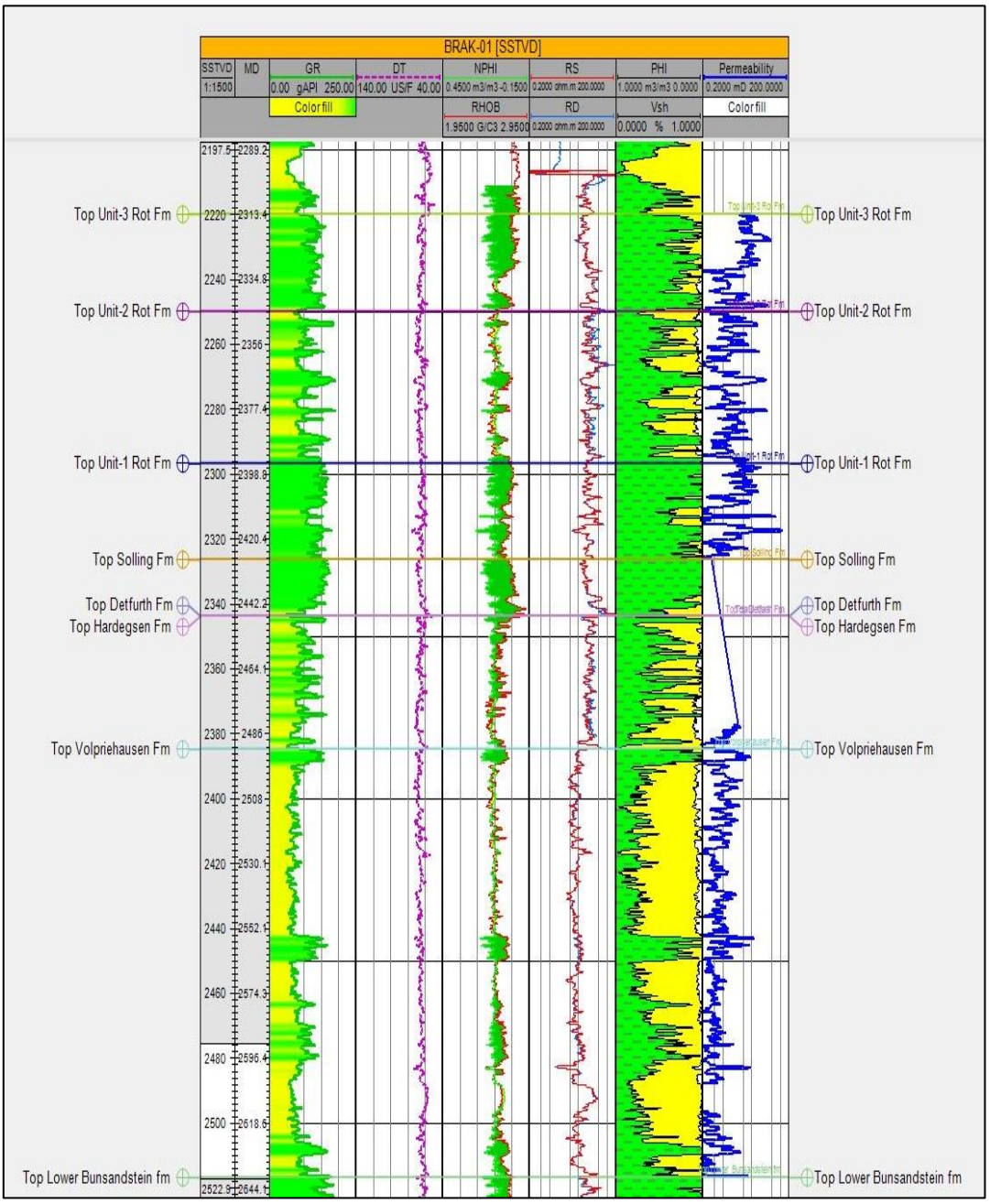

Figure 95. Petrophysical evaluation result for BRAK-01.

E.2 Petrophysical Evaluation of BRTZ-01 Well

GR Max : 135

GR Min : 45

Rho Matrix : 2.65 g/cc

Rho water : 1 g/cc

Rho oil : 0.8 g/cc

Rho gas : 0.25 g/cc

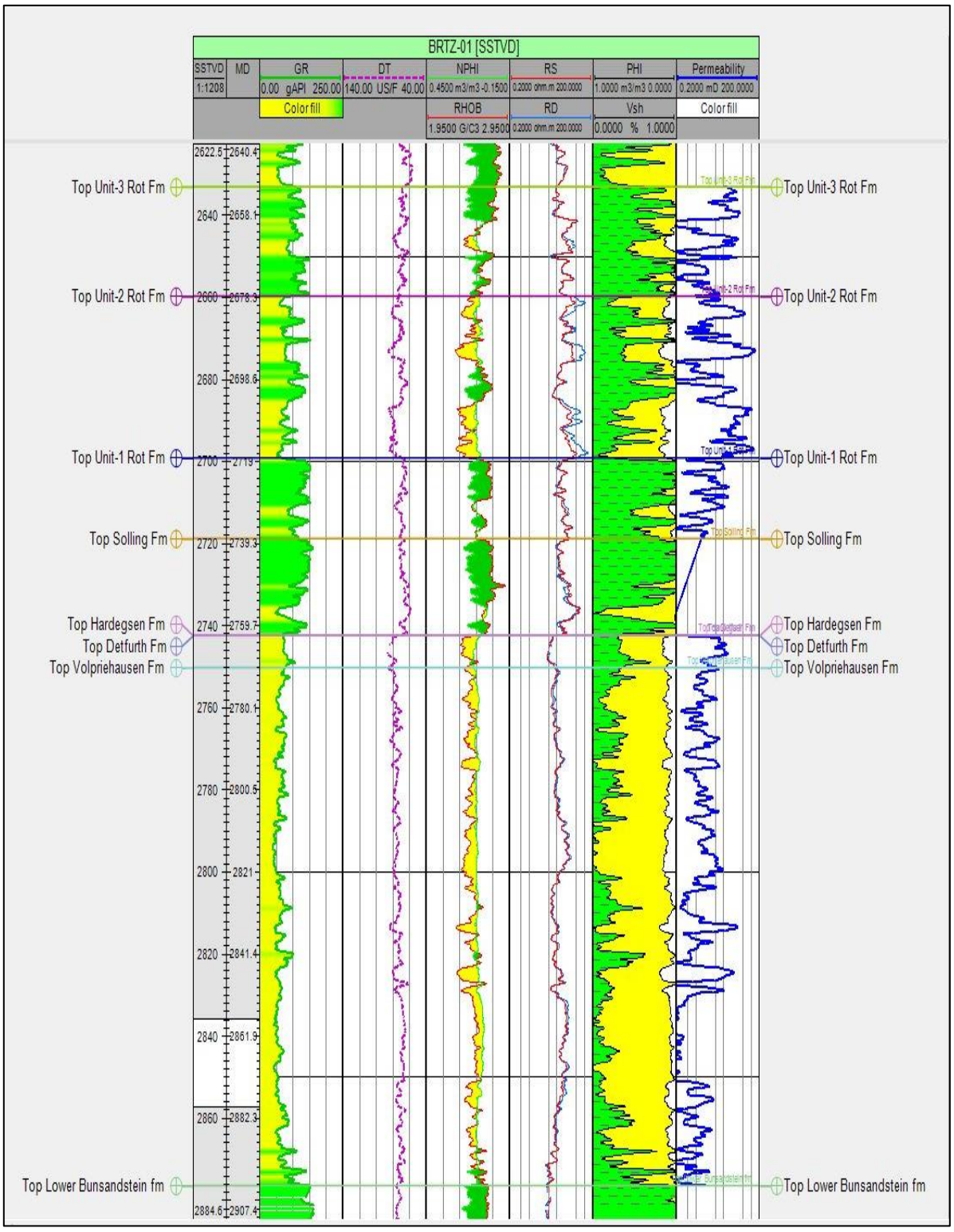

Figure 96. Petrophysical evaluation result for BRTZ-01.

E.3 Petrophysical Evaluation of MOL-02-S2 Well

GR Max : 210
GR Min : 45
Rho Matrix : 2.65 g/cc

Rho water : 1 g/cc
Rho oil : 0.8 g/cc
Rho gas : 0.25 g/cc

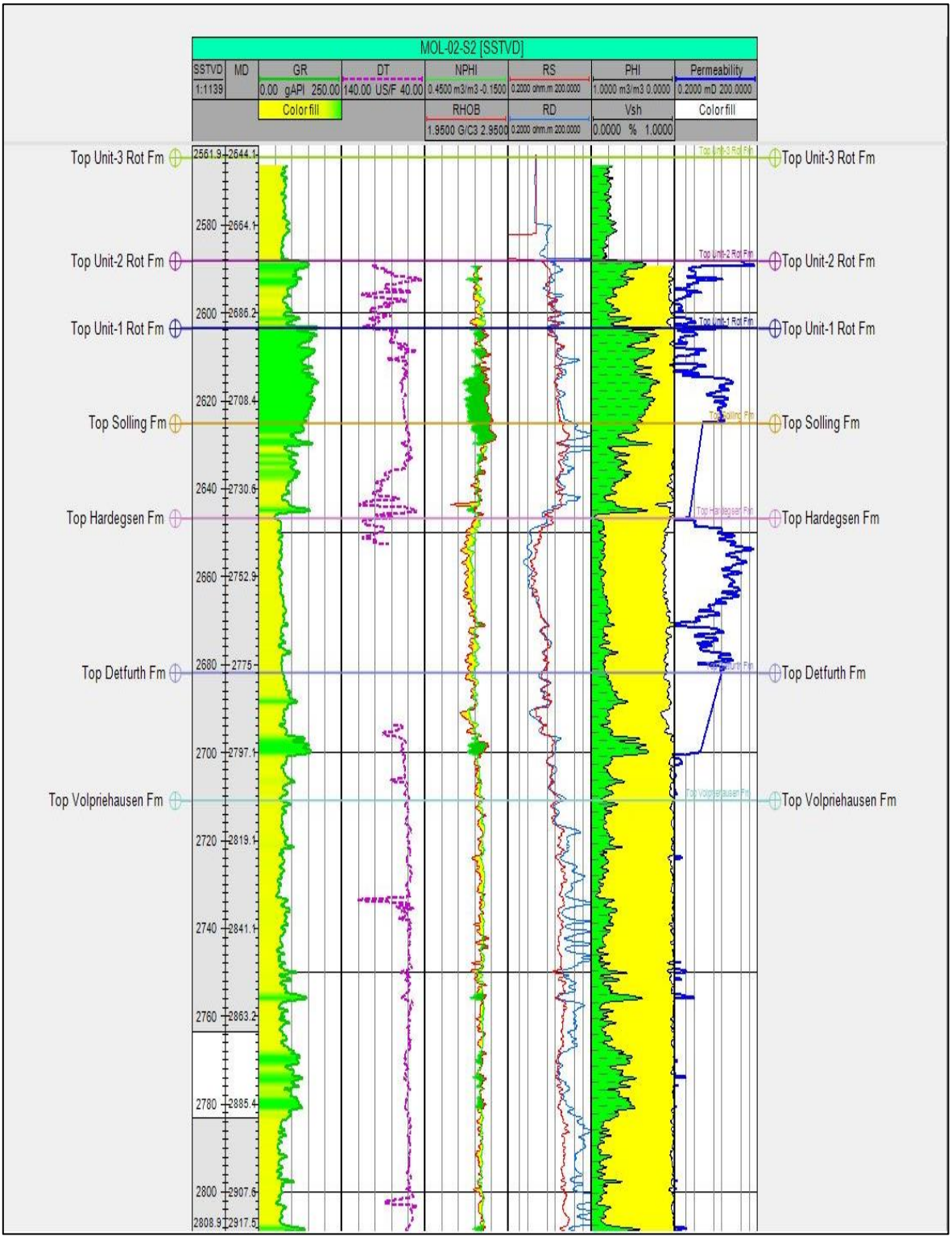

Figure 97. Petrophysical evaluation result for MOL-02-S2.

E.4 Petrophysical Evaluation of OBLZ-01 Well

GR Max : 130
GR Min : 60
Rho Matrix : 2.65 g/cc

Rho water : 1 g/cc
Rho oil : 0.8 g/cc
Rho gas : 0.25 g/cc

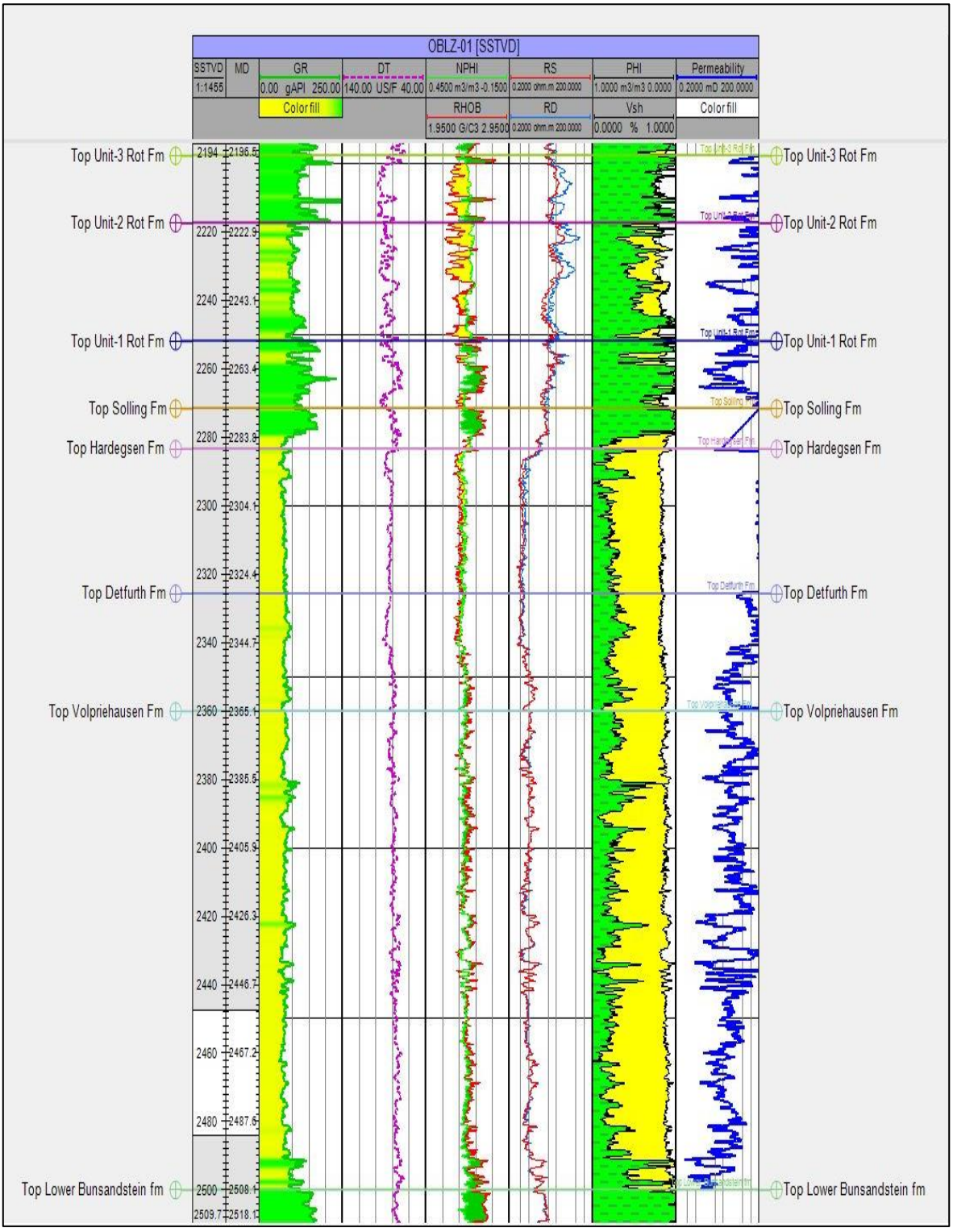

Figure 98. Petrophysical evaluation result for OBLZ-01.

E.5 Petrophysical Evaluation of RDK-01 Well

GR Max : 180
GR Min : 40
Rho Matrix : 2.65 g/cc

Rho water : 1 g/cc
Rho oil : 0.8 g/cc
Rho gas : 0.25 g/cc

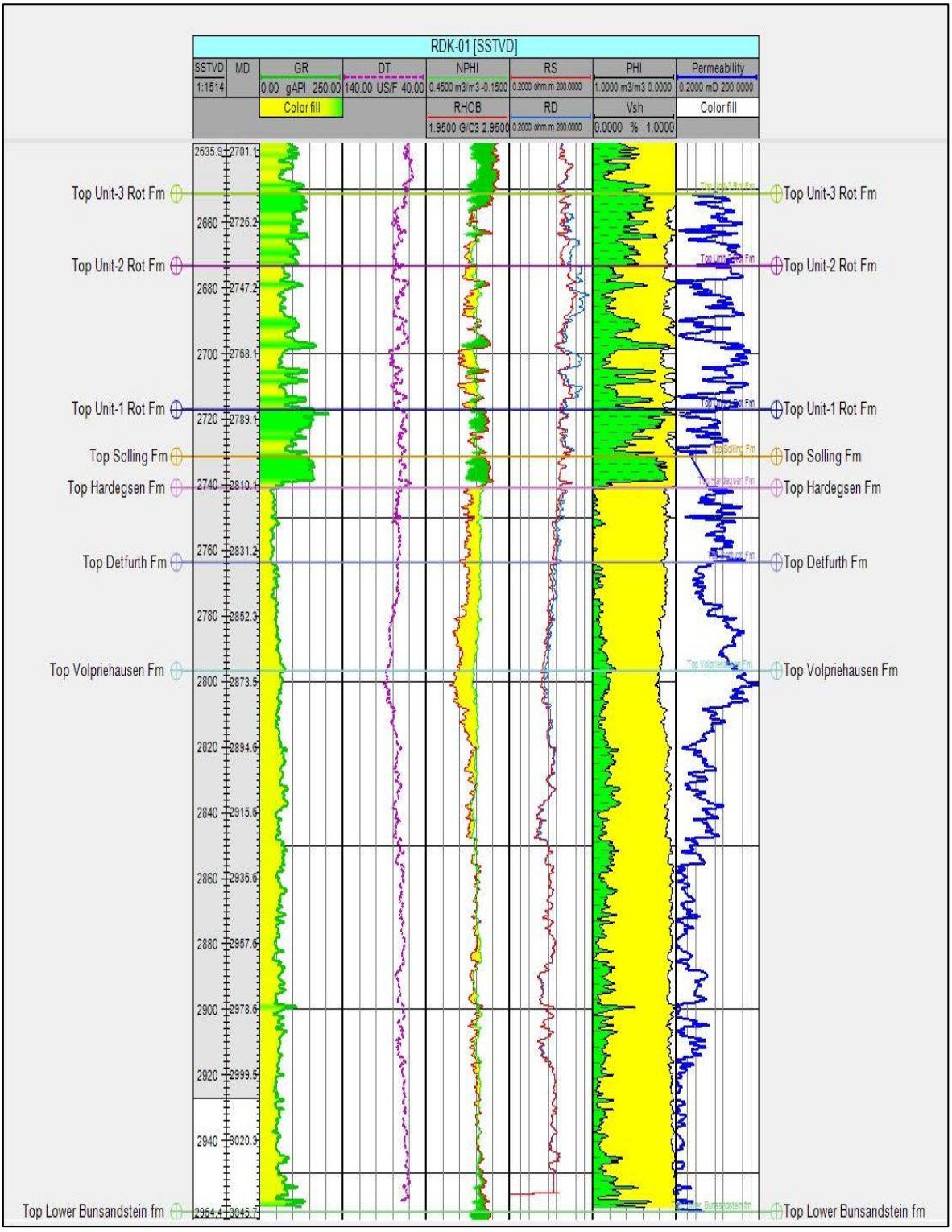

Figure 99. Petrophysical evaluation result for RDK-01.

E.6 Petrophysical Evaluation of WED-03 Well

GR Max : 159
GR Min : 45
Rho Matrix : 2.65 g/cc

Rho water : 1 g/cc
Rho oil : 0.8 g/cc
Rho gas : 0.25 g/cc

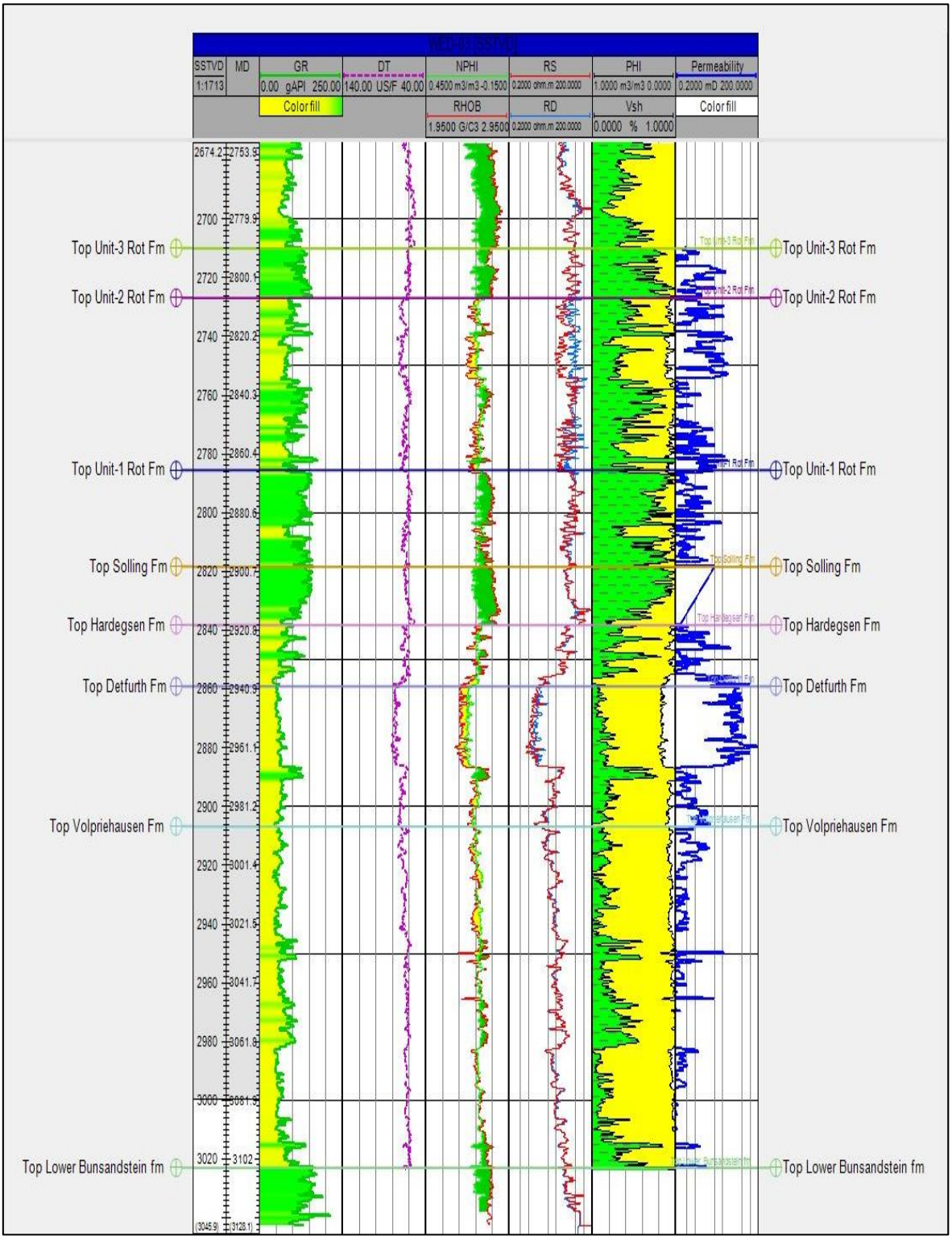

Figure 100. Petrophysical evaluation result for WED-03.

E.7 Petrophysical Evaluation of WGD-01 Well

GR Max : 135
GR Min : 55
Rho Matrix : 2.65 g/cc

Rho water : 1 g/cc
Rho oil : 0.8 g/cc
Rho gas : 0.25 g/cc

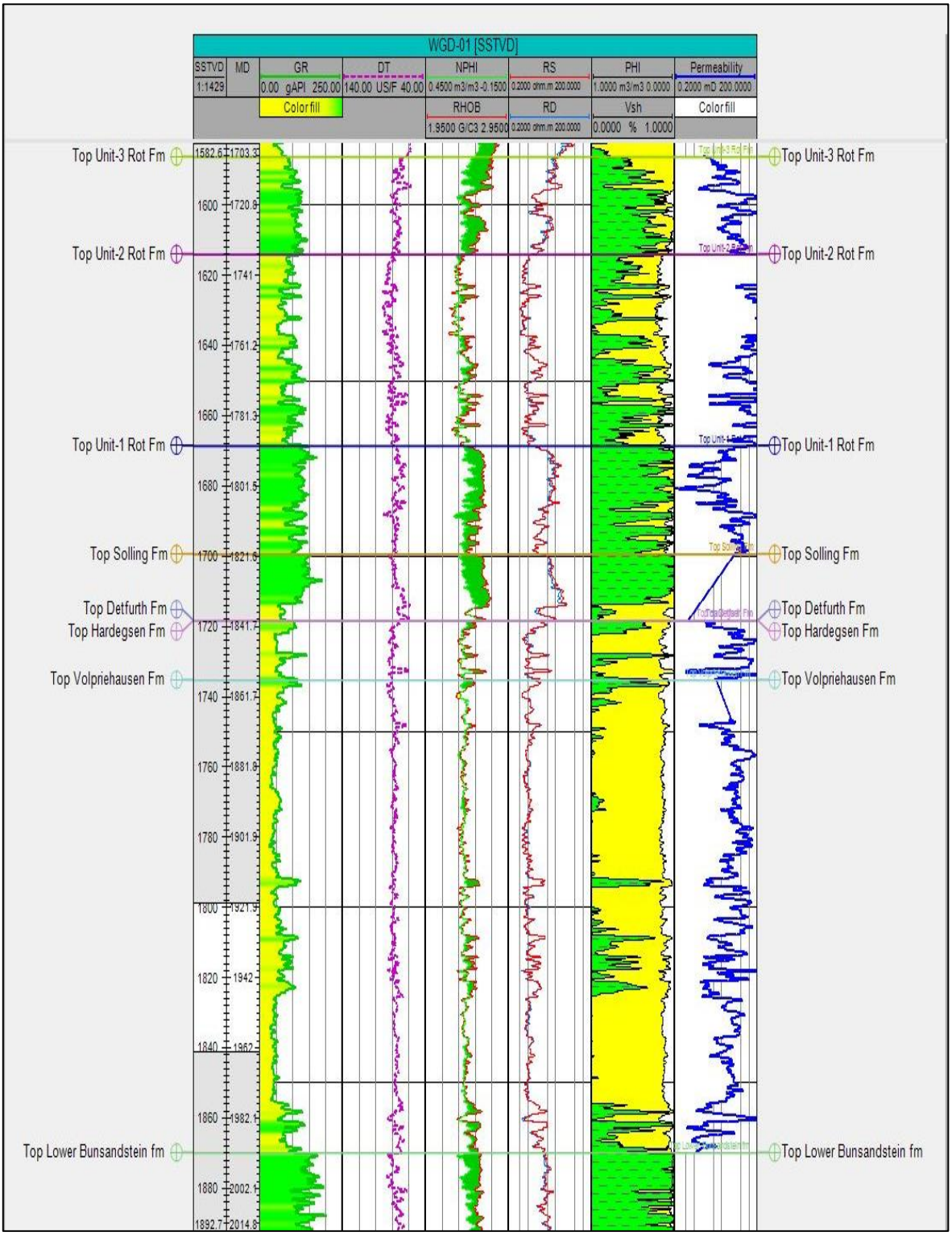

Figure 101. Petrophysical evaluation result for WGD-01.